A. G. Grankov · A. A. Milshin

Microwave Radiation of the Ocean-Atmosphere

Boundary Heat and Dynamic Interaction

Springer

Microwave Radiation of the Ocean-Atmosphere

Alexander Grankov · Alexander Milshin

Microwave Radiation of the Ocean-Atmosphere

Boundary Heat and Dynamic Interaction

🐎 Springer

Alexander Grankov
Institute of Radio Engineering Electronics
Russian Academy of Sciences
Moskva
Russia 125009
agrankov@inbox.ru

Alexander Milshin
Institute of Radio Engineering Electronics
Russian Academy of Sciences
Moskva
Russia 125009
amilshin@list.ru

Cover illustration: Cover Images @ 2009 JupiterImages Corporation

Printed on acid-free paper

Springer is part of Springer Science+Business Media (www.springer.com)

Preface

We will show in this monograph some possibilities of using the potential of satellite passive microwave radiometric methods for the analysis of variations of heat and dynamic processes in the ocean–atmosphere interface in a wide range of time scales – from *mesometeorogical* (hours, daily) to *seasonal* (month) and *multiyear* (climatic) ones.

The most essential mechanisms of intercommunication of natural microwave radiation of the system ocean–atmosphere (SOA) with the vertical turbulence fluxes of sensible, latent heat, as well as the momentum at the boundary of the SOA are studied.

We will consider the turbulence heat fluxes as the factors generated by the chaotic movements in the atmosphere, when every small individual part of air is moved irregularly. Here, one can observe a transfer of the energy from large-scale to small-scales; the average distance between the air particles is increased with a time.

Also, the potential of remote sensing the characteristics of heat and water advection and their accumulation in the atmosphere boundary layer are demonstrated.

In these studies, we mean mainly the middle and high latitudes of the North Atlantic, which are forming the weather conditions and climatic trends over Europe and European territories of the Russia.

Elaboration of the methods of analysis of the processes of the ocean–atmosphere interaction as the factor of seasonal and intraannual climate variability is very important component of international scientific programs such as Global Change Research Program, Earth Observing System (EOS), and climate variability and predictability (CLIVAR). The actuality of these subjects is emphasized and accounted also in special issues of Russian programs on researches of the nature of the World ocean and the development of systems for its studies.

As a result of the steady reduction of the field measurements in the World ocean, the satellite means have become the most perspective tools of its investigation. Additionally, the measurements from vessels and buoys do not provide the required global observations for spatial resolution and time regularity: conventional estimates of global fields of the fluxes between ocean and atmosphere suffer from inadequate spatial and time sampling, with the exception of the North Atlantic.

The parameters measured from satellites such as vertical turbulent fluxes of sensible and latent heat, as well as the impulse (momentum), are considered as the

so-called climate-forming factors. The main problem of retrieving these parameters from satellites is caused by the following reason: an intensity of natural microwave radiation of the SOA brings an information not only on near-surface atmospheric layers (which are most active in forming the processes of energy exchanges with the oceanic surface), but also on the more higher layers.

That is why the satellite passive microwave radiometric methods of analysis of the climate-forming parameters were recognized as the effective tools only in the 1980s and 1990s (mainly in USA, Russia, and Germany), though earlier (in 1960s and 1970s) some encouraging results of the use of the remote sensed data of laboratory studies, as well as the measurements, were obtained from aircrafts and floating platforms at microwaves and infrareds for the analysis of the heat and water exchange at the air–sea boundary.

Conventional estimates of global fields of the fluxes between ocean and atmosphere suffer from inadequate spatial and time sampling with the exception of the North Atlantic. Additionally, the parameters that determine the fluxes are very difficult to measure on buoys and ships or are not measured at all. Satellite measurements probably offer a possibility to circumvent some of these difficulties. In the last two decades, strong efforts have been spent in developing methods to derive geophysical parameters like water vapor content, radiation fluxes, etc. from geostationary and polar orbiting satellites. Retrievals developed for radiometers on polar orbiting satellites like the AVHRR (advanced very high resolution radiometer) on the NOAA series, the SSM/I (special sensor microwave/imager) on the DMSP program and for the instruments onboard the TRMM satellite are distinguished by an accuracy that is competitive to in situ measurements or even better.

The various methods of estimation of the monthly mean latent heat fluxes at the SOA boundary and their seasonal variability are proposed and approved. They are based on the direct (*physical*) properties or indirect (*correlative*) relations between the SOA brightness temperatures measured from satellites and the most important components of the heat and water exchange, such as the sea (ocean) surface temperature, the temperature, moisture, and wind speed of the near-surface atmosphere.

Later, we have examined the potential of the radiometer SSM/I for retrieval of the *synoptic* latent fluxes, but results of these studies were not found so encouraging. At present, we ought to fill out some gaps in researches of real and potential possibilities of the satellite passive microwave radiometric methods conformably to an analysis of the heat and dynamic ocean–atmosphere interaction:

- The methods used are based on the formulas of heat and water exchange between the ocean and atmosphere (*bulk-formulas*), accounting in calculations of the near-surface air temperature and humidity, which are *indirectly* connected to the SOA brightness temperature.
- Usually, only the humidity atmospheric characteristics measured from satellites in the spectral microwave band of the water vapor absorption are taken into consideration as the intermediate characteristic between the SOA brightness temperature and the boundary heat fluxes.
- Relations between the SOA brightness temperature and the boundary heat fluxes have a static character, as they are based on *general* (climatic) regressions

between the air integral and near-surface humidity, which do not reflect their endowment to the effects of various mechanisms of heat and water transfer in the atmosphere (such as the vertical diffusive, horizontal advective, etc.) at the short-period time scales.

What is more important is that the specialists in the field of remote sensing the oceanological and climatic processes did not consider possibilities of using the satellite microwave radiometric methods in the *frontal* oceanic zones, where the effectiveness of bulk-formulas is not clear yet.

Also, the potential of satellite passive microwave radiometric methods for the analysis of energy and circulation characteristics of the boundary layer of the atmosphere and their influence on the heat and water exchange at the boundary of the SOA is still not fully researched.

Finally, the specialists on remote sensing of the World ocean by means of passive radiometric microwave, infrared, and other methods lost sight of the urgent problem concerning the study of initial role of the ocean and atmosphere in their heat and dynamic interaction at various spatial and time scales.

In this connection, first of all, we directed our efforts on the elaboration of the physical backgrounds and approaches of determination of vertical turbulent sensible and latent heat fluxes in a wide range of their variability (*hours, weeks, seasons*, and *years*) using the satellite-derived data measurements of characteristics of natural microwave radiation at millimeters and centimeters.

Toward this end, we solved the following problems and tasks:

- Study of the mechanisms of forming an intercommunication of the SOA natural microwave radiation intensity and an intensity of heat and water exchange at the SOA boundary.
- Searching the spectral intervals, which provide a most close correlation of the SOA brightness temperatures m asured from satellites with vertical turbulent heat and impulse fluxes at the SOA boundary for different time scales.
- Study of ways of using the data of satellite microwave radiometric measurements for an analysis of heat and dynamic interaction characteristics in the frontal zones of the North Atlantic.
- Analysis of satellite passive microwave radiometric methods with a view to use their potential to analyze the ocean and atmosphere roles in the heat interaction over different time scales.

The special aspect of these studies is the research of mechanisms of the SOA natural microwave field reaction to variations of heat properties in the near-surface and boundary layers of the atmosphere, as well as the search of spectral intervals and suitable scales of spatial and time averaging the data of satellite measurements, which provide the immediate (direct) connection between the SOA brightness temperature measured from satellites and an intensity of heat and water exchange at the boundary of the system.

These studies were supported by the Russian Fond of Basic Researches (Grant No.94-05-16234a, 1994–1995). The Russian and American space agencies (Rosaviacosmos and NASA) sponsored our activity in a frame of the contract NAS

15-10110, 1996–1997. The results of our studies of correlation between brightness temperature and the atmosphere boundary layer enthalpy caused by horizontal heat advection were included in the annual report of Russian Academy of Sciences (RAS) in 1998.

Moscow, Russia   A.G. Grankov
Moscow, Russia   A.A. Milshin

Contents

Introduction

The satellite-derived data of passive microwave radiometric measurements have an essential potential to evaluate the parameters of the system ocean–atmosphere (SOA) determining the processes of heat interchange in its interface with use for oceanologists' and climatologists' accuracy. In particular, the brightness temperature of the SOA is directly connected to the water surface temperature and near-surface wind speed, which are the key parameters in the formulas used for computation of heat and water vertical turbulent fluxes at the SOA boundary (bulk-formulas). Such parameters as the near-surface air temperature and humidity only indirectly influence natural microwave radiation of the SOA, but in spacious areas of the North Atlantic (in the middle and high latitudes), the total water vapor of the atmosphere is an effective indicator of variations of these parameters in a wide range of time scales.

An influence of the oceanic water surface temperature T_w on the SOA brightness temperature is the passive factor in comparison with the near-surface air temperature and integral water vapor content of the atmosphere observed in the experiments NEWFOUEX-88 and ATLANTEX-90 in the range of synoptic time scales. This fact, possibly, is not evident for oceanologists and climatologists in their traditional understanding of the role of using the remote sensing methods, when only the partial parameters of the SOA interface are used in retrieving the heat fluxes in the ocean–atmosphere interface with the well-known procedures such as the bulk-formulas. Such result can be justified by an intensive variability of the atmospheric parameters T_a, e, and Q, as well as their close correlation determined by the processes of the horizontal air movements in the near-surface and the boundary layers masses typical for middle and high latitudes. This effect excites the brightness contrasts at the synoptic time scales exceeding in ten times the contrasts produced by variations of the parameter T_w because the influence of the vertical heat transfer on the MCW radiation characteristics is more weak in comparison with the effect of the horizontal heat transfer in the atmosphere.

The significant and unique effect observed in these tasks is a high sensitivity of the SOA brightness temperature at the wavelength 1.35 cm to variations of the atmospheric.

The relations between the SOA natural microwave radiation and the processes of heat interchanges in the system are most indicative at the synoptic range of time scales; the following regularities are observed in this case:

– Parameterizations used for calculating the vertical turbulent fluxes of sensible and latent heat over the ocean can be reconstructed in the form of combinations of only those parameters of the ocean–atmosphere system that are directly related to satellite-derived characteristics.
– A good agreement between theoretical and experimental (satellite) estimates of the brightness temperature of the system ocean atmosphere natural microwave radiation and the results of their processing is observed in the mid- and north latitudes of the North Atlantic.
– An influence of the near-surface wind speed and its direction on synoptic variability of meteorological parameters, total heat (sensible and latent fluxes), and the SOA brightness temperature over the Subpolar Hydrological Front in the North Atlantic has been discovered.

Long-term measurements from the DMSP SSM/I devices help estimate the monthly mean values of most changeable SOA parameters, which are forming the air–sea heat interaction at seasonal and climatic time scales such as the monthly mean wind speed and integral water vapor content in the atmosphere, and whose current values cannot be evaluated with ordinary reference data.

The satellite estimates of the monthly mean estimates of the wind speed and atmosphere integral water vapor content are slightly dependent on the spatial averaging (within the squares varied from $1 \times 1°$ to $5 \times 5°$); the cloudiness and precipitation do not influence essentially an accuracy of these parameters estimation.

A strong correlation between monthly mean values of the SOA brightness temperature at the resonant line of a water vapor absorption in the atmosphere (1.35 cm) and the surface vertical turbulent heat fluxes in some areas of the North Atlantic over a period of years has been discovered.IntroductionIntroduction

Chapter 1
Parameters Accessible for the Satellite Microwave Radiometric Means and Their Relations with the Ocean–Atmosphere Interaction

1.1 Relationship Between Dielectric Properties, Physical and Chemical Parameters of the Water and Physical Characteristics of the Atmosphere

1.1.1 Radiation Models of a Water Surface

The most important characteristics of the sea water are their temperature and salinity. Permittivity of water, ε, is a function of the wavelength λ. The dependence of permittivity ε on the wavelength, temperature, and salinity is approximately described by the Debye's relaxation equations supplemented by an additional term to account for an increase in ionic conductivity at a given wavelength λ due to an increase in salt content in the solution.

Of all the salt solutions present in natural water, the most extensively studied in the radio wavelength range is the NaCl solution proper to sea water (in concentration upto 3–5 moles L^{-1}) (Hasted 1974).

At wind speeds V of about 5–7 m s^{-1}, foam appears on the ocean surface. The water-surface area covered by foam increases with a rise in wind speed. Foam may also be formed as a result of turbulence of the surface and subsurface waves, and also in regions of plankton by a reduced pressure caused by the motion of internal waves. Theoretical estimates show the real and imaginary parts of the foam dielectric constant to vary inversely with the air concentration and constitute several units at concentrations in excess of 0.9. The spectral dependence of foam dielectric constant is due to the frequency dependence of the water dielectric constants.

The dependence of the SOA brightness temperature T^{b} of a calm (not exited by wind force) water surface on temperature and salinity is described in the Kirchoff approximation by the Fresnel reflection equations $R(\varepsilon, \theta)$, which include the characteristics of this medium as the complex dielectric constant ε, observation angle θ and polarization (Basharinov et al. 1974).

$$T^{\mathrm{b}} = \chi\, T_{\mathrm{w}}, \quad \chi = 1 - R, \tag{1.1}$$

where T_w is the water surface temperature.

With vertical observation $\theta = 0$,

$$\chi_v = \chi_h = \chi_0, \tag{1.2}$$

where $|\varepsilon| = \varepsilon_1 \sqrt{1 + tg^2 \delta}$; $tg\delta = \varepsilon_2 / \varepsilon_1$ is the dielectric loss angle;

ε_1 and ε_2 are the real and imaginary parts of the permittivity, respectively.

The angular dependence of the coefficients of horizontally and vertically polarized radiation can be approximated with an accuracy of 2–10% by the following polynomials:

$$\chi_h(\theta) = \chi_0 (1 - A_h \ \theta^2), \ 0 \le \theta \le 0.5\pi,$$

$$\chi_v(\theta) = \chi_0 (1 + A_v \ \chi_v \theta^2 + B_v \ \theta^4), \ 0 \le \theta \le 0.4\pi. \tag{1.3}$$

When the receiving antenna is oriented at an angle α relative to the observational plane,

$$\chi_\alpha(\theta) = \chi_v \cos^2\alpha + \chi_h(\theta) \sin^2\theta). \tag{1.4}$$

The thickness of the efficiently emitting layer (the skin layer) is determined as the inverse of the absorption factor:

$$l_e = 1 / \gamma,$$

where

$$\gamma = \frac{2\pi\sqrt{2}}{\lambda} \sqrt{|\varepsilon| - \varepsilon_1}. \tag{1.5}$$

Analysis of the fresh water dielectric constant data discloses the relation:

$$l_{e1} / l_{e2} = f(\lambda_1 / \lambda_2), \tag{1.6}$$

which is valid for k from 0.94–1 in the 5–30 cm wavelength range

$$l_e(\lambda) \approx 0.01 \ \lambda^{-2}, \tag{1.7}$$

where l_e, λ are in centimeters.

Calculations used (1.1)–(1.7) in *early* works (Nikolaev and Pertshev 1964; Pereslegin 1967; Sirounian 1969; Rabinovich and Melentjev 1970; Matveev 1971; Raizer et al. 1975; Grankov and Shutko 1980) disclosed the frequency dependent relations between the SOA radiation characteristics at microwaves and water

surface temperature and salinity. As an example, a relation for a NaCl solution of varying concentration is presented in Fig. 1.1.

The emissivity of a smooth water surface covered with a uniform foam or an oil layer can be approximated by the equations derived for the stratified models (Basharinov et al. 1974), which account for the dielectric characteristics of individual layers and multiple reflections of electromagnetic radiation fluxes from the boundaries of individual layers. These multiple reflections are responsible for interference effects (foamed mixtures with air content above 95% feature the absence of any interference effects; the emissitivity of a foam-covered water surface in these cases is estimated taking into account the absorption in the foam layer). In later works (Wentz 1983; Shutko 1985; Sasaki et al. 1987; Meissner and Wentz 2004), some considerable revisions of relations between the sea temperature, salinity and wind speed of sea water, its dielectric constants, emissivity, and brightness temperature were made.
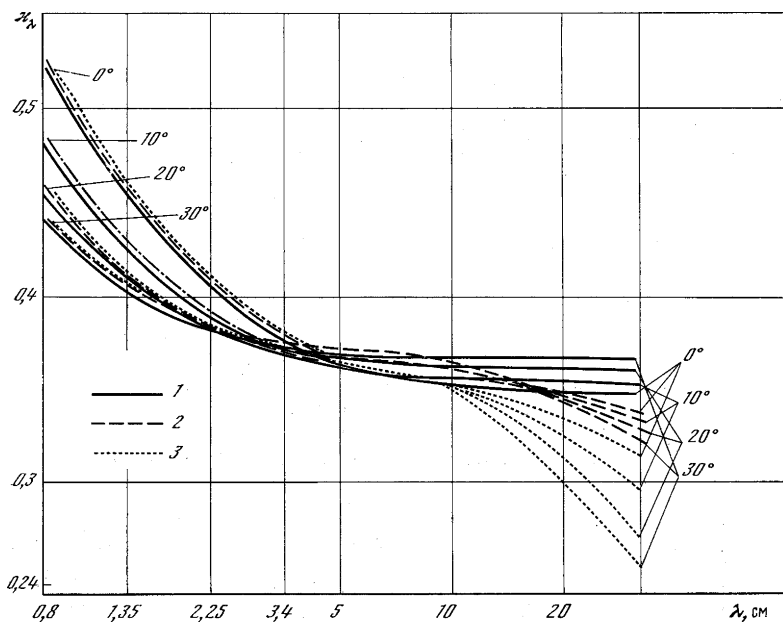
Fig. 1.1 Theoretical dependence of a water surface emissivity χ from the wavelength λ at various temperatures and NaCl solution concentrations: 1–0‰; 2–20‰; 3–40‰

1.1.2   Radiation Models of the Atmosphere and the SOA

A standard cloudless atmosphere is characterized by such parameters as temperature, air density, and water vapor pressure. The height temperature profile T_a is described by the broken line functions T_{a1}, T_{a2}, and T_{a3}:

$T_{a_1} = T_0 - ah$, $0 \leq h \leq 11$km,
$T_{a_2} = T_a(11\text{km})$, $11\text{km} \leq h \leq 20$km,
$T_{a_3} = T_a(11\text{km}) + h - 20$, $20\text{km} \leq h \leq 32$km.

Here, T_0 is the temperature at sea level ($h=0$), and a is the temperature vertical gradient. Due to one of the known (US) standards, $T_0 = 288.15$ K, and $a = 6.5$ K km^{-1}. For an approximate calculation, we can use the simplified formula:

$$T(h) = T_0 \exp^{-h/H}, \; H_T = 4.4 \text{ km.} \tag{1.8}$$

For many preliminary calculations, we can also use the exponential altitude model of atmospheric pressure P:

$$P(h) = P_0 \exp^{-h/H}, P_0 = 1013 \text{ mb}, H_P = 7.7 \text{ km} \tag{1.9}$$

The exponential model is used here to describe the volumetric water vapor density in the atmosphere:

$$\rho_e(h) = \rho_0 e^{(-h/H)} \tag{1.10}$$

Here, ρ_0 is the atmospheric water vapor density at sea level and depends on climatic and seasonal time scales. On the average, it varies from 10^{-2}g m^{-3} for a dry climate upto 30 g m^{-3} for a warm climate. The models (1.8)–(1.10) are fit, to our opinion, also for using in the *climatic* and *seasonal* time scales.

The main absorption and radiation components of the atmosphere are its water vapor and oxygen, which are entirely determined by the atmosphere temperature T, air pressure P, water vapor density ρ_e, and their vertical distribution. Water vapor and oxygen have absorptive lines at wavelength 1.35 cm ($f=22.235$ GHz) and in the region of ~5 mm, respectively; they are, as per our opinion, both attractive for a diagnosis of the atmosphere heat and its interaction with the ocean surface. Namely, in these spectral regions, we can observe the significant brightness contrasts measured from satellites, or artificially derived (simulated) estimates of the SOA physical state.

The brightness temperature of the SOA depends on the radiation properties of the water surface and the absorption of the atmosphere at microwaves; the SOA brightness temperature T^b is given by the following relations (Basharinov et al. 1974):

$$T^b \cdot = T^b_1 \cdot + T^b_2 \cdot + T^b_3 , \tag{1.11}$$

where

$$T^b_1 \cdot = T^b_w \cdot \exp(-\tau) \qquad (1.12)$$

is an intensity of radiation flux from the water (oceanic) surface T^b_w attenuated in the atmosphere (the quantity T^b_w is proportional to emissivity of the water surface and its thermodynamic temperature T_w)

$$T^b_2 \cdot = \cdot \int_0^H \cdot T_a(h) \cdot \exp\left[\tau(h)-(H)\right] \cdot \mathrm{d}h \qquad (1.13)$$

is an intensity of the up-going atmosphere radiation flux;

$$T^b_3 \cdot = \cdot R \cdot \int_0^H \cdot T_a(h) \cdot \exp\left[\tau(h)-(H)\right] \cdot \mathrm{d}h \qquad (1.14)$$

is an intensity of the atmosphere down-going radiation flux reflected by the water surface

$$\tau(h) \cdot = \cdot \int_0^h \cdot \gamma(h') \cdot \mathrm{d}h' \qquad (1.15)$$

τ is the integral attenuation of the radiation by the atmosphere, which depends on the linear absorption factor γ and the thickness h of the absorbing layer counted from the ocean surface ($h=0$); and R is the coefficient of reflection of the atmosphere down-going radiation flux from the water surface.

Figure 1.2 gives the SOA brightness temperature values at millimeters and centimeters, where the resonance effects become apparent.

Besides molecular attenuation in water vapor and oxygen, the microwave propagation at centimeters and millimeters is also greatly affected by various hydrometeors, first of all, rain and clouds; one can evaluate appropriate models from Basharinov et al. (1974), Wentz (1983), and Andreev et al. (1985), for example.

1.2 Methods of Using the Data of Microwave and Infrared Radiometric Measurements for an Analysis of Heat Fluxes at the SOA Boundary

1.2.1 Traditional Approach

The main problem in remote sensing the heat exchange processes in the interface of the SOA is caused by the fact that characteristics of natural microwave and infrared radiation of the ocean–atmosphere system are formed not only in the near-surface atmosphere layer (thick in 10–20 m), but also in its more higher layers (2–5 km),
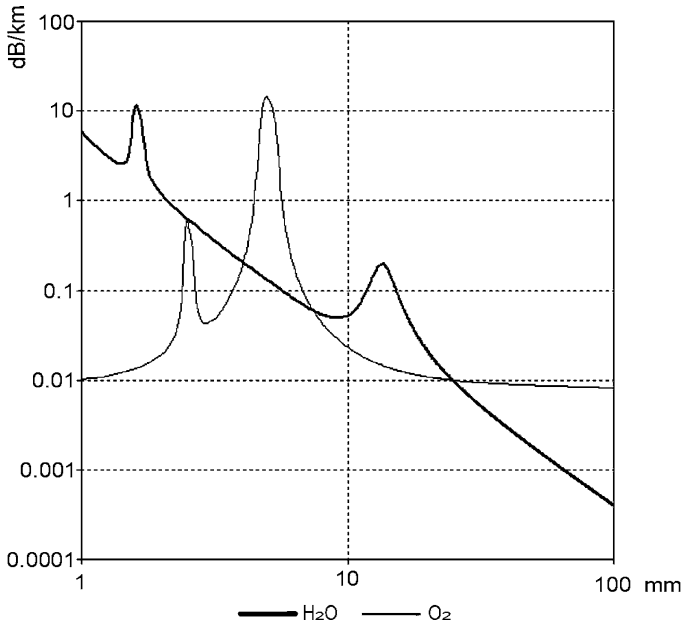
Fig. 1.2 Frequency dependencies of the SOA brightness temperature of the earth atmosphere T^b: (1, 3), the downward atmospheric natural microwave radiation; (2, 4), when the water vapor density at the sea level ρ_0 is 7 $g\,m^{-3}$; (3, 4) ρ_0 is 2 $g\,m^{-3}$

depending on the spectral bands used in satellite measurements. There are different approaches to use the data of microwave and infrared radiometric measurements for estimating the heat fluxes in the SOA interface. For example, one of these is based on retrieving the vertical temperature profiles (gradients) in the oceanic surface layer; it was shown in Khundzhua and Andreev (1973) that their magnitude and the sign let us to judge on intensity of the vertical turbulent flux of sensible heat. The effectiveness of such approach at infrareds is confirmed by results of numerous measurements conducted in laboratories, from stationary coast points, and the floating sea platforms; these results are in a good agreement with the data of aircraft measurements (Bychkova et al. 1988).

The potential of retrieving the vertical temperature (profile) of the sea subsurface layer was investigated theoretically in Sharkov (1978) and Mitnik (1979). Afterwards, these studies were continued by the specialists, which developed and tested the possibilities of retrieving the water surface vertical temperature profile of the ideal (flat) and natural (waved) sea surface (Gaikovich et al. 1987) in the laboratory conditions.

At the same time, we have no evidences of using the microwave and infrared wavelength ranges for determination of heat fluxes based on determination of the water surface vertical temperature profiles with the data of measurements of satellite microwave or infrared means. The modern satellite MCW and IR means, which provide an accuracy of retrieving the sea surface temperature (SST) at best of 0.5–1°C, do not provide the correct estimations of the SST values and their variations. It is even for results of MCW and IR methods of retrieving the air vertical temperature and humidity

profiles in locally bands of radiation (absorption) for the most important atmospheric components – the water vapor and the oxygen, whose accuracy estimates are insufficient for these tasks due to the low spectral resolution and sensitivity of radiometers.

More perspective (the *forced*, at some extent) is the method of determination of heat fluxes based on the statistical correlation between the integral (averaged over the height), whose variations are neatly fixed from satellites with the data of MCW and IR measurements, and its temperature and humidity values.

This correlation is caused by the air near-surface and the boundary layers mechanisms of turbulent the heat and water mixing. These processes are most typical and intensive for the atmosphere (in contrast of the ocean) and become apparent for their monthly (or decade) mean variations, which are free from their more short-period perturbations. That is why the best results of application of satellite radiometric methods obtained are concerned with retrieving *monthly* mean SOA boundary heat fluxes, based, for example, on the data of MCW and IR passive radiometric measurements derived from the satellite Nimbus 7, as well as from the DMSP and NOAA satellite series.

The relation between temperature and humidity characteristics in various atmosphere layers is the starting point for using the data of satellite radiometric methods of analyzing the sensible (q_h) and latent (q_e) vertical turbulent heat fluxes at the SOA boundary, if we use the semi-empirical formulas (bulk formulas), based on the global bulk aerodynamic method. In accordance with this method, the values q_h and q_e are given by the formulas (Ivanov 1978; Lappo et al. 1990):

$$q_h = C_p \rho \; C_T (T_w - T_a) V; \tag{1.16}$$

$$q_e = L \rho (0.622/P_a) \; C_E (e - e_0) V, \tag{1.17}$$

One can see from these formulas that values q_h and q_e depend on such parameters of the SOA as the temperature (T_a), water vapor pressure (e), and wind speed (V) in the near-surface atmosphere, as well as the oceanic water surface temperature (T_w), and maximum for this value, air humidity (e). The following parameters used in bulk-formulas (1.16) and (1.17) are the numbers of Schmidt (C_T), Dalton (C_E), the specific heat of evaporation (L), the specific air heat under constant pressure (c_p), and the air density (ρ).

The frames of aerodynamic method let us also to obtain the simple parameterization of relations between an intensity of *dynamic* air–sea interaction characterized by the turbulent flux of impulse (momentum) (q_v), which can be calculated (Ivanov 1978; Lappo et al. 1990):

$$q_v = \rho \; C_v \; V^2, \tag{1.18}$$

where C_v is the drag coefficient.

The formulas (1.16)–(1.18) enable to determine not only "instant," but also averaged over considerable time scales heat and impulse fluxes. For example, it is possible to estimate the monthly mean ones using the monthly mean parameters T_w, T_a, e, and V as the input data (Ariel et al. 1973; Esbensen and Reynolds 1981; Larin 1984; Gulev 1991).

This peculiarity of the global bulk aerodynamic method attracts an attention of specialists in the field of the oceanology, meteorology, and climatology, who are really interested in the results of the remote sensing means, especially, an

information on the near-surface atmosphere air temperature T_a and humidity e. However, the possibilities of this method are good only in the limited frames: one can envisage some limitations, maintaining this method: the horizontal spatial gradients of the parameters T_w, T_a, e must not exceed some critical values (Lappo et al. 1990). Consequently, the possibilities of its realization are unclear in the oceanic frontal zones, which are characterized by significant geophysical and brightness temperature spatial and temporal contrasts.

It is seen from the formulas (1.16)–(1.18) that the water surface temperature T_w, the near-surface air temperature T_a, humidity e, and wind speed V are playing the main role in the air–sea interchanges.

The estimates of the parameters T_w and T_a can be obtained *directly* from the data of satellite microwave radiometric measurement data. To estimate the parameters T_a and e, we ought to use some *correlative* relations between these parameters and an intensity of the SOA natural MCW and IR radiation, which are manifested only in some spectral intervals.

The extensive studies were devoted to analyze the potential of satellite MCW and IR methods of estimating the characteristics of heat and dynamic interaction between the ocean and atmosphere. For example, in Dymnikov et al. (1984) were obtained some proximate estimates of an accuracy of determining the oceanic layer parameters closely related to the SOA radiation balance. In Grishin and Lebedev (1990) the maximal values of errors of the parameters T_w, T_a, V, and e, when the estimates of the fluxes q_h, q_e, and q_v calculated with the bulk-formulas, are useful for the oceanologists and climatolologists, namely, from this vision angle the possibilities of modern satellite MCW and IR radiometric instrumentation are discussed here. In Taylor (1984) the information content of satellite-derived monthly-mean heat and latent heat fluxes depending on their sampling frequency was studied on the basis of the data obtained during the experiment JASIN in the North Sea. The results of this studies show that the relative error of heat flux determination is estimated to be ~10% for the parameter q_h and 30% for the parameter q_e, if the oceanic areas observed from satellites are covering through every 12 h.

The results of experimental measurements derived from the satellites Nimbus 7, DMSP (at microwaves), and the NOAA satellites (at infrareds) within various physical and geographical zones of the World Ocean (Schulz et al. 1997; Grankov et al. 1999a, b; Liu 1995) justify an effectiveness of this approach. For example, the square root estimates of the month mean latent heat fluxes averaged over $2 \times 5°$ squares on the basis of selected satellite data (September 1987, Global Ocean (Schulz et al. 1997)) is about 15–30 W m^{-2}. The similar results have been obtained in Grankov et al. (1999a, b) (in some energy active zones of the North Atlantics, in February 1994), and in Liu (1995) (in tropical zones of the Pacific Ocean).

As the following important step in the field of remote sensing the processes of the heat and dynamic ocean–atmosphere interaction characteristics, we can consider an appearance of the atlas of the monthly mean sensible and latent heat fluxes, and some other parameters of the SOA typical for the global ocean collected during the period July 1987–December 1998 (Grassl et al. 2000), which are based on the data of satellite MCW and IR measurements.

The evident endowment in an analysis of the potential of satellite microwave radiometric methods in studies of the SOA heat interaction in tropical oceanic zones was introduced by Sharkov from the Institute of Space Research, Russian Academy of Sciences (RAS) (Sharkov 1998).

At the same time, we ought to emphasize the problems of using the bulk-aerodynamic method for retrieving the *synoptic* variations of heat and water vapor exchanges, which are more changeable with the *seasonal* variations. We can explain this features starting from the own experience:

1. When passing on the seasonal to the synoptic time scales, we can observe the relations between the air temperature and humidity in different atmospheric layers become more weakened; hence, we may conclude that the accuracy of determination of the parameters T_a and e, appearing in the formulas (1.16) and (1.18), will be decreased due to the time scale shortening.
2. The role of such factors as the wind speed in the near-surface atmosphere, the atmospheric cloudiness and rainfall, which have limited the satellite estimates of the SST in principle, has become clearly apparent in the range of the *synoptic* time scales.
3. An ambiguity of the coefficients C_T and C_E denoted in the relations (1.16) and (1.17) plays more essential role at the synoptic time scales in comparison with the seasonal ones.

Some efforts were undertaken for solving these problems by way of the modification of the formulas (1.16)–(1.18) taking into account the close correlation between the near-surface air humidity e and the atmospheric total water vapor content Q in the North Atlantic and Pacific oceans (Schulz et al. 1997), the parameters T_a and T_w in the Caspian sea (Il'yin et al. 1986; Panin 1987) as well as the parameters T_a, e, and Q in the Newfoundland active zone of the North Atlantic (Grankov and Novichikhin 1997).

1.2.2 Alternative Approach

Another approach is based on using the data of satellite MCW and IR radiometric measurements as the *direct* characteristics of the heat dynamic interactions between the ocean and atmosphere. This idea was declared first in Dymnikov et al. (1984), where the requirements to the satellite means were discussed from the point of view of the program "RAZREZY" in studies of the heat ocean/atmosphere balance, and in Eyre and Lorence (1989) in interests of the weather forecast. Also, in Lapshin and Ragulin (1989), it was shown that an intensity of the SOA natural MCW radiation (the brightness temperature) in the centimeter range of wavelengths can be considered as the *direct* characteristic of intensity (rate) of exchanges between the ocean and atmosphere through the CO_2 component.

We think that it is an appropriate way to discuss the two conceptions of using the data of satellite MCW radiometric means and methods.

In the first case, we deal with the traditional approach reasonably, when we try to retrieve the information on the near-surface air humidity and temperature characteristics as well as on the SST and near-surface wind speed, which determine the regime of the ocean–atmosphere heat and dynamic interaction. This conception is more convenient and clear for the oceanologists.

In another case, our method corresponds to proposed by A.M Shutko and E.A. Reutov (Reutov and Shutko 1987; Reutov 1989) conception of using the remote sensing data not only for their retrieving into adopted in the geophysics parameters such as the near-surface air humidity and temperature, and wind speed, which are significant factors used in the Bulk-formulas. Following this principle, we can ignore the other factors in details – the vertical distribution of these parameters, for example. When solving this problem, we can decide the typical problems of the extraction (retrieving) of some *partial* characteristics of media state accepted in science and practice (such as the near-surface air temperature, humidity, and wind speed), but also first of all, for a direct use of radiation characteristics such as an intensity, scattering, and polarization electromagnetic properties of natural objects (oceans, basins, lands) for determining their state *at whole*. Some results of realization of these ideas were demonstrated in Reutov and Shutko (1987) and Reutov (1989), where it was shown that the SOA brightness temperature at centimeters and decimeters is closely attached to the so-called *radiation index of dryness* of the land; it is also possible to associate the brightness temperature measured from satellites with an intensity of large-scale ocean–atmosphere heat interaction in the energy-active zones (EAZOs) (Grankov and Shutko 1992a, b; Grankov and Usov 1994), also for estimation of the temporal and spatial variations of the total turbulent (sensible + latent) heat fluxes in the *synoptic* range of time scales (Grankov and Resnjanskii 1998; Grankov and Mil'shin 1999; Grankov et al. 2000, 2002), as well as for an analysis of the *multiyear* changeability of their month mean values in the middle and high latitudes of the North Atlantic (Grankov and Mil'shin 2001).

To our opinion, the satellite microwave radiometric of the direct analysis of heat and water exchanges in the SOA interface should be based on the following principles:

1. The methods used must be based on the models of interrelations between radiation characteristics of the SOA and the boundary heat processes using a clear physical interpretation, which includes a minimal number of transit parameters; in other words, the most simple parameterizations of these relations are preferable.
2. It is a desirable and effective approach when the models used will include the oceanic and atmospheric parameters, which are accessible for the satellites methods of remote sensing of the SOA; it is very important that these parameters should provide strong response of the SOA natural MCW and IR radiation in contrast of other parameters of the system.
3. The parameterizations used must be universal enough to provide their accommodation to different parts of the World ocean (at least, in the middle and high

latitudes) for various seasons. Also these approaches must be suitable for the cyclonic and frontal zones, when the classic insight on the ocean–atmosphere heat and water interchanges are effective even we will be use the *climatic* data, accumulated by means of satellite and vessel measurements.

The following examples have met the requirements listed above, such as the example (Grankov and Usov 1994), which illustrates the close relation between seasonal variations of the month mean of the SOA brightness at the specific pieces (intervals) at microwaves and the air–sea temperature differences $\Delta T = T_w - T_a$, which is considered as one of the key characteristics of heat and water interchange in the ocean–atmosphere interface (at least, in the middle and high latitudes of the World ocean) (Shuleikin 1968; Nikolaev 1981). The results of regressions between the values ΔT (taken from the atlas of the climatic-mean hydrometeorological parameters for the Gulf Stream active zone) with their calculated MCW estimates ΔT^* show us that the value of the correlation coefficient r is about 0.92; the values of the root-mean-square (*rms*) discrepancy σ is about 0.6°C. Such approach demonstrates the evident advantage in comparison with the methods of the singly determination T_w and T_a and the following calculations of their difference. Let us note that an accuracy of a single estimation of the month mean values of the SST (the parameter T_w) *only* is about 1°C (see details in Chap. 3).

More possibilities of a direct use of satellite data measurements at microwaves demonstrates the method (Grankov and Shutko 1992a, b) elaborated for an analysis of the integral (averaged per year) vertical turbulent heat fluxes and their year-to-year variability. This approach is based on the method of calculation of the heat fluxes, which was founded by Lappo et al. (1990) and takes into account not only the month mean values of the parameters T_w and T_a (and their annual amplitudes), but also the estimations of the time shift between them. The method is more presentable, if we draw the line (phase) trajectories in the form of the T_w–T_a loops. The geometric characteristics of these loops such as the square, orientation, and their distinctions from the ideal (rectangular) form let us to estimate the annual heat fluxes in different regions of the World ocean and to evaluate their intra-annual variability. The advantage of this procedure is in its resistance to all kinds of the measurement noises, as far as the final estimates of the heat fluxes include not only some separate data of satellite measurements, but also take into account the general (seasonal) tendencies. The similar approach is used in radioengineering and radiolocation, when we operate with the low-level in contrast with noises; in this case, besides the amplitude (intensity) of the signals measured, the other properties (spectrum form, energy, time delay) are actively used (Kharkevich 1962; Frenks 1969).

The effectiveness of a direct use of satellite MCW radiometric measurements for analysis of the heat and water exchanges in the SOA interface is endorsed also in the *synoptic* range of time scales. It is important in this case that the satellite methods are quite efficient in the cyclonic zones as well as in the hydrological and atmospheric frontal areas, where the oceanologists cannot use effectively

their traditional methods and instrumentations. This approach was examined also for an analysis of the climatic variability of the month mean values of the parameters q_h, q_e, q_{he} in the Gulf Stream, Newfoundland, and Norwegian EAZOs of the North Atlantic.

1.3 Parameters of Heat Interchanges in the SOA, which are Directly Determined by Means of Satellite Microwave Radiometry

1.3.1 Preamble

One can select only a row of the SOA parameters, which are directly accessible for the satellite passive MCW radiometric method. In this turn, we must underline the oceanic (sea) surface temperature and the near-surface wind speed, which play a significant role in forming the heat and dynamic processes in the SOA interface. We consider the task of retrieving these parameters from satellite microwave and radiometric data as the important one from the theoretical and practical points of view for studies of the ocean–atmosphere interaction. A long time this problem is in a focus of scientific specialists of leading research Russian centers such as the Moscow and Fryazino departments of the IRE (RAS), the Research Institute of Radiophysics (Nizhnij Novgorod), the Institute of Atmospheric Physics (Moscow, RAS), the Sevastopol Sea Hydrophysical Institute (Ukraine Academy of Sciences), the Institute of the Space Research (Moscow, RAS, the Voejkov's Main Geophysical Observatory (St. Petersburg, Hydrometeorological Service of the Russia), the Shirshov's Institute of Oceanology (Moscow, RAS), the Scientific Research Center for Exploration of Natural Researches (Moscow, Russian Hydrometeorological Service), etc. The interest to these themes simulated a lot of *monographs* based on theoretical and experimental studies in Russia and abroad (Nikolaev and Pertshev 1964; Basharinov et al. 1974; Bogorodskii et al. 1977; Twomey 1977; Kondrat`ev and Timofeev 1978, 1979; Ulaby et al. 1981, 1982, 1986; Tsang et al. 1985; Nelepo et al 1985; Shutko 1986; Kochergin and Timchenko 1987; Bychkova et al. 1988; Chavro 1990; Kondrat`ev et al. 1992; Raizer and Cherny 1994; Cherny and Raizer 1998; Sharkov 1998; Grankov and Mil'shin 2004; Armand and Polyakov 2005).

The important endowment in a theory and practice of using the satellite passive microwave radiometric methods was made by Sergey V. Pereslegin in its pioneer work (Pereslegin 1967) devoted to an analysis of relations of the oceanic surface temperature and the brightness temperature contrasts observed from satellites.

Let us make a brief review of some relations between the ocean surface brightness temperature and its thermodynamic (kinetic) temperature, and near-surface wind speed.

1.3.2 Relations Between MCW Radiation, the SST, and the Wind Speed

An effectiveness of satellite passive microwave radiometric methods of determining the SST (except for an influence of the noise temperature (sensitivity) of radiometers, an attenuations in feeders, the directional patterns, etc.) depends upon the natural sensitivity (q^T) of natural MCW radiation intensity (brightness temperature T^b) to variations of SST ($q^T = \Delta T^b / \Delta T^s$), and its steadiness to variations of the near-surface wind speed and the atmosphere meteorological parameters. The main problem is an extraction of the component of the SOA brightness temperature related to the SST variations against a background of its variations caused by the water surface roughness and its foam cover as well as an influence of the atmosphere cloudiness and rainfall intensity (Basharinov et al. 1974; Shutko 1986; Grankov and Shutko 1992b).

The value of the parameter q^T reaches a maximum in the centimeter range of wavelengths (see Fig. 1.3); at the wavelength 8.5 cm, a close linear correlation between the SOA brightness temperature – measured from the firstling of radiophysical researches of the Earth from space, the soviet satellite "Cosmos-243," and in situ SST estimates is observed (see Fig. 1.4).

The satellite estimates of SST are especially critical (sensible) to a water state excitable by the wind at the SOA boundary. There are two suitable reasons: (1) the roughness of the water surface causes the appreciable brightness temperature contrasts, which are comparable with ones induced by the SST variations and (2) the spectral distinctions between the SST and near-surface wind speed effects on the SOA brightness temperature at the centimeter range of wavelengths are quiet slight; their resolution will be possible by expanding the wavelength range from centimeters to
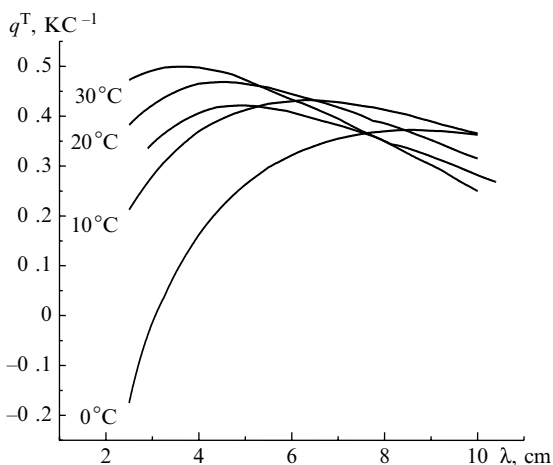
Fig. 1.3 Sensitivity of brightness temperature to SST variations calculated for values of the parameter T_w: 0, 10, 20, 30°C as function of wavelength (Grankov and Shutko 1980)

Fig. 1.4 Brightness temperature variations obtained from the satellite "Cosmos-243" at the wavelength 8.5 cm, plotted as function of SST (Shutko 1986)
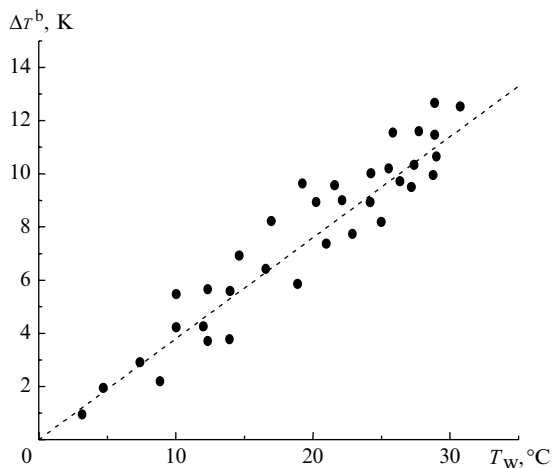
millimeters, i.e., by increasing the number of radiometric channels and losing a simplicity of a radiation model used (Grankov and Shutko 1992b). That is why, already in the first experiments on remote of the ocean from the satellites "Cosmos-243" (1968), "Cosmos-1076" (1979), "Cosmos-1151" (1980), and Nimbus 5 (1979), four spectral channels operated in the centimeter and millimeter ranges of wavelengths were used.

As early as the *first*, researches on remote sensing displayed the close correlation between the microwave radiation characteristics of sea surface and the near-surface wind speed: some results of systematization of experimental data obtained are demonstrated in the Figs. 1.5–1.8.

Figure 1.5 shows the dispersion of a sensitivity of brightness temperature to near-surface wind speed variations ($q^v = \Delta T^b / \Delta V$) in the centimeter range of wavelengths with an account of roughness and the foam characteristics observed in different experiments.

Figure 1.6 shows the dispersion of a sensitivity of the coefficient of polarization p to variations of parameter V in two subranges: $0 < V < 8$ m s^{-1} (without a foam cover) and $8 < V < 25$ m s^{-1} (in presence of foam). Let us note that the polarization characteristics of MCW radiation give us an additional information about the sea surface state. It follows from Fig. 1.6 that an account of such information at least at the wavelength of 3 cm for the angle of observation of 55^0 gives 4–5 gradations of wind speed. Data obtained in this way may be used as some of the basic values for the parameter V (similarly to averaged climatic data of the SST).

Figures 1.7 and 1.8 compare the brightness temperature contrasts ΔT^b measured from satellite "Cosmos-243" and their scattering with the wind speed V.

Fig. 1.5 Sensitivity of brightness temperature to wind speed variations as function of wavelength (Grankov and Shutko 1980)
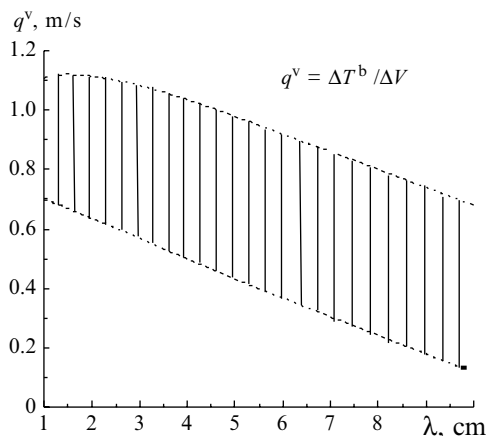
Fig. 1.6 Coefficient of polarization at the wavelengths 3.2–3.6 cm under the angle of observation 55° as function of wind speed (Shutko 1986)
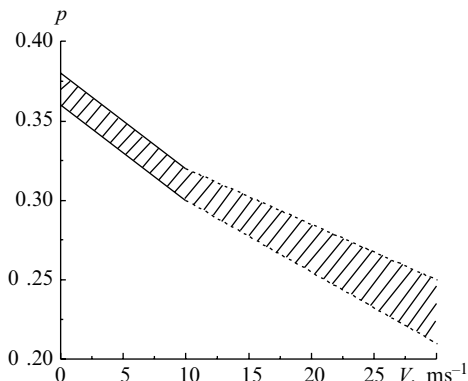
These (or similar) data are very important for solving the problem of determination of the brightness temperature component caused by the SST variations of rough water surface.

1.3.3 Estimates of an Accuracy of the SST Determination

Already in 1960s and '70s a large number of investigations were devoted to a theoretical analysis of the accuracy of estimates of the SST derived from the data of satellite MCW radiometric measurements; one can find some results of these investigations

Fig. 1.7 Brightness temperature contrasts of sea surface at the wavelength 8.5 cm observed in nadir from satellite "Cosmos-243" as function of wind speed (histogram in plan) (Shutko 1986)
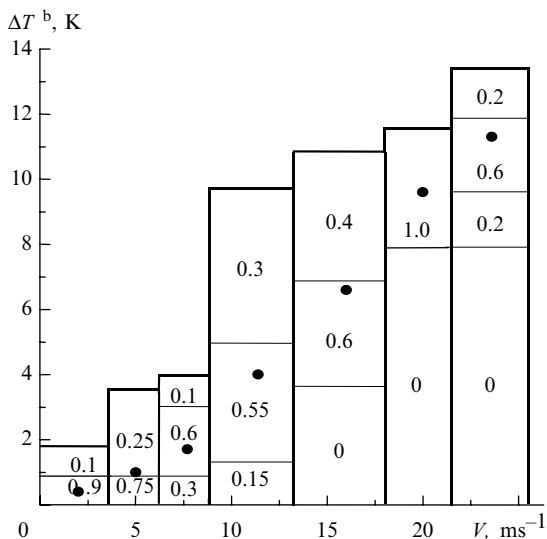
Fig. 1.8 Brightness temperature contrasts of sea surface observed from satellite "Cosmos-243" at the wavelengths 0.8, 1.55, 3.4, and 8.5 cm as function of wind speed (Matveev 1971)
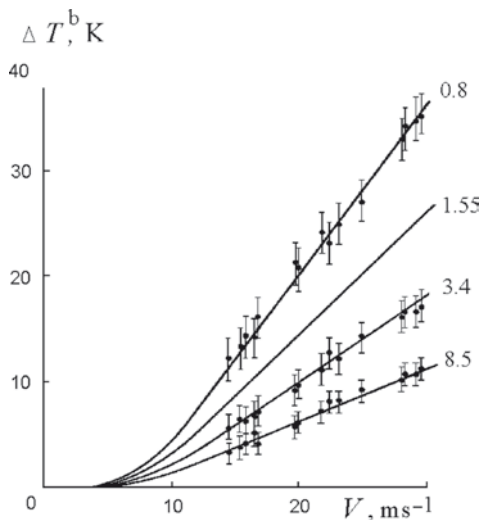
in Basharinov et al. (1974), Wilheit (1978), Kondrat`ev and Timofeev (1979), Nelepo et al. (1985), Shutko (1985), Robinson (1985), and Bychkova et al. (1988).

Table 1.1 shows some estimates of potential accuracy of the SST determination – minimum *rms* error σ_{T}, which is accessible for satellite passive MCW radiometric methods in the centimeter wavelength range. Here, we take into account first of all such interfering factors as the near-surface wind speed V and the integral liquid water content in the clouds W.

Table 1.1 Root-mean-square errors of the sst estimates under various weather conditions, °C

W (kg m⁻²)	V (m s⁻¹)		
	$0 < V < 8$	$8 < V < 15$	$V > 15$
$0 < W < 0.2$	0.6 (0.5)	1 (0.1)	
$0.2 < W < 1$	0.8 (0.1)	1.2°C (0.15)	
$W > 1$			1.2–2 (0.15)

Its frequency is indicated in brackets (Shutko 1986; Grankov and Shutko 1992b)
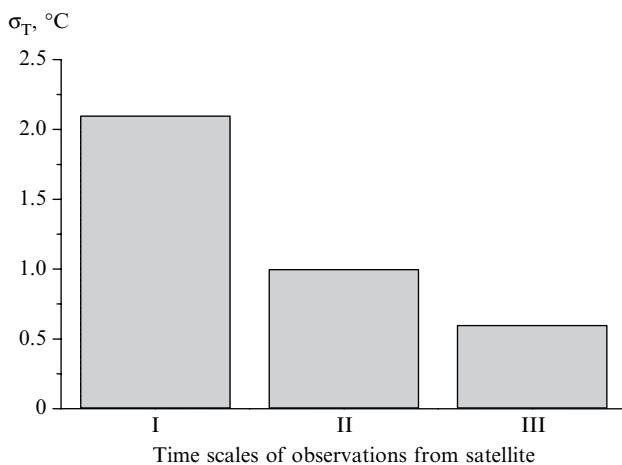
Fig. 1.9 Estimates of the SST errors σ_T for various time scales: mesometeorological (I), synoptic (II), and seasonal (III) (Grankov and Shutko 1992a, b)

The table shows that if the wind speed does not exceed the value 8 m s⁻¹ (when a sea surface is free from the foam) and water content in clouds less than 0.2 kg m⁻² (a week cloudiness), the *rms* error of the SST determination reaches its margin, which is specified by a natural sensitivity of the SOA brightness temperature to the SST variations. Only in this case the satellite means can provide a determination of SST with the accuracy acceptable for the oceanologists.

An accuracy of the SST determination at more complicated weather conditions ($V > 8$ m s⁻¹ and $W > 0.2$ kg m⁻²) may be increased in 1.5–2 times in comparison with the data shown in Table 1.1 due to an appropriate selection and averaging the results of *long-term* satellite MCW radiometric measurements. This conclusion is confirmed by results of calculations (see Fig. 1.9).

These results are in a good agreement with the data of spacious studies fulfilled in one's time in Jet Propulsion Laboratory with the radiometers AVHRR, HIRS/MSU, and SMMR from the satellites NOAA, Seasat, and Nimbus 7 (Hofer et al. 1981; Njoku et al. 1985; Susskind and Reuter 1985; Bernstein and Chelton 1985; Hilland et al. 1985).

Table 1.2 Results of comparison of satellite and vessel monthly SST averages in $2^0 \times 2^0$ bins and the rms values of their differences (Bernstein and Chelton 1985), °C

Satellite sensor	November 1979	December 1981	March 1982	July 1982
AVHRR				
Mean value	0.19	−0.30	−0.36	−0.48
rms	0.61	0.58	0.62	0.92
Number of measurements	723	729	795	644
HIRS				
Mean value	−0.04	0.13	0.30	−0.07
rms	1.01	0.89	0.97	0.69
Number of measurements	735	729	795	662
SMMR				
Mean value	0.52	0.72	−0.21	−0.43
rms	1.37	1.37	1.13	1.06
Number of measurements	395	677	690	522

An effectiveness of using the satellite passive radiometric methods of the SST determination with the radiometer SSMR (*at microwaves*), AVHRR (*at infrareds*), and HIRS/MSU (at *microwaves and infrareds*) in climatologic studies of the ocean is summarized in Table 1.2. In Bernstein and Chelton (1985) are presented some important and edifying results relating to a choice of the time intervals reasonable for comparison of remotely sensed and in situ data obtained in different physical and geographical oceanic zones characterized by a considerable variability and changeability of their meteorological and oceanographic parameters.

1.3.4 Perspective Methods of Resolution of the Problem of the SST Determination

We intend to analyze an effectiveness of some methods of increasing the accuracy of the SST determination; the following ways of their realization can be used here:

1. Searching the new features in the SOA field of natural MCW radiation as the characteristics of the SST in the tradition for satellite passive radiometric measurements *centimeter range* of wavelengths.
2. Using the SOA brightness temperature in the more long-wave (*decimeter*) range of wavelengths.

It was shown in Grankov and Shutko (1980) and Shutko and Grankov (1982) that a position of the spectral maximum of a sensitivity of the brightness temperature of the SOA in the wavelength range 3–8 cm (3.75–10 GHz) to the SST can be used as its quantitative characteristics in the interval of the SST variations from 0 to 30°C.

Based on these idea, we proposed the method of determination of the spectral maximum and the method of estimating the SST from satellites. This method can

be realized with the special radiometer-spectrometer, which can provide a periodical scanning of the SOA brightness temperatures in the wavelength range 3–8 cm during the traveling satellites over the ocean.

In our opinion, this method provides some advantages in comparison with the known methods of passive microwave radiometric determination of the SST, which will provide the following advantages: (a) a possibility of calibrations of satellite data in terms of absolute SST values with the use of several data on the SST and other SOA parameters and (b) the steadiness of the satellite SST estimates to variations of the radiometers parameters (stability, sensitivity) and their variations caused by instability of the temperature regime of radiometers and antennas in open space. Some results of this method were testified by laboratory experiments in the range of the water surface temperature variations from 11 to 23°C using the sweeping radiometer PK7-19 operating in the frequency range 3.9–6.0 GHz (Grankov 2003).

We also studied the potential of passive microwave radiometric methods of determination of the SST from satellites. The results of these studies at the waves 20–40 cm show that an accuracy of determination of the sea surface parameter (i.e., their local spatial variations) is comparable with an accuracy achievable at the centimeters. In addition, we can obtain additional information on the local variations of the ocean surface salinity (Grankov and Shutko 1986; Grankov and Mil'shin, 1988). An essential limitation for exploration of the passive radiometric means designed for operating on the space orbit in the decimeter wavelength range is the antennas' sizes (10–30 m), which can provide useful information on the water surface temperature and salinity spatial variations for the oceanologists.

In the near future, the Russian Cosmic Agency is planning the placing of decimeter radiometers operating in radioastronomical "window" 21 cm on the board of the "Lavochkin" satellites. We believe that these data will improve the estimates of parameters obtained by traditional radiometric means in the centimeter wave range of wavelengths.

Additionally, the following methodological aspect of these studies is seemed as an actual problem of development of satellite MCW radiometric methods: we see here the only way, instead of a *demonstration* to oceanologists some possibilities of the remote sensing of the SST and the other SOA parameters from the aerospace levels, we have to *develop* the common (integrated) models of heat and radiation processes at the ocean–atmosphere boundary. Let us note that the specialists engaged in the physics and mathematics applied a strong force to solve this problem (Kochergin and Timchenko 1987; Armand et al. 1987; Fedorov and Ginsburg 1988). It is very important to understand for everybody the following: in what segments of these models (and in a what form) we have to assimilate the data of satellite measurements; only after that, we can formulate demands to the technical means and to their engineering requirements such as an accuracy and spatial and time resolution. For example, a slight spatial resolution (countable in tenths of kilometers) and a low accuracy of the SST determination are not sufficient in the practice of the operative oceanic studies from satellites. At the same time, one can see that the SOA brightness temperature is be used as the *direct* characteristic of

the monthly-mean SST values and their seasonal variations with an accuracy of 0.5–0.6°C (Fig. 1.9); some interests of the climatologists may be awaken in this respect. The demands to the satellite estimates of the SST may be reduced also, if we will use the remote sensed data not only as the local (spotted) values, but as their spatial and temporal images. Another side of this methodology (and philosophy) is based on combination of the satellite MCW radiometric methods with the methods of mathematical modeling of the processes observed from the space, which let us to raise the information content of satellite methods of studies the "invisible" for these methods processes. In terms of the words of the academician Konstantin Fedorov, these peculiarities let us "to use the remote sensors to look into in the ocean, which surface as the screen illuminates various deep-sea processes" (Fedorov and Ginsburg 1988). In this respect, the very interest results were obtained from the vessel and satellite levels by Raizer and Cherny (1994) and Cherny and Raizer (1998).

1.4 Potential of Satellite Microwave Radiometric Methods for Determining the Meteorological Parameters of the Near-Surface Atmosphere

1.4.1 Climatic and Seasonal Scales

As it was mentioned above, the relation between temperature and humidity characteristics in various atmosphere layers is the starting point for using the data of satellite passive radiometric methods of determining the surface heat fluxes. From this point of view, the analysis of correlations between total water vapor content of the atmosphere Q and its near-surface parameters T_a and e in the ranges of seasonal, synoptic, and mesometeorological time scales is a required stage in studies of heat and water interchanges at the SOA interface from satellites. Some examples of such analysis can be found in the works, which are based on the results of systematization of the long-term oceanological, meteorological, and aerologic measurements (Snopkov 1977; Liu 1986; Hsu and Blanchard 1989; Grankov and Mil'shin 1994, 1995). Besides, the latest researches testify that the results of satellite MCW and IR passive radiometric measurements can essentially supplement the data of direct meteorological and aerologic measurements when analyzing relations between the atmosphere total and near-surface humidity and temperature (Liu 1988; Schulz et al. 1993; Shibata and Konda 1996; Liu et al. 2003).

At least, the two circumstances denote the specific role of the total water vapor of the atmosphere – parameter Q:

1. Parameter Q is closely related to an intensity of the water vapor radiation in the resonant line 1.35 cm, which variations are reliable measured from satellites.
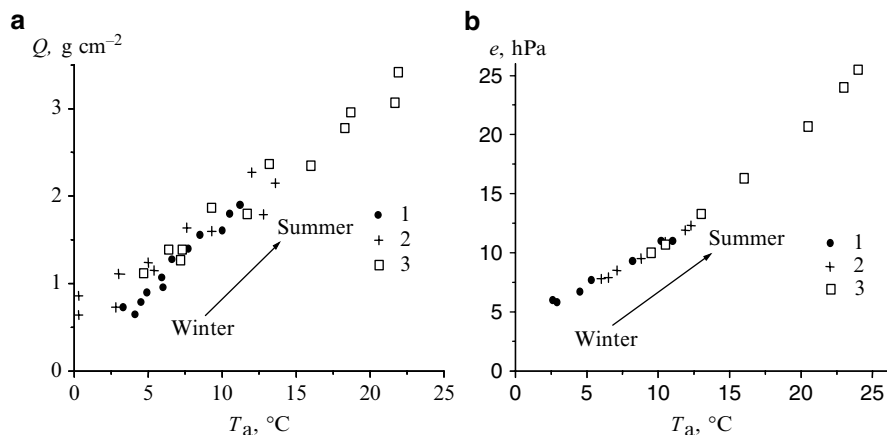
Fig. 1.10 Correlations between monthly mean parameters Q and T_a during the period January–December (**a**) and the parameters e and T_a during the period February–August (**b**) in the Norwegian (1), Newfoundland (2), and Gulf Stream (3) EAZOs

2. A significant fraction of the total quantity of heat in the SOA is concentrated in a water vapor.

The premise for joint analysis of the parameters e, T_a, and Q is the correlations between them, which are conditioned by the processes of vertical diffusion as well as horizontal (advective) heat and water transfer in the near-surface and boundary layers of the atmosphere.

The results of numerous experimental investigations (shipborne, satellite), performed in different regions of the ocean in limited time intervals (hours, days), show that under these conditions, the relations between Q and e and between Q and T_a are not single-valued. The reason is that the parameter Q is not determined only by e and T_a, but rather it is a sum of many factors: wind speed, vertical stratification of the air temperature and humidity, etc. More definite estimates of the relationships between water vapor content of the atmosphere and its near-surface temperature and humidity should be expected when they are significantly averaged in space and time as indicated in Fig. 1.10. We analyzed the results of comparison of monthly mean parameters e, Q, and T_a for their $5° \times 5°$ spatial averaging in some fragments of Norwegian, Newfoundland, and Gulf Stream EAZOs of the North Atlantic based on various climatic archives: the estimates of T_a are taken from Handbook (1977), Q from Tuller (1968), e – from Handbook (1979), Snopkov (1981), Timofeev (1979), and Drozdov and Grigor`eva (1963).

We also studied the problem to what extent the relations between monthly mean of the atmospheric water vapor and near the surface values of the air temperature and humidity could be stable (universal), if we will use the different archival data on the parameters Q, e, and T_a. The result of this study confirms our idea and experience that one can reduce the dispersion of the dependencies $Q(T)$ and $Q(e)$ essentially, if

a

b
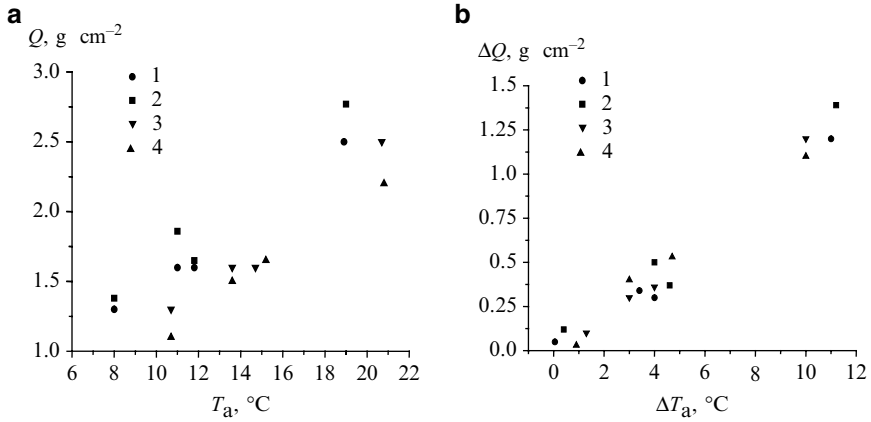
Fig. 1.11 Estimates of relations between month mean *(climatic)* values of the parameters Q and T_a (**a**) and their variations (**b**) during February–May–August–November in the Newfoundland EAZO taken from: 1 – T_a and Q (Handbook 1977); 2 – T_a (Handbook 1977) and Q – (Snopkov 1981); 3 – T_a (Handbook 1977) and Q (Timofeev 1979); 4 – T_a (Handbook 1977) and Q (Drozdov and Grigor`eva 1963)

a

b
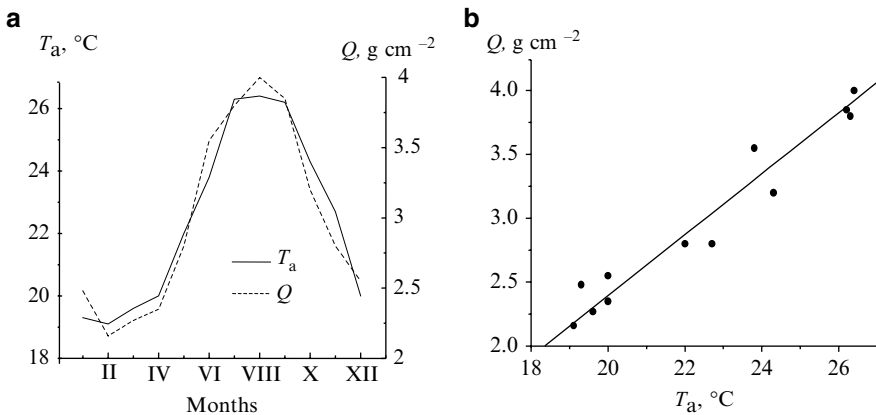
Fig. 1.12 Annual values of month mean water vapor of the atmosphere Q and its near-surface temperature T_a (**a**) in the island Midway) in the Pacific ocean (28.2˚N, 177.4˚W); linear regression between them (**b**): Q – data of interpretation of the radiometer Nimbus 7 SMMR radiometer (Liu 1988) averaged during the period 1980–1983 years, T_a – climatic data (Handbook 1977)

operating not with the *absolute*, but *relative* values (variations) of this parameters (Grankov and Mil'shin 1994, 1995). Taking as the examples the data accumulated in the Newfoundland EAZO for confirmation of this idea, we see that this approach will be as is quite effective (Fig. 1.11).

   Figure 1.11 shows that the strong relationships between seasonal variations of the month mean parameters Q and T_a are obvious under these conditions, in spite of the diversity of initial archival data. The distinctions of using the means and

Table 1.3 Intraannual variability of the slope of regressional relations $\Delta Q/\Delta e$ and $\Delta Q/\Delta T_a$ observed by the island meteorological station St. Paul in the Pacific Ocean

Years	1964	1965	1966	1967	1968	1969	1970	1971	1972	1973	1974
$\Delta Q/\Delta e$	0.16	0.19	0.14	0.18	0.15	0.17	0.16	0.17	0.20	0.15	0.15
$\Delta Q/\Delta T_a$	0.17	0.13	0.13	0.15	0.13	0.18	0.13	0.14	0.18	0.13	0.13

methods of the Earth observation as well as the time and spatial scales of averaging the data obtained are very important for solving the problem of validation of the data of passive MCW radiometric measurements derived from satellites.

One can see that in selected EAZOs the relationships between the monthly mean values Q and T_a in the entire range of their variations are very strong. Change of the 5° oceanic areas by 1–2° ones in the chosen EAZOs has virtually no effect on the results of the comparison. It is remarkable that the slope of the regression dependence Q (T_a) is slightly varied in the middle latitudes of the North Atlantic from the value 0.1 in the Norwegian EAZO to 0.13 g cm^{-1}K^{-1} in the EAZO Gulf Stream. In the equatorial zones of the Pacific Ocean, this characteristic is twice as much of this, at which, a correlation between the values ΔQ and ΔT_a is more than 0.9 (Fig. 1.12).

We analyzed the intra annual variability of the regressions between the month mean values of the atmospheric water vapor and its near-surface temperature and humidity using the data of meteorological and aerologic measurements from the Pacific island station St. Paul (52.7°N, 170.2°W) during the period 1964–1974 years figured in Liu (1988). The results of analyzing these data demonstrate a steadiness of the dependences $\Delta Q/\Delta e$ and $\Delta Q/\Delta T_a$ (see Table 1.3), where the variation coefficients are 9.4 and 13.6% accordingly.

The results presented indicate that averaged microwave radiometric data measured from satellites at the wavelength 1.35 cm can be used as the indirect characteristics of the near-surface atmosphere temperature T_a. Let us note that the averaging scales required in order to reveal the statistically significant microwave radiometric estimates of the parameter T_a (during every 30 days with a spatial resolution of several degrees) correspond to the characteristics adopted in the problems of modeling the global interaction of the ocean and atmosphere (Dymnikov et al. 1984) and can be realized by periodic (with an interval of several days) and long-term (for several years) surveying (monitoring) of the EAZOs with the satellite method of passive microwave radiometry. In addition, the averaging of satellite microwave radiometric data gives us some auxiliary possibilities for improving the accuracy of remote sensed estimates of seasonal variations of the SST up to 0.5–0.6°C as a result of smoothing the noise components of the instrumental (radiometric) errors and selection (rejection) of the measurement fragments with a thick cloudiness in the atmosphere and the storm zones in the ocean (Grankov and Shutko 1992a, b) (see again Fig. 1.9).

In general, results of analysis and systematization of long-term data show that the correlation of monthly mean values Q, e, and T_a is stable in the wide range of their variations ($0.5 < Q < 4.5$ g cm^{-2}, $5 < e < 30$ hPa, $0 < T_a < 30$°C). The results obtained illustrate clearly the seasonal variations of the monthly mean parameters

Q, e, and T_a and, in the same time, demonstrate some individual features of the dependencies $Q(e)$ and $Q(T_a)$, as well as the dependence $e(T_a)$ in different physical and geographical zones of the North Atlantic and the Pacific Ocean.

1.4.2 Synoptic Scales

Results of the experiments NEWFOUEX-88 (November 1987–April 1988) and ATLANTEX-90 (November 1989–June 1990) on observation of the ocean–atmosphere interaction in the Newfoundland EAZO give us the spacious information useful for studies of relationships between synoptic variations of the parameters Q, e, and T_a in the middle latitudes.

     We extracted from these archives the data obtained from the research vessels (R/Vs) *Victor Bugaev*, *Musson*, and *Volna* in the *stationary* phases of these experiments (March 1988 and April 1990), when the vessels were immovable. The initial data in each phase include the following:

(a) More than 2,000 meteorological measurements in the near-surface atmosphere with the 1-h time resolution.
(b) More than 400 aerological measurements in the interval of heights 10–16,000 m (at 20 levels) with the 6-h time resolution.
(c) More than 2,000 measurements of the water vapor content with the 15–20-min resolution obtained from the ship-boarding microwave-radiometers at the 1.35 and 0.8 cm wavelengths (R/V *Volna*) in the experiment ATLANTEX-90).

The results of these measurements show that the relation between synoptic variations of the atmospheric water vapor obtained from microwave radiometric measurements and the variations of the near-surface air determined directly from meteorological measurements is very strong (Fig. 1.13).
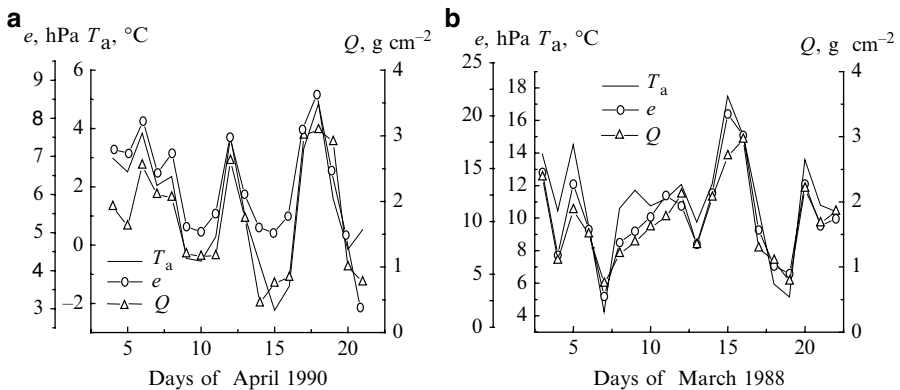
Fig. 1.13 Correlations of daily the parameters e, T_a, and Q observed at the stationary phases of the experiments ATLANTEX-90 (*Volna*) (**a**) and NEWFOUEX-88 (*Musson*) (**b**)

Figure 1.14 illustrates the results of our comparison of the data of synchronous measurements of passive MCW radiometers derived from the satellite level (with down-looking radiometer SSMI of the satellite F 08 of the DMSP series) and the vessel level (up-looking radiometric complex of the Voeikov Geophysical Observatory, operated at wavelengths 0.8 and 1.35 cm) derived at the stationary phase of the experiment ATLANTEX-90.

Table 1.4 shows the data of a regression analysis presented in the form of linear relations (of a kind $y=A+B\,x$) between current daily values of the parameters Q, e, and T_a measured during the periods in turn 4–8 April, 4–10 April, 4–20 April,
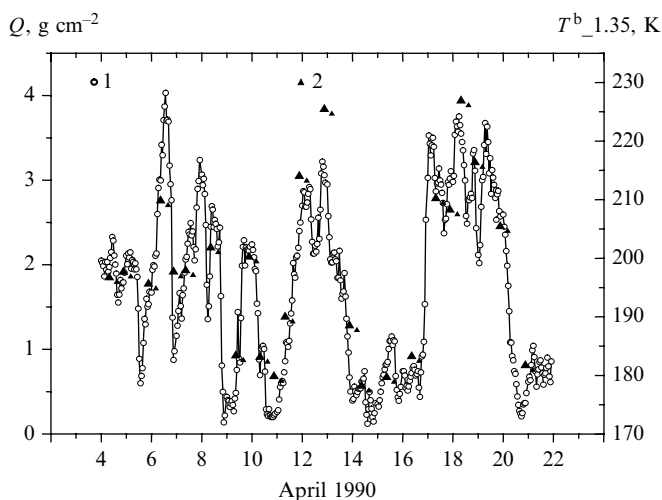
Fig. 1.14 Results of comparison of the total water vapor content in the atmosphere Q retrieved with the looking-up MCW radiometric complex operated at the wavelengths 0.8 and 1.35 cm from R/V *Volna* (1) with the SOA brightness temperature derived from the radiometer SSM/I of the satellite F-08 at the wavelength 1.35 cm (2). The stationary phase of the experiment ATLANTEX-90

Table 1.4 Parameters of regressions between daily parameters T_a, e, and Q at the stationary phase of the experiment ATLANTEX-90 (R/V *Volna*) (Grankov and Novichikhin 1997)

Data	Regression parameters								
April 1990	T_a and e			e and Q			T_a and Q		
Coefficients	A	B	r	A	B	r	A	B	r
4–8	5.33	0.67	0.96	−0.86	0.41	0.59	1.24	0.30	0.62
4–10	5.40	0.64	0.99	−0.93	0.42	0.90	1.31	0.27	0.90
4–12	5.39	0.63	0.99	−1.34	0.48	0.91	1.25	0.31	0.92
4–14	5.42	0.62	0.99	−1.83	0.55	0.89	1.15	0.35	0.91
4–16	5.67	0.51	0.96	−2.08	0.59	0.91	1.23	0.32	0.92
4–18	5.67	0.55	0.97	−2.33	0.63	0.93	1.24	0.35	0.93
4–20	5.62	0.56	0.96	−2.24	0.63	0.89	1.29	0.36	0.88

which characterize the history of evolution of the atmospheric temperature and humidity characteristics at the stationary phase of the experiment ATLANTEX-90 derived from the R/V *Volna*.

Strong correlations between these parameters and their stability at once are observed, in spite of their intense variability caused by cyclones typical of these areas. The results of observational data processing in the initial phase of the experiment (4–7 April) are excluded from consideration because they have a low statistical significance. As evident from the table, the current samples of the mean daily values of the parameters T_a and e and also of T_a and Q have the most stable regressions: the coefficient of variations of the parameter   for these combinations is half as large as the respective coefficients for the combination of e and Q values (the coefficient of variation of the parameter A is an order of magnitude less). The analogical results were obtained with R/Vs *Victor Bugaev* and *Musson* in the March of 1988.

The analysis of relations between the atmosphere water vapor and its near-surface temperature and humidity within the *mesometeorological* time scales (hours, days) is very important in the two aspects as follows (Grankov and Resnjanskii 1998):

1. An understanding and interpretation these processes on the synoptic and seasonal time scales
2. Estimating the possibilities of using the parameter Q, which are easily accessible for satellite microwave radiometric means, as the reliable criteria for estimating not only seasonal, but for more dynamic (short-period) values of the parameters e and T_a

Based on these ideas, we used the data accumulated in the stationary phases of the experiments ATLANTEX-90 and NEWFOUEX-88 for an analysis of relations between the *mesometeorogical* variations of the parameters Q, e, and T_a, which are varied intensively in the ocean (especially, in their active zones). Some results of this analysis are presented in Fig. 1.15 where the results of comparison of the 1-h readings of the parameters e, T_a and 6-h indications of the parameter Q are illustrated.
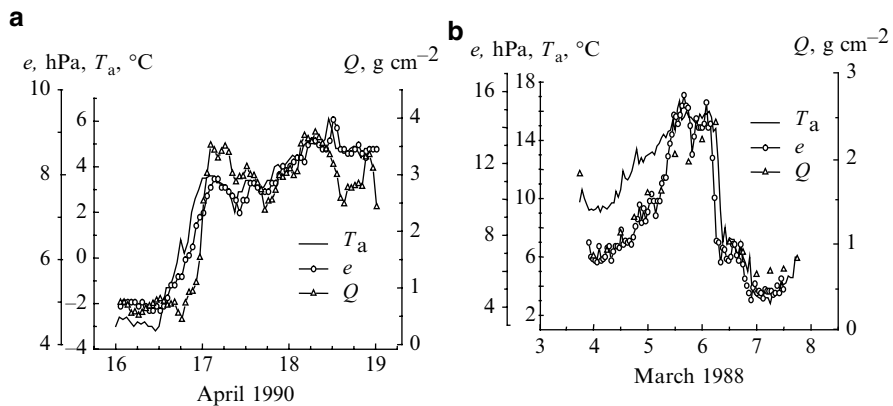
Fig. 1.15 Comparison between daily variations of the parameters e, T_a and Q: (**a**): ATLANTEX-90 (R/V *Volna*, April 16–19, 1990); (**b**) NEWFOUEX 88 (R/V *Musson*, March 3–8, 1988)

Results of the analysis show that the relations between the atmosphere water vapor and its near-surface temperature and moisture are developed on the daily intervals. One can see the following peculiarities: (a) a most close correlation existing between the parameters e and T in the atmosphere near-surface layer is mostly observed. These regularities conform the rules of the ideal gas and (b) under influence of energetic (cyclonic) processes of tuning the atmosphere, the variations of the parameter Q are following often to variations of the parameters e, T_a with a time lag of a few hours (Grankov and Novichikhin 1997).

The atmosphere horizontal circulation plays a key role in forming the vertical distribution of the air temperature and humidity, which immediately influence the SOA brightness temperature measured from satellites. First of all, this rule becomes apparent for middle latitudes of the North Atlantic, especially in the periods of the cyclonic activity of the atmosphere. This reason is confirmed by the data presented in Fig. 1.16, which shows the data of the aerologic testing of the atmosphere from the R/V *Victor Bugaev* during the experiment ATLANTEX-90.

Figure 1.16 illustrates variations of the temperature and humidity of the atmosphere boundary layer for its different layers during April 8–13, 1990 with 6-h resolution; Table 1.5 demonstrates some results of their correlation analysis.
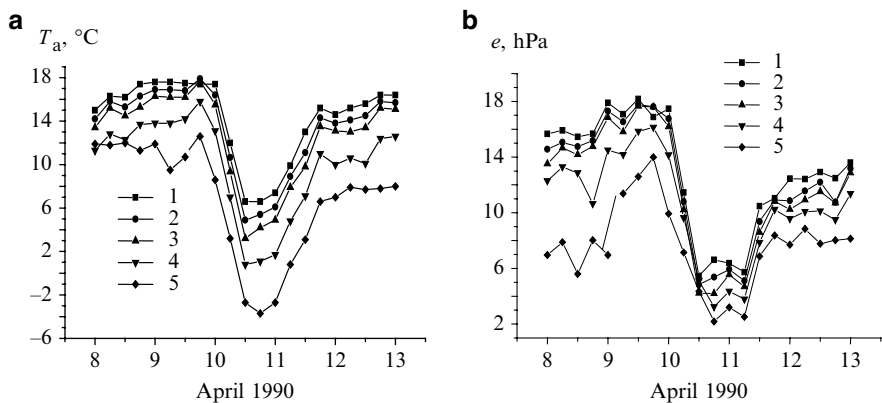
Fig. 1.16 Variations of the temperature T_a and humidity e in the atmosphere boundary layer during a passage of powerful cyclone in the point of location of the R/V *Victor Bugaev* at the horizons: 1–10 m, 2–100 m, 3–200 m, 4–500 m, 5–1,000 m

Table 1.5 Correlation of the air temperature T_a and humidity e in various horizons of the atmosphere boundary layer

h (m)	10	100	200	500	1,000
10	1	0.993	0.988	0.968	0.788
100	0.995	1	0.998	0.979	0.812
200	0.990	0.999	1	0.982	0.827
500	0.988	0.996	0.996	1	0.857
1,000	0.948	0.954	0.953	0.962	1
Near-surface air temperature			Near-surface air humidity		
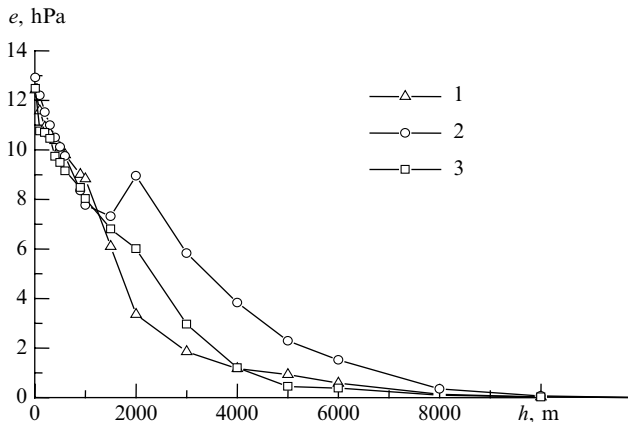
Fig. 1.17 Results of upper-air sounding the atmospheric water vapor pressure e at various horizons h from the R/V *V.Bugaev* in the experiment in April 12, 1990: 1–6 h; 2–12 h; 3–18 h

Once, such cooperativeness in variations of the air temperature and humidity at various horizons can be disturbed due to an appearance of inversions in vertical distribution of these parameters in the atmosphere (see Fig. 1.17).

As seen from the illustration, a life time of the inversion in this case in no way exceed 12 h; more certain estimates of its are difficult because the periodicity of the aerologic soundings from vessels is 6 h. Let us note that this phenomena was observed at the stationary phases of the experiments ATLANTEX-90 and NEWFOUEX-88, but not frequently – some tens advents in hundreds aerologic soundings.

1.5 Conclusion

The satellite-derived data of passive microwave radiometric measurements have an essential potential to evaluate the parameters of the system ocean–atmosphere (SOA) determining the processes of heat interchange in its interface with useful information for oceanologists and climatologists accuracy. In particular, the brightness temperature of the SOA is directly connected with the water surface temperature and near-surface wind speed, which are the key parameters in the formulas used for computation of heat and water vertical turbulent fluxes at the SOA boundary (bulk-formulas). Such parameters as the near-surface air temperature and humidity only indirectly influence natural microwave radiation of the SOA, but in spacious areas of the North Atlantic (in the middle and high latitudes), the total water vapor of the atmosphere is an effective indicator of variations of these parameters in a wide range of time scales.

References

Andreev GA, Zrazhevskii AYu, Kutuza BG et al (1985) Propagation of millimeter and submillimeter waves in the troposphere. In: Kotelnikov VA (ed) Problems of modern radio engineering and electronics. General Editorial Board for Foreign Publications, Moscow, pp 151–178

Ariel NZ et al (1973) On calculation of month mean values of heat and moisture heats over the ocean. Meteorol Gidrol 5:3–11 (in Russian)

Armand NA, Krapivin VF, Mkrtchyan FA (1987) Methods of processing the data of radiophysical studies of the environmental. Nauka, Moscow In Russian

Armand NA, Polyakov VM (2005) Radio propagation and remote sensing of the environment. CRC Press LLC, Boca Raton

Basharinov AE, Gurvich AS, Egorov ST (1974) Radio emission of the planet Earth. Nauka, Moscow In Russian

Bernstein RL, Chelton DB (1985) Large-scale sea surface temperature variability from satellite and shipboard measurements. J Geophys Res C6:11619–11630

Bogorodskii VV, Kozlov AI, Tuchkov LT (1977) Radiothermal emission of the Earth's covers. Gidrometeoizdat, Leningrad In Russian

Bychkova IA, Victorov SV, Vinogradov VV (1988) Remote sensing of sea temperature. Gidrometeoizdat, Leningrad In Russian

Chavro AI (1990) Physical base and the methods of the sea surface determination from satellites. OVM AN USSR, Moscow In Russian

Cherny IV, Raizer V Yu (1998) Passive microwave remote sensing of oceans. Wiley, UK

Drozdov OA, Grigor`eva AS (1963) Water vapor exchanges in the atmosphere. Gidrometeoizdat, Leningrad In Russian

Dymnikov VP, Korotaev GK, Galin VYa (1984) Atmosphere, ocean, space – "Razrezy" program. VINITI, Moscow In Russian

Esbensen SK, Reynolds RW (1981) Estimating monthly averaged air-sea transfers of heat and momentum using the bulk aerodynamic method. J Phys Oceanogr 11:457–465

Eyre JR, Lorence AC (1989) Direct use of satellite sounding radiances in numerical weather prediction. Meteorolog Magaz 118:13–16

Fedorov KN, Ginsburg AI (1988) The subsurface layer of the ocean. Gidrometeoizdat, Leningrad In Russian

Frenks LE (1969) Signal theory. Prentice Hall, NY

Gaikovich KP et al (1987) Determination of the temperature profile in the water surface layer with microwave radiometric measurements. Fiz Atmos Okeana 23:761–768 In Russian

Grankov AG (1992) Microwave-radiometric diagnostics of integral fluxes of sensible heat at the ocean-atmosphere boundary. Izvestija, Atmosph Oceanic Phys 28:883–889

Grankov AG (2003) Thermal analysis of atmosphere-ocean interaction by means of satellite microwave radiometry in the 0.5 and 1.35 cm resonance bands. Tech Phys 48:906–913

Grankov AG, Mil'shin AA (1988) Effect of the Earth's ionosphere brightness temperature on the underlying surface in the decimeter range of wavelengths for satellite measurements Radiotekhnika i electronika (Radioengineering and Electronics) 33:1345–1351 (in Russian)

Grankov AG, Mil'shin AA (1994) On correlation of the near-surface and total atmosphere humidity with the near-surface air temperature. Meteorol Gidrol 10:79–81 In Russian

Grankov AG, Mil'shin AA (1995) A study of intercorrelation between thermodynamical parameters of the atmosphere for validating satellite MCW and IR-radiometric methods of determining its near-surface temperature. Institute of Radioengineering and Electronics RAS (Preprint No. 3(603), Fryazino

Grankov AG, Mil'shin AA (1999) Interrelation between the Microwave Radiation of the Ocean-Atmosphere System and the Boundary Heat and Momentum Fluxes. Izvestiya, Atmosph Oceanic Phys 35:570–577 In Russian

Grankov AG, Mil'shin AA (2001) Evaluation of usefulness of the SSM/I data for study of climatic parameters of the ocean and atmosphere in the North Atlantic. Issled Zemli iz kosmosa 5:70–78 In Russian

Grankov AG, Mil'shin AA (2004) Intercorrelation between natural microwave radiation of the ocean-atmosphere system and its boundary heat and dynamic interaction. Nauka, Moscow In Russian

Grankov AG, Novichikhin YeP (1997) Formulas oh heat and moisture exchange between ocean and atmosphere used in radiometric satellite data assimilation. Russian Meteorology and Hydrology, Allerton Press 1:81–90

Grankov AG, Resnjanskii JuD (1998) Modeling the response of the ocean-atmosphere natural radiation system to the pertrubation of a thermal equilibrium at the interface. Russian Meteorology and Hydrology, Allerton Press 11:57–65

Grankov AG, Shutko AM (1980) Assessment of the effectiveness of estimates of parameters of the sea surface and the atmosphere. Radiotekhnika 35:38–41 In Russian

Grankov AG, Shutko AM (1986) Use of decimeter wavelength range to study water surface by means of microwave radiometry. Issledovanija Zemli iz kosmosa 5:78–89 In Russian

Grankov AG, Shutko AM (1992a) Use of remote radiophysical methods to determine the role of energy-active zones of the ocean in the development of the weather on the continents. Sov J Remote Sens 9:926–941

Grankov AG, Shutko AM (1992b) Accuracy of estimates of the surface temperature and its variations using spectral techniques of satellite microwave radiometry. Sov J Remote Sens 10:169–198

Grankov AG, Usov PP (1994) Intercommunication between monthly mean air-sea temperature differences and natural microwave and infrared radiation. Meteorol Gidrol 6:79–89 In Russian

Grankov AG, Mil'shin AA, Petrenko BZ (1999a) Natural radiothermal radiation as a characteristic of seasonal and synoptic variation at the ocean-atmosphere heat interfaces. Dokl Earth Sci 367A:839–842

Grankov AG, Gulev SK, Mil'shin AA, Shelobanova NK (1999b) Experimental studies of the ocean-atmosphere brightness temperature as a function of near-surface heat and impulse exchanges in the range of synoptic time scales. Issled Zemli iz kosmosa 6:3–7 In Russian

Grankov AG, Mil`shin AA, Novichikhin EP (2000) Interconnection between the brightness temperature and the intensity of the thermal ocean-atmosphere interaction (Based on the data Atlantex-90 experiment). Earth Obs Rem Sens 16:457–467

Grankov AA, Mil'shin AA, Shelobanova NK (2002) Specific features of the subpolar hydrological front from microwave radiometric satellite data. Russian Meteorology and Hydrology, Allerton Press 8:34–40

Grassl H, Jost V, Schulz J et al (2000) The Hamburg ocean-atmosphere parameters and fluxes from satellite data (HOAPS): a climatological atlas of satellite-derived air-sea interaction parameters over the world oceans. Report No. 312. MPI, Hamburg

Grishin GA, Lebedev NE (1990) Use of IR data from satellites for monitoring the ocean and atmosphere: state of the problem. Issled Zemli iz kosmosa 6:97–104 In Russian

Gulev SK (1991) Effects of spatial and temporal averaging in estimating of energy exchange parameters between ocean and atmosphere. Fiz Atmos Okeana 27:204–213 In Russian

Handbook (1977) Atlas of the oceans: Atlantic and Indian oceans. MO SSSR, Moscow (in Russian)

Handbook (1979) Averaged month, 10 and 5-day periods values of the air water and temperature, their difference and wind speed in selected regions of the North Atlantic (1953–1974 years). VNII GMI, Obninsk In Russian

Hasted JB (1974) Aqueous dielectrics. Chapman and Hall, London

Hilland JE, Chelton DB, Njoku EG (1985) Production of global sea surface temperature fields for the Jet Propulsion Laboratory workshop comparisons. J Geophys Res 90:11642–11650

Hofer R, Njoku EG, Waters JW (1981) Microwave radiometric measurements of sea surface temperature from the SEASAT satellite: first results. Science 212:1385–1387

Hsu SA, Blanchard BW (1989) The relationship between total precipitable water and surface-level humidity over the sea surface: a further evaluation. J Geophys Res 94:14539–14545

Il'yin Yu A, Kuznetzov AA, Malinnikov VA (1986) On the method of remote sensing of heat fluxes at the boundary of the system ocean-atmosphere. Izv VUZov 6:117–120 In Russian

Ivanov A (1978) Introduction to oceanography. Mir, Moscow In Russian

Kharkevich AA (1962) Spectrums and analysis. GIFML, Moscow In Russian

Khundzhua GG, Andreev EG (1973) On determination of heat and water vapor fluxes in the ocean-atmosphere system from measurements of the temperature profile in a thin water layer. Dokl Akad Nauk SSSR 208:841–843 In Russian

Kochergin VP, Timchenko IE (1987) Monitoring the hydrophysical fields of the ocean. Gidrometeoizda, Leningrad In Russian

Kondrat`ev KJa, Melent`ev VV, Nazarkin VA (1992) Remote sensing of waterareas (microwave methods). Gidrometeoizdat, St. Petersburg In Russian

Kondrat`ev K Ya, Timofeev Yu M (1978) Meteorological probing of atmosphere from space. Gidrometeoizdat, Leningrad In Russian

Kondrat`ev K Ya, Timofeev Yu M (1979) Meteorological sensing of underlying surface from space. Gidrometeoizdat, Leningrad In Russian

Lappo SS, Gulev SK, Rozhdestvenskii AE (1990) Large-scale heat interaction in the ocean–atmosphere system and energy-active zones in the world ocean. Gidrometeoizdat, Leningrad In Russian

Lapshin VB, Ragulin IG (1989) The rate of air-sea gas exchange from microwave radiometric measurements. Meteorol Gidrol 3:113–115 In Russian

Larin DA (1984) On calculations of heat and moisture fluxes with averaged values of meteoparameters. Tr. VNIIGMI MCD, Obninsk 110:87–93 (in Russian)

Liu WT (1986) Statistical relations between monthly mean precipitable water and surface-level humidity over global oceans. Mon Wea Rev 114:1591–1602

Liu WT (1988) Moisture and latent flux variabilities in the tropical Pacific derived from satellite data. J Geophys Res 93:6749–6760

Liu WT (1995) Satellite remote sensing of ocean surface forcing and response, COSPAR Colloq., Taipei, 15B2-1-15B2-3

Liu C-C, Liu G-R, Chen W-J, Yuang H-Y (2003) Modified Bowen ratio method in near-sea-surface air temperature estimation by using satellite data. IEEE Trans Geosci Remote Sens 41:1025–1033

Matveev DT (1971) On the microwave spectrum emission of the rough sea surface. Fiz Atm Okeana 7:1070–1076 In Russian

Meissner T, Wentz FJ (2004) The complex dielectric constant of pure and sea water from microwave satellite observations. IEEE Trans Geosci Remote Sens 42:1836–1849

Mitnik LM (1979) Possibilities of remote sensing the temperature of a thin oceanic layer. Fiz Atmos Okeana 15:344–347 In Russian

Nelepo BA, Korotaev GK, Suetin VS, Terekhin Ju V (1985) Research of the ocean from space. Naukova Dumka, Kiev In Russian

Nikolaev JuV (1981) The role of the large-scale interaction of the ocean and the atmosphere in the development of weather anomalies. Gidrometeizdat, Leningrad In Russian

Nikolaev AG, Pertshev SV (1964) Passive radiolocation. Sovetskoe Radio, Moscow In Russian

Njoku EG, Barnett TP, Laurs RM, Vastano AC (1985) Advances in satellite sea surface temperature measurement and oceanographic applications. J Geophys Res 90:11573–11586

Panin GN (1987) Evaporation and heat exchange over the Caspian sea. Nauka, Moscow In Russian

Pereslegin SV (1967) On relations between thermal and radiobrightness contrasts of the sea surface. Fiz Atmos Okeana 3:47–51 In Russian

Rabinovich JA, Melentjev VV (1970) Influence of temperature and salinity on the emission of plane water surface at centimeter wave band. Trudy Glavnoi Geofizicheskoi Observatorii, 235:78–123, Leningrad (in Russian)

Raizer V Ju, Cherny IV (1994) Diagnostics of the ocean surface layer at microwaves. Gidrometeoizdat, St. Petersburg In Russian

Raizer V Ju, Sharkov EA, Etkin VS (1975) Influence of temperature and salinity on the flat sea surface in the decimeter and meter wavelength ranges. Fiz Atm Okeana 11:652–656 In Russian

Reutov EA (1989) On intercorrelation of microwave and IR radiation of natural objects with their state. Issled Zemli iz kosmosa 1:70–76 In Russian

Reutov EA, Shutko AM (1987) On correlation of radiobrightness temperature with the radiative index of dryness. Issled Zemli iz kosmosa 6:42–48 In Russian

Robinson IS (1985) Satellite oceanography. An introduction for oceanographers and remote sensing scientists. Ellis Horwood Series Marine Science, Chichester e.a

Sasaki Y et al (1987) The dependence of sea-surface microwave emission on wind speed, frequency, incidence angle, and polarization over the frequency range from 1 to 40 GHz. IEEE Trans Geosci Remote Sens GE-25:138–146

Schulz J, Schluessel P, Grassl H (1993) Water vapour in the atmospheric boundary layer over oceans from SSM/I measurements. Int J Remote Sens 14:2773–2789

Schulz J, Mejwerk J, Ewald S, Schlussel P (1997) Evaluation of satellite-derived latent heat fluxes. J Climate 10:2782–2795

Sharkov EA (1978) On use of thermal microwave system for investigation heat interchanges in a transient layer at the ocean-atmosphere boundary. Radiotekh Elektron 23:656–658 In Russian

Sharkov Je A (1998) Remote sensing of tropical regions. Wiley, NY

Shibata A, Konda MN (1996) A new method to determine near-sea surface air temperature by using satellite data. J Geophys Res 101:14349–14360

Shuleikin VV (1968) Physics of the sea. Nauka, Moscow In Russian

Shutko AM (1985) The status of the passive microwave sensing of the waters – lakes, seas, and oceans – under the variation of their state, temperature, and mineralization (salinity): models, experiments, examples of application. IEEE J Ocean Eng OE-10:418–435

Shutko AM (1986) Microwave radiometry of water surface and soils. Science, Moscow In Russian

Shutko AM, Grankov AG (1982) Some peculiarities of formulation and solution of inverse problems in microwave radiometry of the ocean surface and atmosphere. IEEE J Oceanic Eng OE-7:40–43

Sirounian V (1969) Effect of temperature, salinity, and thin ice on the microwave emission of water. J Geophys Res 73:4481–4496

Snopkov VG (1977) On correlation between the atmosphere water vapor and the near surface humidity seasonal variations of the water vapor content over the Atlantic. Meteorol Gidrol 12:38–42 In Russian

Snopkov VG (1981) On seasonal variations of the water vapor content over the Atlantic. In: Atmosphere circulation and its interaction with the ocean in the tropical and subtropical latitudes of the Atlantic Nauka, Moscow (in Russian)

Susskind J, Reuter D (1985) Retrieval of sea surface temperatures from HIRS/MSU. J Geophys Res 90:11602–11608

Taylor PK (1984) The determination of surface fluxes of heat and water by satellite radiometry and in situ measurements. In: Gautier C, Fleux M (eds) Large-scale oceanographic experiments and satellites. Reidel, Dordrecht, pp 223–246

Timofeev NA (1979) On vertical distribution of the air humidity and the atmosphere water content over the oceans. Meteorol Gidrol 8:55–62 In Russian

Tsang L, Kong JA, Shin RT (1985) Theory of microwave remote sensing. Wiley, NY

Tuller ST (1968) World distribution of mean monthly and annual precipitable water. Mon Wea Rev 96:785–797

Twomey S (1977) Introduction to the mathematics of inversion in remote sensing and indirect measurements. Elsevier, Amsterdam

Ulaby FT, Moor RK, Fung AK (1981, 1982, 1986) Microwave remote sensing. Addison-Wesley, NY

Wentz FJ (1983) A model function for ocean microwave brightness temperatures. J Geophys Res 88:1892–1908

Wilheit TT (1978) A review of applications of microwave radiometry to oceanography. Boundary-Layer Meteorol 13:277–293

Chapter 2
Modeling of the SOA MCW and IR Characteristics and Their Relations With the Air–Sea Heat Interaction

2.1 Sensitivity of Microwave and Infrared Radiation of the System Ocean–Atmosphere to Mesometeorological Variations of Heat Interchanges Between the Oceanic and Atmospheric Boundary Layers

2.1.1 Model of Heat Interchanges Between the Oceanic and Atmospheric Boundary Layers

To study the thermal response of the atmospheric and oceanic boundary layers (hereafter, ABL and OBL, respectively) to a heat perturbation at their interface:

$$dT_1 / dt = (q_{ha} - q_{hs}) / (\rho_a c_a h_1),$$
$$dT_2 / dt = (q_{hs} - q_{hw} - Le_s + R) / (\rho_w c_w h_2),$$
$$dq / dt = (e_a - e_0) / (\rho_a h_1),$$
$$(2.1)$$

$$T_1 = T_{10}, T_2 = T_{20}, q = q_o \ (t = 0) \qquad (2.2)$$

Here, the values T_1 and T_2 are denoted as the temperatures of the atmospheric and oceanic boundary layers, respectively; q is the specific humidity in the ABL; h_1 and h_2 are the thickness of the ABL and OBL, respectively; ρ_a and ρ_s are the air water densities; C_a and c_w are the air and water specific capacities, respectively; q_{ha} and q_{hw} are the latent heat fluxes at the sea-air interface; e_s is the moisture flux (rate of evaporation/condensation) at the water surface; L is the specific heat of evaporation; and R is the sun shortwave radiation flux heated the water surface.

The temperature-moisture regime of the SOA is parameterized under the following assumptions:

– The simulated system is laterally homogeneous
– The boundary layers of the atmosphere and ocean are well mixed, so that T_1, T_2, and q values are independent of the height (depth) within the ABL and OBL

– The boundary-layer thicknesses h_1 and h_2 remain unchanged with time
– The ABL heat budget is controlled only by sensible heat fluxes q_{ha} and q_{hs}
– The OBL heat budget is controlled only by sensible heat q_{hw} and q_{hs} and also by the latent heat Le_s, resulting from a water surface evaporation (condensation), and by the solar radiation flux R, which is entirely absorbed within the OBL
– The ABL moisture budget is determined by the surface evaporation e_s and the moisture exchange e_a with the overlying air layer; phase conversions of water do not occur in the ABL
– ABL and OBL temperature regime is independent of the electromagnetic radiation intensity in the ocean–atmosphere system

The problem is formulated analogously to Grankov and Resnjanskii (1998), with the only difference that in the evolution of the ABL moisture regime, the respective component of the OBL heat budget is taken into account inconvenience.

To close the problem, it is necessary to express the fluxes q_h, q_{hs}, q_{ha}, q_{hw}, e_s, and e_a in terms of the sought variables and q as well as the external conditions. The radiation flux R is assumed to be specified. It serves as a thermal perturbation. The simulation of the response to this perturbation is the essence of the given problem. To determine the fluxes, the following expressions are used:

$$
\begin{aligned}
q_{hs} &= c_1\, \rho_a\, c_a\, V_a\, (T_1 - T_2), \\
e_0 &= c_2\, \rho_a\, V_a\, (q - q_s), \\
q_{ha} &= c_3\, \rho_a\, c_a\, V_a\, (T_a - T_1), \\
e_a &= c_4\, \rho_a\, V_a\, (q_a - q), \\
q_{hw} &= c_5\, \rho_w\, c_w\, u_w\, (T_2 - T_w),
\end{aligned} \tag{2.3}
$$

where the first two are conventional bulk formulas, and the last three are based on the assumption that the fluxes q_{ha}, q_{he}, and q_{hw} at the outer boundaries of the ABL and OBL, to first approximation, can be expressed similarly through the values of the q_{hs} and q_{hs} and q_{es} with a proper choice of the transfer coefficients c_3, c_4, and c_5.

In formulas (2.3), T_a is the air temperature just above the ABL; T_w is the water beneath the OBL; q_w is the saturation specific humidity at the water temperature T_2; V_a is the mean near-surface wind speed; u_w is the mean oceanic current; c_1, c_2, …, c_5 are some nondimensional transfer coefficients.

Using one more assumption of the linearized dependence of a saturation humidity q_w vs. the temperature T_2,

$$
q_w = q_r + a\, (T_2 - T_r) \tag{2.4}
$$

where, q_r and T_r are the reference humidity and temperature; the set of equations (2.1) taking into account (2.3) and (2.4) can be rewritten in a vector form as follows:

$$
d\mathbf{y}\,/\,dt = A\mathbf{y} + \mathbf{f}, \tag{2.5}
$$

where $\mathbf{y} = (T_1, T_2, q)$ is the vector of the sought variables; $\mathbf{f} = (f_1, f_2, f_3)$ is the vector of three terms:

Table 2.1 Matrix of the coefficients *aij* characterized the equation of the system (2.7)

$a_{11} - r$	a_{12}	a_{13}
a_{21}	$a_{22} - r$	a_{23}
a_{31}	a_{32}	$a_{33} - r$

$$f_1 = (c_3\ u_a\ /h_1)\ T_a,$$
$$f_2 = [R + c_5\ \rho_w\ c_w\ u_w\ T_w - c_2\ \rho_a\ u_a\ L\ (q_r - a\ T_r)\ )]; \qquad (2.6)$$
$$f_3 = (u_a\ /h_1)\ [c_4\ q + c_2\ (q_r - aT_r)];$$

$A = |a_{ik}|$, $i, k = 1, 2, 3$, is the matrix of coefficients. Unlike f, the expressions for a_{ik} comprise only the model parameters h_1, h_2, a, c_1, c_2, …, but not R, T_a, T_w, and q_a, which characterize the external conditions of forcing with respect to the ABL (OBL).

The solution of (2.5) is written as follows:

$$T_1 = C_1\ e^{r_1 t} + C_2\ e^{r_2 t} + C_3\ e^{r_3 t} + T_1^*,$$
$$T_2 = C_1\ p_1\ e^{r_1 t} + C_2\ p_2\ e^{r_2 t} + C_3\ p_3\ e^{r_3 t} + T_2^*, \qquad (2.7)$$
$$q = C_1\ s_1\ e^{r_1 t} + C_2\ s_2\ e^{r_2 t} + s_3\ C_3\ e^{r_3 t} + q^*,$$

Here, r_i ($i = 1, 2, 3$) are the roots of a characteristic equation of the homogeneous system (2.5) as shown in the Table 2.1.

The values T_1^*, T_2^*, and q are the partial solutions of the inhomogeneous system (2.7), sought by the method of variation of constants and expressed in terms of a_{ik}, f_i, and r_i; p_i, s_i and C_i are some combinations of coefficients and initial values T_{10}, T_{20}, and q_0 from condition (2.2).

Numerical estimates show that for typical values of the model parameters, the determinant of the characteristics of (2.8) is negative, and all its roots r_j, ($j = 1, 2, 3$) are real, different, and negative. Hence, the solution (2.7) describes the adaptation of the ABL-OBL system to the external conditions (factors) R, T_a, T_w, q_a, which tend with time to a stable state (T_1^*, T_2^*, q^*). The characteristic adaptation time [min ($|r_i|$)]$^{-1}$ is about 18 h for typical values of the parameters: $\rho_a = 1.25$ kg m^{-3}; $\rho_w = 10^3$ kg m^{-3}; $c_a = 10^3$ J kg deg^{-1}; $c_w = 4{,}100$ Jkg deg^{-1}; $h_1 = 1{,}500$ m; $h_2 = 30$ m; $L = 2.4 \times 10^6$ J kg^{-1}; $R = 200$ W m^{-2}; $V_a = 10$ m s^{-1}; $u_w = 0.1$ m s^{-1}; $c_i = 1.3 \times 10^{-3}$ ($i = 1, 2, …, 5$); $T_r = 10°C$; $q_r = 7.5 \times 10^{-2}$ kg kg^{-1}; and $a = 5 \times 10^{-4}$ deg^{-1}.

2.1.2 Interrelations of MCW and IR Radiation Fluxes with Heat Fluxes in the System Ocean–Atmosphere

In the framework of a plane-layered model of thermal radiation (absorption) in the ocean–atmosphere system (Fig. 2.1), it is possible to analyze the processes of the

SatellIte level (A)
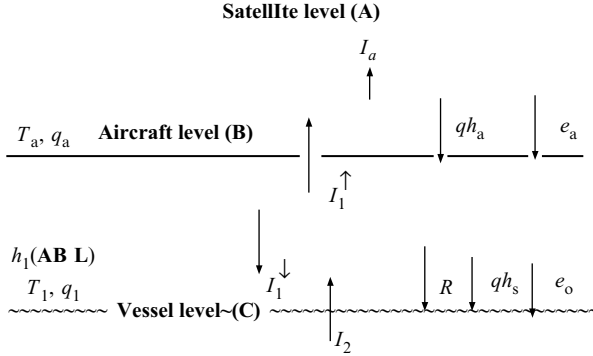
Fig. 2.1 Parameterization scheme of the main characteristics of thermal and electromagnetic energy transfer in the ocean–atmosphere system

electromagnetic energy transfer in various layers, as well as to estimate an intensity of these radiation components, which can be registered with satellite (A), airplane (B), and shipboard (C) equipment.

A: In satellite observations, the ocean–atmosphere natural microwave radiation I_{sat} is composed of the intensity of the free-atmosphere radiation I_a and an intensity of the up-going radiation flux $I_1^{\uparrow}$ at the top of the ABL attenuated in the free atmosphere (multiplier G_a):

$$I_{sat} = I_a + I_1^{\uparrow} G_a, \tag{2.8}$$

where $I_1^{\uparrow} = I_1 + (I_1^{\downarrow} R_{21} + I_2) G_1$ is an intensity of the up-going radiation flux at the top of the ABL; $I_1 = I_1 + I_a$; G_1 is an intensity of the down-going radiation flux at the bottom of the ABL; $I_1(G_1)$ is an intensity of the integral (total) attenuation in the ABL; I_2 is an intensity of the ABL natural radiation; G_1 is the integral attenuation of radiation in the ABL; and R_{21} is the coefficient of reflection of the down-going radiation flux $I_1^{\downarrow}$ from the water surface.

It is assumed that the electrophysical parameters of the ABL and the free atmosphere, in spite of the difference (in a general case) between their temperature and humidity characteristics, are consistent with each other, that is, the reflectivity at their interface is absent or negligibly small compared with R_{21}.

B: In observations from an aircraft (at the top of the ABL), the ocean–atmosphere radiation intensity I_{air} is determined solely by the component $I_1^{\uparrow}$:

$$I_{air} = I_1^{\uparrow} \tag{2.9}$$

C: In shipboard observations (at the lower boundary of the ABL), an intensity of radiation I_{ship} is computed as follows:

$$I_{ship} = I_2 + I_1^{\uparrow} R_{21} \tag{2.10}$$

The characteristics of natural radiation of the boundary (I_1) and free (I_a) atmosphere in expressions (2.8)–(2.10) are related to the corresponding values of temperature T_1, T_a and of the integral absorption G_1, G_a of this media:

$$I_1 = T_1 (1 - G_1); \ I_a = T_a (1 - G_a). \qquad (2.11)$$

An intensity of the thermal radiation of the water surface I_2 is proportional to

$$I_2 = æ \ T_2 \ in \ the \ MCW \ wavelength \ range;$$
$$I_2 = \delta \ B(T_2) \ in \ the \ IR-band,$$

where T_2 is the OBL temperature; $B(T_2)$ is the Planck's function with T_2 as an argument; æ is the emissivity of the water surface at microwaves; and δ is the IR-emissivity of the ocean surface.

In the MCW range of wavelengths, where the Rayleigh-Jeens approximation is valid, respective values of the brightness temperature T^b are used as a measure of the radiation intensity of different components of the ocean–atmosphere system. To characterize the IR radiation intensity I here and below, we will use the concept of the effective (radiation) temperature T^r, defining it from the equation $B(T^r)$, that is, as a thermodynamic temperature of the absolute (ideal) black body with a radiation intensity is equal to I.

2.1.3 Results of Numerical Analysis of the Dynamics of Thermal and Electromagnetic Fluxes and Their Correlations in the Ocean–Atmosphere System

The numerical estimates were obtained for the temporal evolutions of fluxes q_h and q_e at the ABL-OBL interface boundary and the radiation fluxes I_{sat}, I_{air}, and I_{ship} in terms of the corresponding values of the brightness temperature at the wavelength range (5 mm–3 cm) and infrared radiation temperatures (8–12 mcm) after the ocean–atmosphere system was forced out of the state of a thermal equilibrium. They were obtained for typical values of thermal constants (air humidity and density, heat capacity, specific heat of evaporation (condensation), heat and humidity interchange coefficients), ABL and OBL thickness, mean wind, and current velocities, given above.

The computations were performed in the following sequence: (a) derivation of the system solution (2.7) as related to the tasks (2.1), (2.2) in terms of the ocean–atmosphere interface layer variables T_1, T_2, and q_a for given values of the thermodynamic parameters T_w, T_1, and q_a at the outer boundaries of the ABL and OBL and of the solar heat flux R at the water surface; (b) determination of heat fluxes q_h and q_e at the ocean–atmosphere interface from the defined values of T_1, T_2, and q_a; and (c) determination of electromagnetic fluxes I_{sat}, I_{air}, and I_{ship} from the calculated values of parameters T_1, T_2, and q_a and specified values of T_1, T_2, and q_a; and (d) regression

analysis of the interrelation between the evolutions of the q_h and q_e parameters and the evolutions of the I_{sat}, I_{air}, and I_{ship} values in various MCW and IR spectral bands.

The analysis of the ocean–atmosphere brightness temperature has been carried out for the range of wavelengths from 5 mm to 3 cm, where the natural MCW radiation of the system is most sensitive to variations of thermal and humidity characteristics, the radiation temperature being used as a measure of natural IR radiation in the atmospheric window of 8–12 mcm. The atmospheric absorption was computed with an account of the effect of the water vapor content (in MCW and IR bands), molecular oxygen (in the MCW bands), and the aerosol component (in the IR band) on the basis of theoretical relations (Zhevakin and Naumov 1964, 1965) and semi-empirical relations (Arefjev 1991; Paramonova 1985) mainly used at infrareds.

The simulation of the dynamics of thermal and electromagnetic fluxes and an analysis of their interrelations have been performed for several variants differing in the character of the thermal energy outflow from the ocean–atmosphere interface toward the outer boundaries of the ABL and OBL and beyond their borders. This was achieved by a proper choice of parameters of the free atmosphere and of the lower quasi-homogeneous ocean in reference to the initial ABL and OBL conditions invariant in all cases ($T_{10} = T_{20} = 10°C$, $q_o = 6$ g kg^{-1}). The results given below illustrate the following variants: (1) $T_w = T_a = 5°C$; $q = 4$ g kg^{-1} (the heat propagates toward the outer boundary of the ABL and simultaneously to the outer boundary of the OBL); (2) $T_w = 5°C$; $T_a = 10°C$; $q = 6$ g kg^{-1} (heat propagates only to the lower oceanic layer); and (3) $T_w = 10°C$; $T_a = 5°C$; $q = 4$ g kg^{-1} (heat propagates only to the free atmosphere).

Figure 2.2 demonstrates the results of an analysis of the response of the ABL and OBL parameters T_1, T_2, and q, which determine a natural MCW and IR radiation of the SOA, for the first (most general of the above-mentioned) variant.
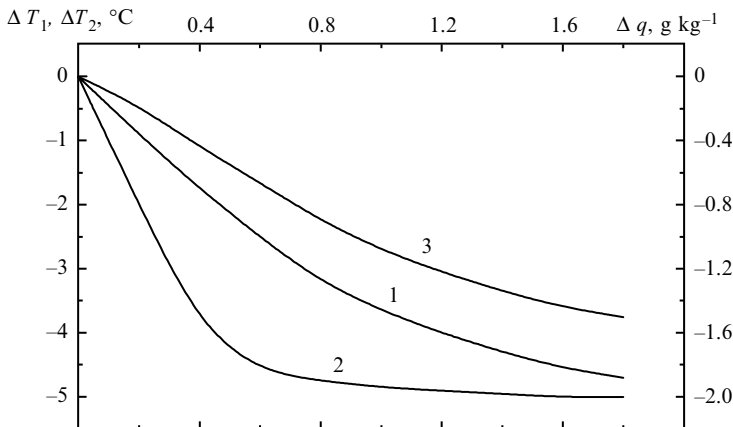
Fig. 2.2 The response of (1) ABL temperature T_1, (2) OBL temperature T_2, and (3) ABL humidity q to the thermal excitation of the SOA in the case of heat outflow from the ocean–atmosphere interface toward the outer boundaries of the ABL and OBL

As seen from the figure, the complete adaptation of the SOA parameters to the impact of the solar radiation flux R occurs during 1–2 days; the adaptation of the ABL temperature occurs about twice as fast as that of the ABL parameters T_1 and q.

The analysis of corresponding variations of sensible and latent heat fluxes q_h and q_e shows that the response of heat fluxes and of the ocean–atmosphere brightness (radiation) temperature is also formed during 1–2 days, that is, it agrees with the time of adaptation of the ocean–atmosphere characteristics to the external influx R.

A regression analysis has been performed to derive some relations between variations of sensible and latent heat fluxes, Δq_h and Δq_e, and brightness ΔT^b (radiation ΔT^t) temperature variations at microwaves and infrareds, accordingly, for versions I, II, III at different observation levels (from satellites, aircrafts, vessels). In particular, the feasibility of an approximation of Δq_h and Δq_e has been examined for the case of the heat outflow in both directions from the ocean–atmosphere interface; the approximations were constructed as linear pair combinations of ΔT in different spectral bands (if meaning the satellite level) and are shown in Fig. 2.3. The solution of this problem involves: (1) determination of regression coefficients between Δq_h, Δq_e, and ΔT in the initial stage of formation of the SOA response to a thermal perturbation (hatched area in Fig. 2.3); (2) approximation of Δq_h and Δq_e using the computed regression coefficients; and (3) extrapolation (prediction of the subsequent evolution) of Δq_h and Δq_e with the regression relations derived in the initial stage with an account for the evolution of ΔT in the final stage of formation
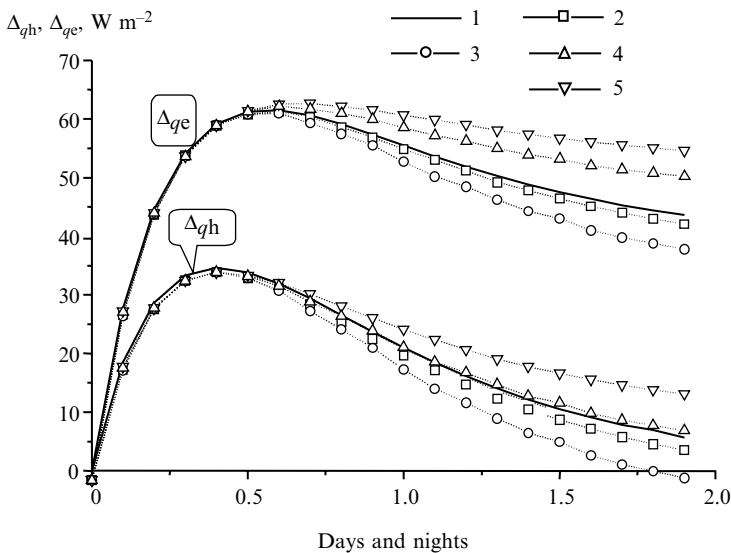
Fig. 2.3 Simulated results of approximation and extrapolation of sensible q_h and latent q_e fluxes (1) with the data of satellite passive radiometric measurements at the spectral intervals: 10 mcm, 5.7 mm (2), 10 mcm and 1.35 cm (3), 1.35 and 3.2 cm (4), 5.7 mm and 3.2 cm (5)

of the ocean–atmosphere response. As seen from the Fig. 2.3, the variations of an intensity of the ocean–atmosphere natural radiation in the spectral windows ~10 microns and ~5.7 mm provide the best reconstruction of the q_h and q_e fluxes in the entire time interval (2 days) of a formation of the radiation and heat response.

The results of a regression analysis for different versions of heat outflow from the interface to the outer boundaries of the ABL and OBL are given more completely in Table 2.2.

It follows from the table that the lowest estimation errors $\delta(q_h)$ and $\delta(q_e)$ (a few percent of the amplitude of natural variations of these parameters) correspond in most cases to spectral intervals 10 and 5.7 micrometers microns as well as 1.35 and 3.2 cm; the increase in the number of spectral intervals as degrees of freedom from two to three or more in the approximation of heat fluxes by MCW and IR radiation characteristics does not lead to any significant reduction of the errors.

The results of a regression analysis of heat fluxes at the micrometers (mycrons) ocean–atmosphere interface and electromagnetic fluxes at the top of the ABL (the aircraft level) are quite close to those given in the table. At the same time, the results of regression analysis of the heat and electromagnetic fluxes at the lower boundary of the ABL (the vessel level), where the atmosphere influence is minimal, differ from the data in the table by substantially larger values of q_h and q_e, which in this case equal 5–6 W m^{-2} and are scarcely affected by the selection of the spectral intervals.

As a whole, the idea of studying the response of the ABL heat features on the air–sea boundary perturbations give us the following results:

1. The heat and water exchange processes in the ocean–atmosphere interface layer have a profound effect on the MCW and IR radiation characteristics not only in the interface layer, but also in the entire atmosphere. This is evident from analysis of the evolutions of the SOA brightness temperatures at the top of the ABL and in the free atmosphere, as well from comparison of these data with the evolutions of heat fluxes at the ocean–atmosphere interface. One can see that the response of thermal and electromagnetic fluxes to the excitation of the system is developing during about the same time period (several days, typically).

2. A connection of brightness and radiation temperatures at the top of the ABL and in the free atmosphere with sensible and latent heat fluxes in the SOA interface is best pronounced in certain spectral intervals; the main effect of the outflows from the ocean–atmosphere interface toward the outer boundaries of the ABL and OBL becomes more apparent in the regions of the atmospheric resonance absorption by molecular oxygen (~5 mm) and in the water vapor line 1.35 cm. Hence, the oxygen and water vapor atmospheric factors can serve as some transient parameters ("bridges") between the natural radiation of the SOA and the heat exchange intensity at its interface not only on seasonal and synoptic scales, but also on smaller (daily, for example) time scales.

3. Because of theoretical analysis fulfilled in the framework of the plane-layered problem, the brightness (radiation) temperature variations at the top of the ABL and in the free atmosphere caused by vertical transfer of heat and water transfer

Table 2.2 Approximation errors δq_h and δq_e for Fluxes qh and q_e in different spectral bands for overall (2-day) cycle of the SOA response as observed from satellite

Wavelength (cm, mcm)						Version I		Version II		Version III	
10 (mcm)	0.57 (cm)	0.8 (cm)	1.35 (cm)	1.6 (cm)	3.2 (cm)	δq_h (W m⁻²)	δq_e (W m⁻²)	δq_h (W m⁻²)	δq_e (W m⁻²)	δq_h (W m⁻²)	δq_e (W m⁻²)
+	+					0.14	0.13	0.10	0.13	0.05	0.24
+						0.40	0.37	0.40	0.31	0.06	0.26
	+	+				0.91	1.18	0.91	1.21	0.08	0.25
	+				+	0.64	0.86	0.67	0.90	0.08	0.22
			+		+	0.20	0.46	0.16	0.46	0.42	0.27
				+	+	0.64	0.23	0.97	0.32	0.42	0.27
+	+	+				0.11	0.09	–	–	–	–
+	+	+				0.10	0.08	–	–	–	–
+	+				+	0.10	0.08	–	–	–	–

The wavelengths involved into the analysis are marked by the sign "+"

in the interface of the system are of a few degrees of Kelvins (K). At the same time, as it will be shown below, the satellite-derived estimates of the SOA brightness temperature variations can reach the tens of K measured at the wavelength 1.35 cm.

2.2 Correlation of the Brightness Temperature with an Intensity of the Ocean–Atmosphere Heat Interaction in the Synoptic Range of Time Scales

2.2.1 Initial Data

We will use in this study the results of the experiments ATLANTEX-90 and NEWFOUEX-88 obtained from the research vessels (R/Vs) *Victor Bugaev*, *Musson*, and *Volna*, which manifested and completed a final phase of the scientific project "RAZREZY" devoted to an analysis of the large-scale air–sea heat and dynamic interaction in the North Atlantic energy active zones.

First of all, from these unique experiments, we extracted the data that are obtained during the so-called stationary phases (April 4–21, 1990 and March 3–23, 1988), which are distinguished by the following features:

(a) Maximum regularity of the meteorological and, especially, aerologic measurements fulfilled during this period
(b) Possibility of a fine analysis of the temporal dynamics of the oceanic and atmospheric parameters due to the fixed (stationary) positions of the R/Vs *Victor Bugaev*, *Musson*, and *Volna*

The research vessels were settled in the three areas of the Gulf Stream delta: in a southern periphery of the basic Gulf Stream water flow (R/V *Victor Bugaev*), in its southern stream (R/V *Musson*), and in an eastern branch of the Labrador Current (R/V *Volna*). This zone is characterized by a strong synoptic variability of the oceanic and atmospheric parameters, which is caused by an influence of the subpolar hydrological front (SHF) as a result of interaction between the cold Labrador Current and the warm quasi-stationary anticyclone rings of the Gulf Stream. The important attribute of this zone is an intensive horizontal circulation of the atmosphere – about 50% of all the time this area of the North Atlantic feels an influence of the powerful midlatitude cyclones, which excite intensive variations of the atmospheric temperature and humidity as well as the boundary heat fluxes (Lappo et al. 1990).

The fragments of stationary phases of the experiments ATLANTEX-90 (from April 8 to 13, 1990) and NEWFOUEX-88 (from March 10 to 15, 1988) were analyzed in details, because just in these periods one could see a synchronous response of all vessel oceanographic and meteorological sensors on the strong mid latitude cyclones in this area of the North Atlantic.

2.2.2 Methods of Computation of the SOA Radiation

We compared the results from the two methods of calculating the average daily values of the SOA brightness temperature in the spectral regions affected by absorption in molecular oxygen (5−6 mm) and the atmospheric water vapor line (1.35 cm) for the case of satellite-borne observations.

In the first case, the simplified model (2.8) was used, which cannot take into account a detailed information on the atmospheric characteristic vertical distribution, but is more accessible for various oceanic regions in every times.

In another case, the plane-layer model of radiation (Basharinov et al. 1974) similar to the model described in Sect. 1.1 of Chap. 1 was used. In terms of this model, proper for MCW range as well as the infrareds, for observations in the nadir direction from an altitude H, the SOA natural radiation I consists of three components:

$$I = I_1 + I_2 + I_3, \qquad (2.12)$$

where the components I_1, I_2, and I_3 can be determined by the relationships (1.12)–(1.15).

Here, in comparison with the model used in Sect. 2.1, this one enable us to assimilate the spacious data on vertical distribution of the air temperature, humidity, and pressure obtained from the aerologic measurements. But the sample frequency specific for the aerologic measurements (every 6 h) is less in comparison with the first case where the SOA brightness temperature is computed based on the 1-hourly values of the oceanographic and meteorological measurements.

An intensity of the SOA radiation I at the level h is determined as follows:

$$
\begin{array}{ll}
\textit{at microwaves} & \textit{at infrareds} \\
I_a(h) = T_a(h)\,\gamma(h); & I_a(h) = B[T_a(h)]\,\gamma(h),
\end{array}
\qquad (2.13)
$$

where $T_a(h)$ is the thermodynamic temperature of the atmosphere at the level h; $B[T_a(h)]$ is the Plank function with the argument $T_a(h)$.

Relationships (2.12), (2.13) and formulas figured in Chap. 1 (1.11–1.15) will be used later in Sect. 2.3 of this chapter.

Right now, using this model, we will analyze the daily and synoptic variations of the SOA brightness and radiation temperatures in the wavelength range 0.5–5.0 cm at the stationary phases of the experiments ATLANTEX-90 and NEWFOUEX-88 aboard the *Victor Bugaev*, *Musson*, and *Volna*.

From the field data we extracted the following:

– Hourly values of the oceanic water surface temperature T_w and near-surface wind speed V to calculate the brightness (radiation) temperature of the surface.
– Total water vapor content in the troposphere to evaluate the integral absorption τ both with and without cloudiness.
– The temperatures T_a, relative humidity q (or water vapor pressures e), and the air pressures P measured at 20 levels between 10 and 16,000 m every 6 h to estimate

not only the total absorption τ, but also the linear absorption factor $\gamma(h)$, from which the accurate estimates of the atmospheric transfer function and, hence, the SOA brightness (radiation) temperature can be found.

– Estimates of turbulent sensible q_h and latent q_e heat at the SOA interface, which were calculated in the State Institute of Oceanography using parameterizations (Gulev et al. 1994) based on hourly observational data for T_w, T_a, V, and e.

The contributions from different layers to radiation properties of the SOA and their interrelations with the heat fluxes at the interface on the synoptic time scale were evaluated theoretically for various cases. In the first case, the down-looking sensors (radiometers) are placed in free air to simulate satellite observations. In the second case, which simulates measurements aboard an aircraft, the down-looking sensors are placed at the boundary between free air and the atmospheric boundary layer. In the third case, the up- and down-looking sensors are placed 10–20 m above the water surface to simulate aboard the vessels.

One more method of calculating the satellite-derived SOA brightness temperature in the spectral regions caused by the absorption of oxygen (~5 mm) and water vapor (1.35 cm) in the atmosphere was tested in our investigations. The idea was to use the minimum data on the atmosphere absorption characteristics – without any detailed information on its vertical temperature and humidity distribution within the ABL (see Fig. 2.4).

Partial interest of comparison of these data with the results of more accurate procedures of calculating the SOA brightness temperature was obtained with an account of the temperature and humidity vertical distribution in the ABL.

It follows from a comparison of the results of the calculations that both methods give a similar picture of the variations of the daily averaged brightness temperature at the wavelengths 5.6 mm and 1.35 cm during the stationary phase of the experiment ATLANTEX-90, though individual differences between the results may account to several Kelvin degrees at the wavelength 5.6 mm and of 15−20 K at the wavelength 1.35 cm.

2.2.3   Results of Computations of the SOA Brightness Temperatures and Their Comparison with Heat Fluxes (Experiment ATLANTEX-90)

The response of the SOA natural MCW radiation to the variability of heat fluxes at the ocean–atmosphere interface was the most distinct in April 8–13, 1990, when the strong cyclone was ranged.

Over this period, the variations of the total (sensible + latent) heat fluxes were more than 800 W m^{-2} for the *Victor Bugaev*, 500 W m^{-2} for the *Musson*, and about 400 W m^{-2} for the *Volna* (Gulev et al. 1994). Among the spectral ranges used to calculate the SOA brightness temperature (5.4, 5.6, 5.9 mm, 0.8, 1.0, 1.35, 1.6, 3.2, and 5.0 cm), the temperature brightness contrasts over this time interval was found
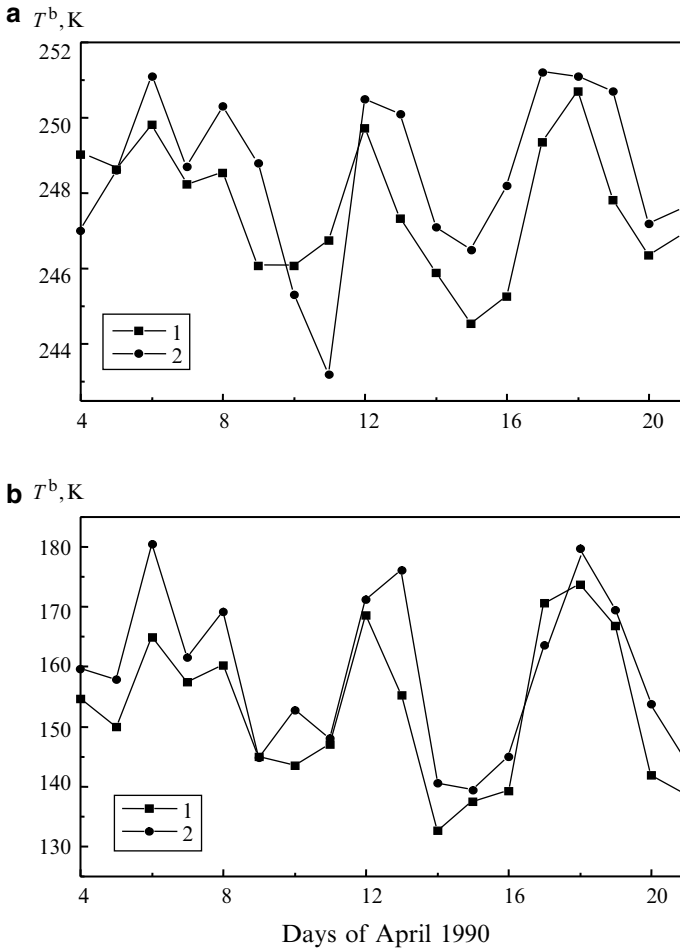
Fig. 2.4 Comparison of the SOA brightness temperature calculated from integral MCW radiometric (1) and aerologic (2) measurements of the temperature and humidity characteristics of the atmosphere at the wavelengths 5.6 mm (**a**) and 1.35 cm (**b**)

to be the greatest in the wavelength range 0.59–1.60 cm, which corresponds to the resonant effect of the atmospheric oxygen and water vapor on the water surface up-going radiation (Fig. 2.5).

One can observe in this piece of electromagnetic spectrum a close correlation between estimates of variations of the SOA brightness temperature T^b and near-surface heat fluxes q_{he} at the *satellite*, *aircraft*, and *vessel* levels of simulated results of outer observations.

This idea is illustrated by Figs. 2.6a, b, c, which compare the values of the q_{he}, and T^b_0.59 (the brightness temperature at a wavelength of 5.9 mm) and T^b_1.35 (the brightness temperature at a wavelength of 1.35 cm) obtained aboard the *V: Bugaev*, *Musson*, and *Volna*.
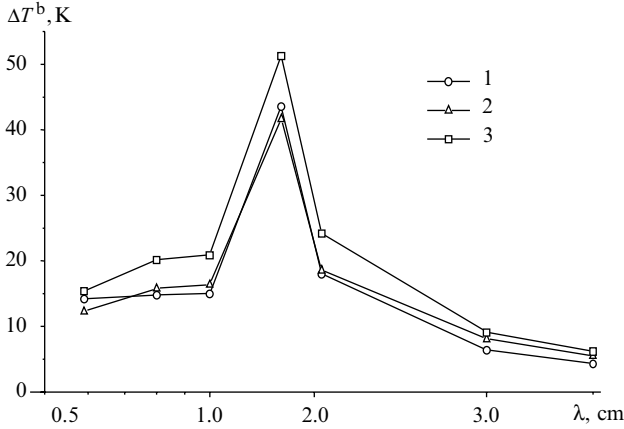
Fig. 2.5 Spectral dependence of the SOA brightness temperature contrast ΔT^{b} in the wavelength range 5 mm–5 cm during the passage of a cyclone (April 8–13) through the places of location of the RV/s *V. Bugaev* (1), *Musson* (2), and *Volna* (3)

It is seen that, in response to the increase in the fluxes q_{he}, the SOA microwave radiation diminishes its brightness temperature T^{b} and vice versa: as the value of q_{he} decreases, T^{b} grows. Over this period, the brightness temperature variations are, on average, 15–20 K at the wavelength 5.9 mm and 30–40 K at 1.35 cm.

We analyzed more rigorously the phenomena of a time delay of the SOA brightness temperature response in the resonant spectral domains 0.59 and 1.35 cm compared to the variations of surface heat fluxes resting upon the results adjusted above (see Fig. 2.7).

The Duamel's integral equation let us to calculate the function $r(t)$ of the brightness temperature T^{b} response (sensitivity) to the total heat flux q_{he} variations:

$$T^{b}(t) = \cdot \int_{0}^{t} q(\tau) \cdot r(t - \tau) \cdot d\tau \qquad (2.14)$$

One can consider (2.14) as a modification of the classic Volterra's equations of the first kind inherent to the class of equations of the convolution type. We proposed some iterative procedure determining the function $r(t)$ as a linear superposition of the exponential functions:

$$r(t) = \sum_{i=1}^{N} a_{i} \exp(-b_{i}t) \qquad (2.15)$$

where coefficients a_{i} and b_{i} are calculated from the condition of minimal discrepancy between the SOA brightness temperature values and their approximations, characterized by values of the root-mean square (*rms*) error.

The calculations show that the value $N = 6$ in the formula (2.15) is acceptable for this task; a mean value of the *rms* error in this case does not exceed 5–7%.
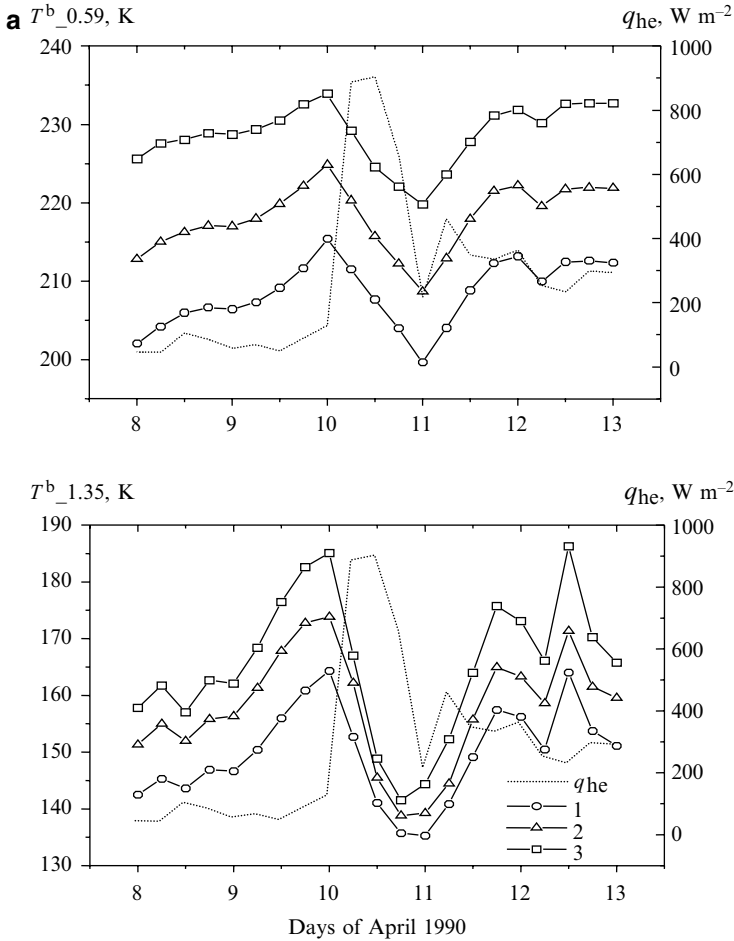
Fig. 2.6 (**a**) Comparison of the total heat flux q_{he} with the simulated SOA brightness temperature estimates T^b_0.59 and T^b_1.35 in the places of location of the R/V *V. Bugaev* during the period April 8–13, 1990 (experiment ATLANTEX-90). Simulation of satellite (1), aircraft (2), and vessel (3) observations

The result shown in the Fig. 2.7b for the vessel *Volna* is especially useful for us due to a fuzziness of variations of the parameters T^b and q_{he} (see Fig. 2.6c). This case is distinguished from the cases illustrated in the Figs. 2.6a and b where the fact of the time shift between these parameters is obviously noticeable without any mathematical analysis.

Table 2.3 illustrates results of an analysis of the role of a time delay of the SOA response on the synoptic surface heat fluxes. Here, we presented the data of a regression analysis (the coefficient of correlation R and discrepancy d (*rms*))
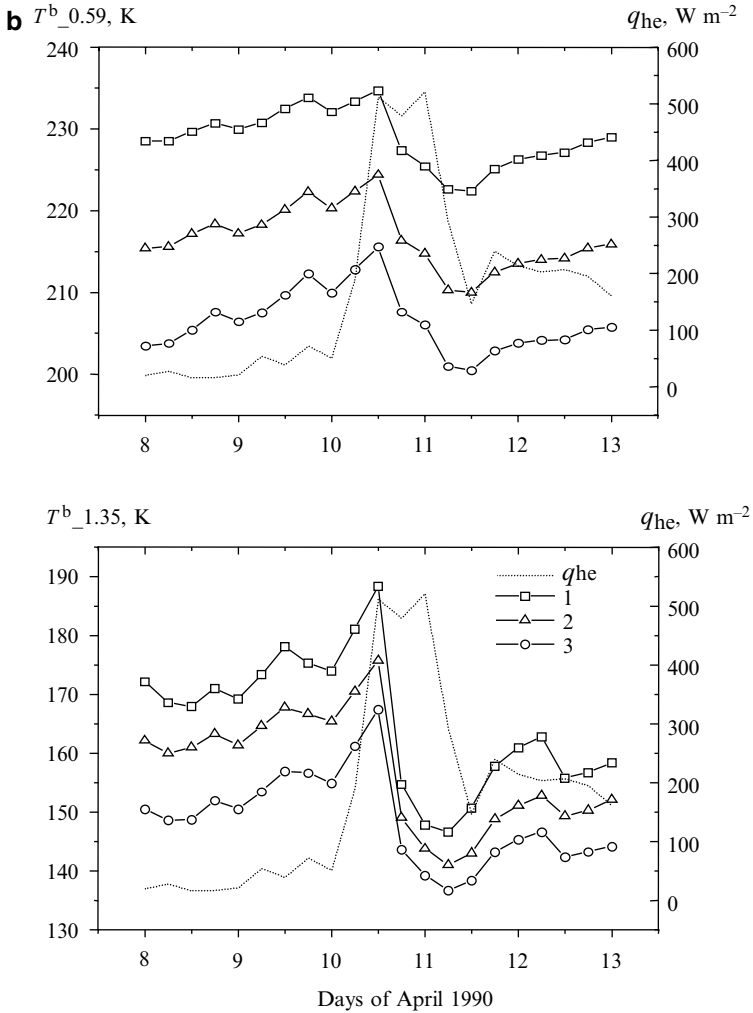
Fig. 2.6 (continued) (**b**) The same as in (**a**), but for the vessel *Musson*.

between simulated estimates of the SOA brightness temperatures at the wavelengths
0.59 and 1.35 cm and the heat fluxes data collected from the vessel *Musson* during
the stationary phase of the experiment ATLANTEX-90. Thus, while carrying out
comparison of these data, we have to take into account the factor of a time shift
between the surface heat fluxes and the SOA brightness temperature variations in
the synoptic range of time scales.

We studied regression relationships in the form of linear correlations between
6-h samples (Fig. 2.8) of the total heat flux q_{he} at the ocean–atmosphere interface
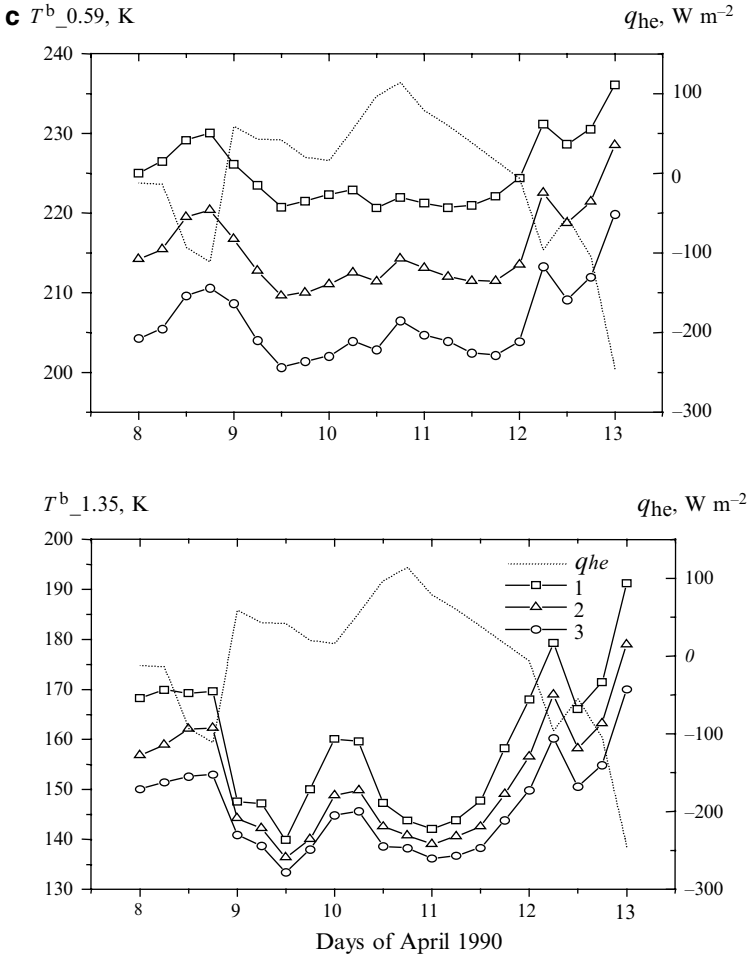
Fig. 2.6 (continued) (**c**) The same as in (**a**) and (**b**), but for the vessel *Volna*

and the brightness temperature of the SOA microwave radiation (the simulation of satellite measurements) at wavelengths of (a) 5.9 mm and (b) 1.35 cm (the temperature was calculated from the oceanographic and aerologic measurements aboard the *Volna*), and the model estimates of the SOA brightness temperature. It is seen that there is an intimate relation between the synoptic variations of the heat fluxes (recorded by the *Volna*) and the model estimates of the SOA brightness temperature. For the 6-h samples of the parameters q_{he} and T^b in the resonance ranges of molecular oxygen and atmospheric water vapor, the least absolute error of approximating the total heat flux q_{he} by the brightness temperature T^b is of 26–28 W m^{-2} for a flux variation amplitude of 320 W m^{-2}.
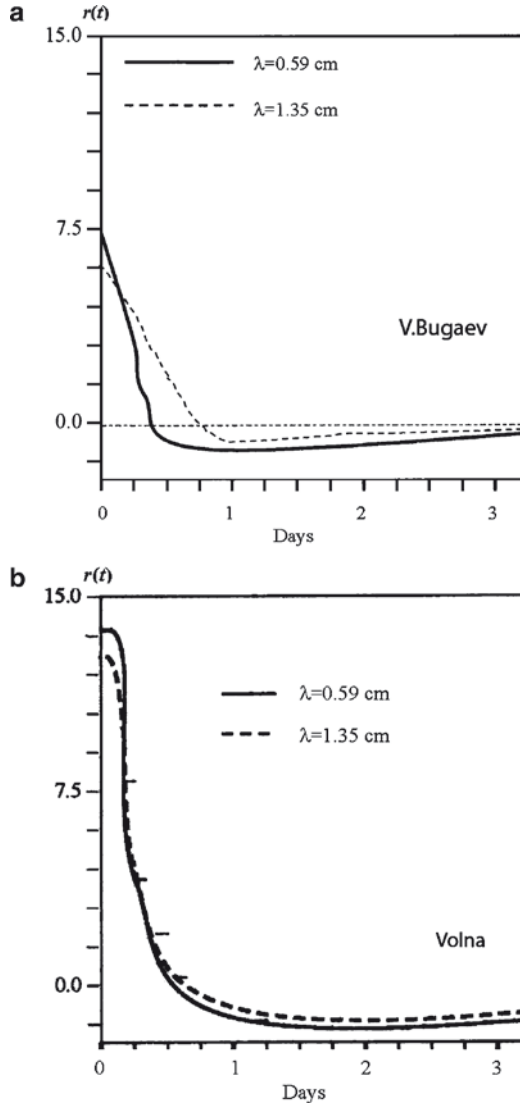
Fig. 2.7 Sensitivity of the SOA brightness temperature at the wavelengths 0.59 and 1.35 cm to heat flux variations (in K $W m^{-2}$)$^{-1}$days^{-1} in the areas observed by the R/Vs – *V. Bugaev* (**a**), and *Volna* (**b**)

Table 2.3 Influence of the time shift Δt between the time samples of the SOA brightness temperature at the wavelengths 0.59 cm (1) and 1.35 cm (2) and heat fluxes on their correlation R and *rms d* (*R/V Musson*). The peak of heat flux variations is of 900 $W m^{-2}$

Time shift Δt (h)	0	6	12	18
Correlation R (1)	0.25	0.67	0.86	0.84
Correlation R (2)	0.34	0.74	0.85	0.71
Discrepancy d ($W m^{-2}$ (1))	160	124	85	98.7
Discrepancy d ($W m^{-2}$ (2))	157	113	93	127.3
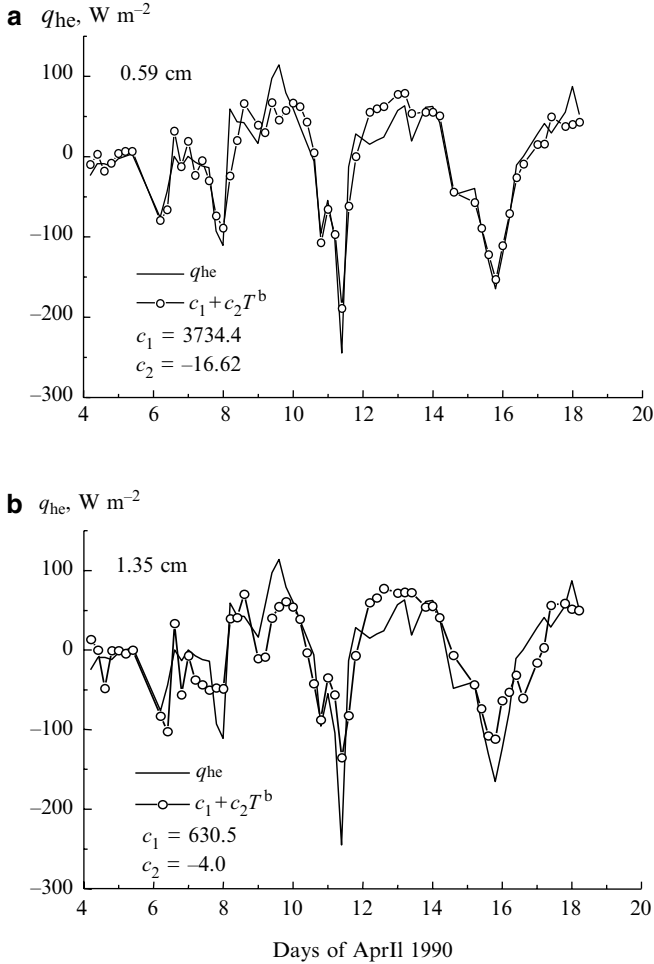
Fig. 2.8 Six-hour samples of the total heat fluxes q_{he}, as the linear combinations of the SOA brightness temperatures at the wavelengths 0.59 and 1.35 cm computed from the meteorological and aerologic data obtained during the stationary phase of the experiment ATLANTEX-90 (R/V *Volna*)

The relative variations of the regression coefficients c_1 and c_2 are of 13–15%, with the regression coefficient c_2 being negative in both cases. This means that the heat flux and the brightness temperature vary in antiphase: an increase in the parameter q_{he} causes T^b to decrease and vice versa. It is remarkable that the intensity variations of the SOA natural microwave radiation correlate well with variations of the heat fluxes in this case, though the accuracy of finding the brightness temperature, and especially, the heat fluxes is not very high. The relative error involved in the model brightness temperature values found under the hydrometeorological conditions of the ATLANTEX-90 experiment is estimated as 5–10%, while that of

the heat fluxes determined by the bulk-parameterizations (1.11–1.13) given in Chap. 1 may be as great as several tens of percent (Gulev et al. 1994). This factor substantiates the idea of using passive MCW radiometric data as *natural* characteristics of ocean–atmosphere heat interaction.

2.2.4   On the Mechanism of a Correlation Between the SOA Brightness Temperature and Interfacial Heat and Momentum fluxes

The problem of how the SOA brightness temperature (simulated or satellite-measured), for which an effectively radiating 2- to 5-km-thick stratum is responsible, can be related to the temperature and humidity properties of a much thinner (roughly 10-m-thick) near-water atmospheric layer has been repeatedly discussed by teams at the Institute of Radioengineering and Electronics, Russian Academy of Sciences; the Institute of Space Research, Russian Academy of Sciences; and the Institute of Oceanology, Russian Academy of Sciences.

Here, we will study the importance (priority) of water surface parameters and some parameters of different atmospheric layers, i.e., their effect on the correlation between the heat and humidity exchange characteristics and the MCW radiation of the SOA on the *synoptic* time scales. To this end, the regression analysis of relationships between variations of simulated brightness temperatures ΔT^b and total heat fluxes Δq_{he} was made based on the data accumulated from the R/V *Volna* at the ATLANTEX-90 experiment stationary phase with the following formulas:

$$\Delta q_{he} \ = \ k_1\, \Delta T_{i1} \ + \ k_2\, \Delta T_{i2}; \ i \ = \ 1,..., \ 4, \tag{2.14}$$

where the indices 1 and 2 are attached to the SOA brightness temperature of natural radiation in certain pieces of the MCW spectrum characterized by the wavelengths λ_1 and λ_2; due to the index i we can divide an influence of parameters forming the air–sea heat interaction such as the sea surface temperature T_w ($i=1$), the near-surface wind speed V ($i=2$) and temperature T_a ($i=3$), as well as the total water vapor content Q ($i=4$); ΔT_{i1} and ΔT_{i2} are the brightness temperature variations at these wavelengths caused by variations of these parameters.

Then, we used the ordered elimination method to reveal the contribution of one or another parameter simultaneously to the heat exchange process and the SOA natural radiation in different parts of the MCW range of wavelengths. Table 2.4 lists the errors due to the approximation of the total heat fluxes q_{he} by the brightness temperatures of the SOA radiation in the wavelength range 0.56–3.2 cm.

Here, the column d is the discrepancy (*rms*) between the parameter q_{he} and the linear combinations of the parameters ΔT_{i1} and ΔT_{i2}, whose values were computed from the formulas of the least-squares method taking into account variations of all the basic parameters of the SOA (T_w, T_a, V, and Q) in the frames of generalized and simplified radiation models.

Table 2.4 Root-mean-square errors of approximation of the total heat fluxes by the sea brightness temperatures simulated with various radiation models (the generalized model – the column "*d*," and the simplified ones – the other columns)

Wavelength (cm)	Approximation error (W m^{-2})				
	d	*d_T*$_w$	*d_V*	*d_T*$_a$	*d_Q*
0.56	27.8	27.8	28.2	48.5	27.8
0.8	26.6	26.8	27.3	27.0	37.8
1.35	27.0	27.2	28.4	27.5	35.9
1.6	26.1	26.3	27.8	26.5	35.9
3.2	34.2	34.2	30.2	34.3	394

Table 2.5 Correlation between simulated values of the SOA brightness temperature from various levels of observations at the millimeters and centimeters and the parameter qh_e controlled from the vessel *volna* in April 1990

Wavelength (cm)	0.54	0.56	0.59	0.80	1.0	1.35	1.6	3.2	5.0
Satellite	0.48	0.69	**0.92**	**0.87**	**0.87**	**0.83**	**0.88**	0.77	0.74
Aircraft	0.77	**0.90**	**0.89**	**0.84**	**0.85**	**0.86**	**0.88**	0.75	0.73
Vessel (1)	**0.86**	**0.87**	**0.85**	**0.80**	**0.81**	**0.84**	**0.86**	0.74	0.72
Vessel (2)	**0.81**	0.73	0.71	**0.80**	**0.82**	0.78	**0.82**	**0.80**	0.70

The cells marked in the Table by a **bold** characterize the correlation equal or above the level 0.8

In the columns *d_T*$_w$, *d_V*, *d_T*$_a$, and *d_Q*, the effects of the ocean surface temperature T_w, the near-surface wind speed V and temperature T_a, and the integral water vapor content Q, respectively, are excluded (neutralized). Table 2.4 shows that an influence of the sea surface temperature is more easy in comparison with the atmospheric parameters T_a and Q (this question was one of actual point in our regular discussions conducted with some leading specialists of the P.P. Shirshov's Oceanologic Institute Russian Academy of Sciences, in particular, with Prof. Vadim Pelevin and Dr. Sergey Pereslegin).

We analyzed also the relations between synoptic variations of the parameter q_{he} and the model estimates of variations of the SOA brightness temperature derived as a result of an imitation of satellite and aircraft measurements with the down-looking MCW sensors, as well as the ship measurements with up-looking (1) and down-looking (2) sensors (antennas): these results are presented in Table 2.5. Computations of the SOA brightness temperatures were performed using the radiation model (2.8)–(2.11) for the 6-hourly samples taken from the measurements of the parameters T_w, V, T_a, and Q observed aboard the vessel *Volna* at the stationary phase of the experiment ATLANTEX-90.

The results given in Tables 2.4 and 2.5 point to the primary role of the parameters T_a and Q in forming relations between the SOA brightness temperatures in the atmospheric resonance lines 1.35 cm and in the regions (5.4–5.9 mm) of the oxygen (O_2) attenuation (radiation) with the near-surface heat fluxes. This analysis also

shows that independently from the methods of observations used (*satellite*, *aircraft*, *or vessel*), an influence of the sea surface temperature on the SOA brightness temperature is the *passive* factor in comparison with an influence of the atmospheric parameters T_a and Q in the *synoptic* range of time scales.

Figures 2.9a, b, c, given below, illustrate an important role of the air temperature parameter T_1500 measured at the height of 1,500 m (the top of the ABL) and the atmospheric total water vapor content Q as the transient (transmitting) factors forming relations between the SOA brightness temperatures and the near-surface heat fluxes.

We estimated the parameters T_1500 and Q from aerological measurements carried out with the R/Vs *Victor Bugaev*, *Musson*, and *Volna* during April 8–13, 1990.
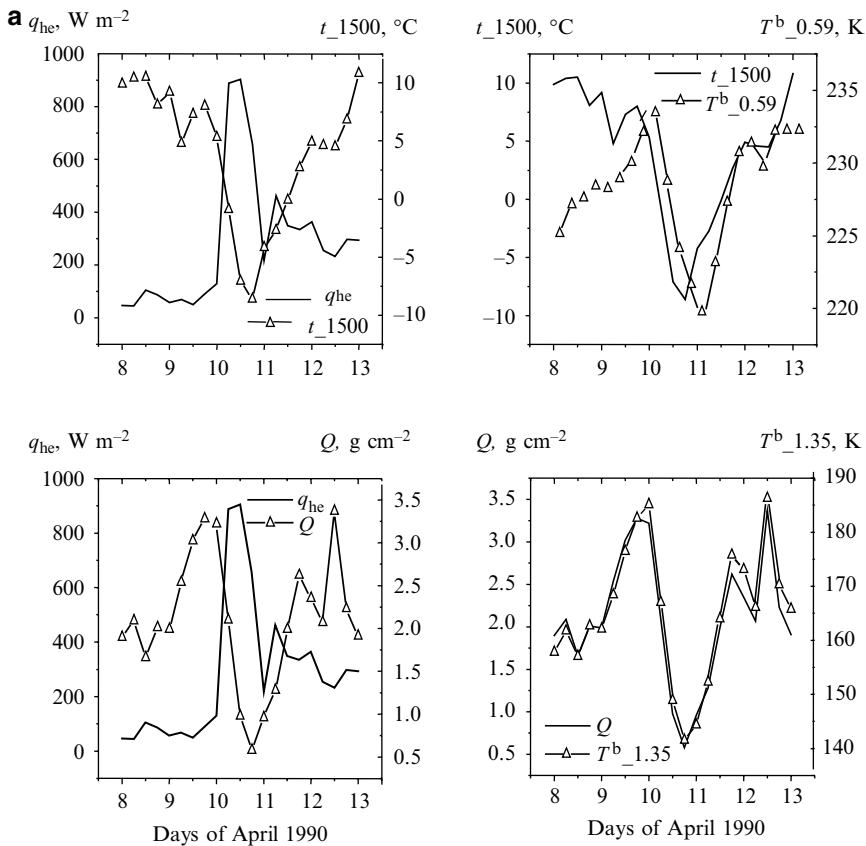
Fig. 2.9 (**a**) Results of comparison the heat fluxes q_{he}, the atmosphere temperature t_1500 at the top of the ABL, the total water vapor content of the atmosphere Q, and the SOA brightness temperature at the wavelengths 5.9 mm and 1.35 cm at the point of location of the R/V *Victor Bugaev* during 8–13 April, 1990.
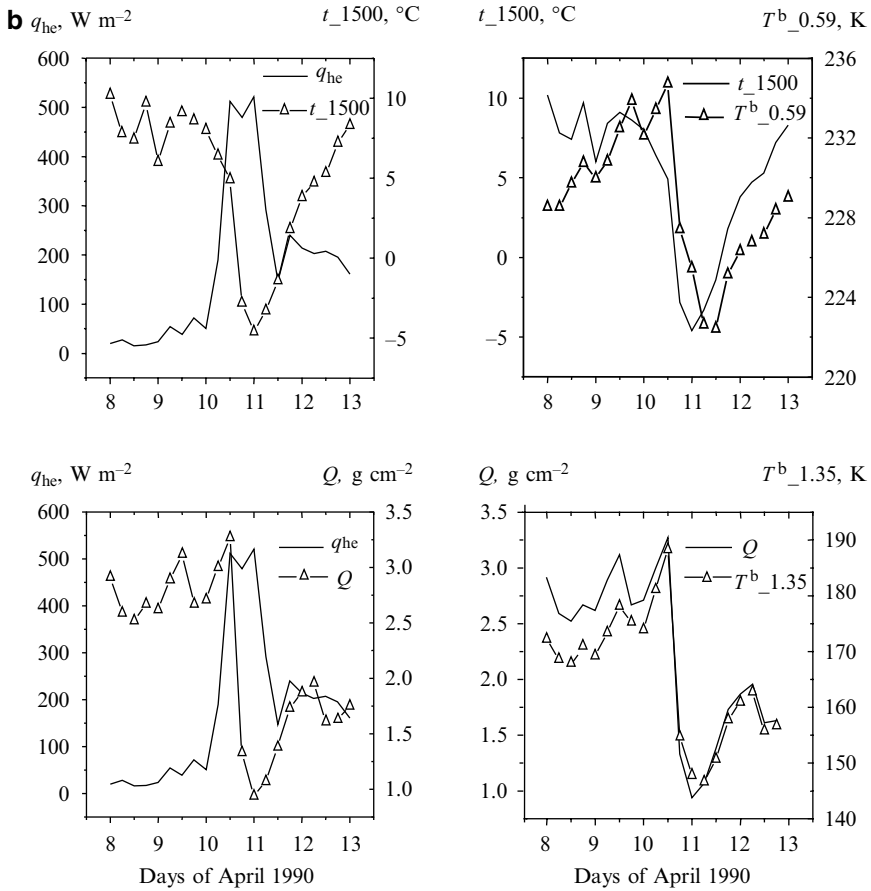
Fig. 2.9 (continued) (**b**) The same as (**a**), but for the vessel *Musson*.

A close correlation between the vertical turbulent flux of momentum q_v and the near-surface wind speed V is observed. Figure 2.10 demonstrates this effect with data of the experiment ATLANTEX-90 derived from the R/V *Volna*.

This regularity predetermines a clear *direct* correlation between the SOA brightness temperature and the momentum fluxes. For example, we revealed a close interrelation between the momentum fluxes at the ocean–atmosphere interface and the model estimates (corresponding to the satellite level of observations) of the SOA brightness temperature in the wavelength range between 3 and 5 cm, which is not affected by the atmosphere, and where the brightness temperature variations are governed mainly by variations of an intensity of a wind stress of the water surface (see Fig. 2.11).
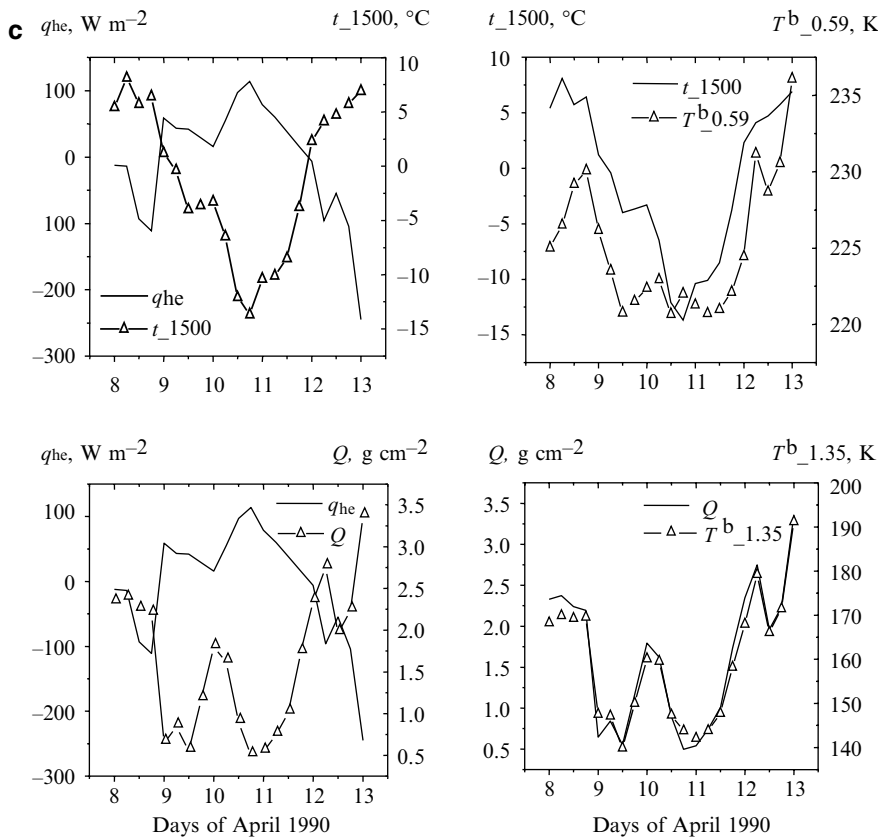
Fig. 2.9 (continued) (**c**) The same as (**a**) and (**b**), but for the vessel *Volna*

During April 8–13, the correlation coefficient of variations of the brightness temperature T^b at the wavelength 3.2 cm and the parameter q_v observed from the vessel *Victor Bugaev* was as high as $R = 0.96$ and the discrepancy (*rms* error) between such variations was of $d = 0.043$ for the values of parameter q_v varying from 0.044 to 0.9 $N\,m^{-2}$ (in Newton per square meter). For the R/V *Musson*, the corresponding parameters were as $R = 0.95$ and $d = 0.05$ in the range of variations of q_v 0.013–0.57 $N\,m^{-2}$. At last, for the vessel *Volna*, the values of its corresponding parameters were of $R = 0.89$ and $d = 0.06$ for q_v varying from 0.014 to 0.42 $N\,m^{-2}$. Hence, we can observe a *direct* correlation between the SOA natural MCW radiation (its brightness temperatures estimated in the millimeter and centimeter range of wavelengths) and the impulse (momentum) fluxes in the synoptic scales.
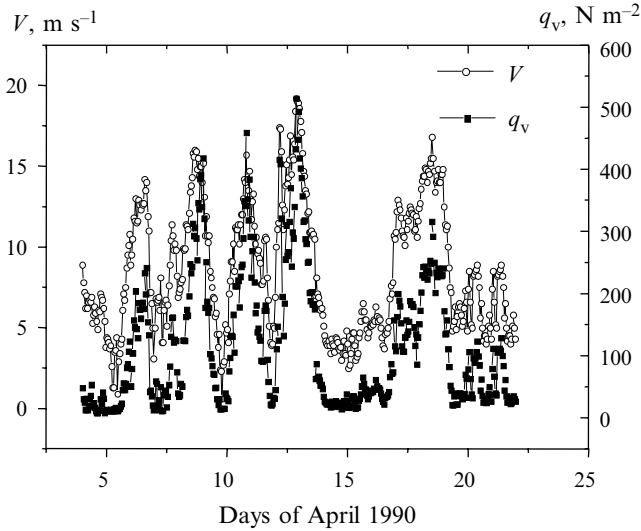
Fig. 2.10 Results of comparison of the near-surface wind speed and momentum fluxes observed during the stationary phase of the experiment ATLANTEX-90 with the 1-h time resolution of these parameters

2.2.5 Response of the SOA Heat and MCW Radiation Characteristics on the Atmospheric Horizontal Circulation

It follows from illustrations shown at the Figs. 2.5 and 2.6 as well as from an analysis of characteristics of spatial and temporal variability of the atmosphere that the SOA brightness temperature contrasts in the oceanic areas observed where the experiment ATLANTEX-90 was made are strongly dependent on the processes of the horizontal circulation in the near-surface atmosphere, which produce, in particular, intensive advection fluxes of heat and water. We have discovered that this effect exceeds *in an order* an influence of the factor of vertical turbulent heat and water transfer, which was analyzed and demonstrated in Sect. 2.1 of this chapter. The processing of the aerological data array gained afloat has made it possible to put forward a concept of the large-scale horizontal (*advective*) heat and water transfer as a factor provoked the vertical turbulent fluxes arising for regulating the heat balance between the ocean and atmosphere. The essence of this idea is that the horizontal heat transfer leads to a periodical sharp heating (cooling) of air in a given oceanic area. This effect (1) intensifies heat fluxes directed from the atmosphere to the ocean (or vice versa) because of a greater difference between the water and air; and (2) increases (or decreases) the integral absorption of electromagnetic fluxes, based on the model of the SOA brightness temperature (2.12). Such a supposition follows from the comparison of synoptic variations of the enthalpy (heat content),
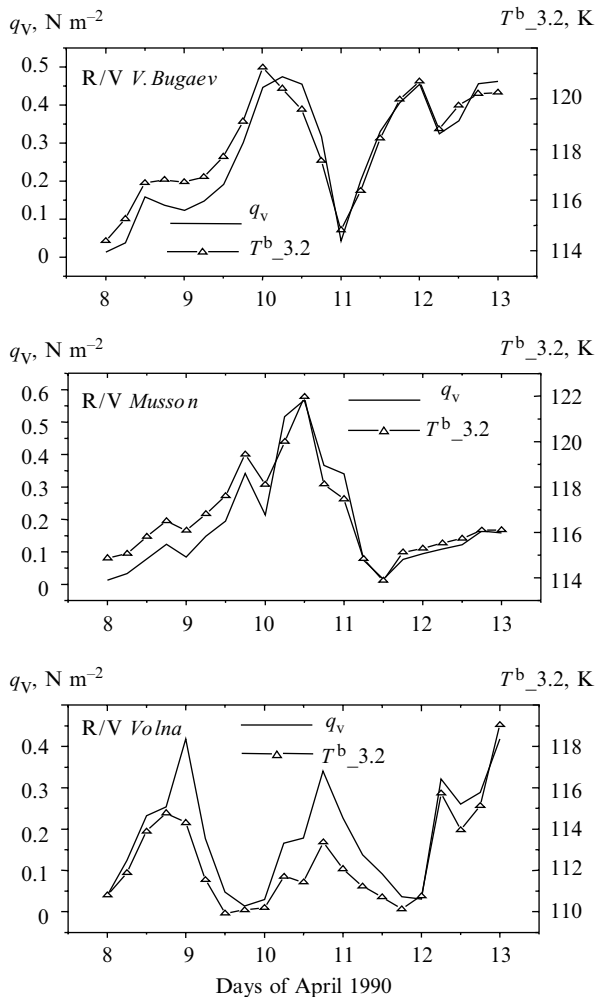
Fig. 2.11 Comparison of the momentum fluxes q_v with simulated ocean–atmosphere brightness temperature at 3.2 cm in the areas where the R/Vs *Victor Bugaev*, *Musson* and *Volna* were resided during April 8–13, 1990

kinetic, and potential energy in the ABL, which experience the regular influence of the horizontal heat and energy transfer, with the vertical heat fluxes at the SOA interface and the brightness temperature of the system.

Figure 2.12 compares the values of the ABL enthalpy (computed from the aerologic sounding data for horizons on altitude of 10, 100, 200, 300, 400, 500, 900, and 1,000 m gathered aboard the *V. Bugaev* and *Musson* vessels and estimated with the methods stated in Pinus (1982) and Perevedentsev (1984)) with the total heat fluxes excited by the deep cyclone originated during the stationary phase of the
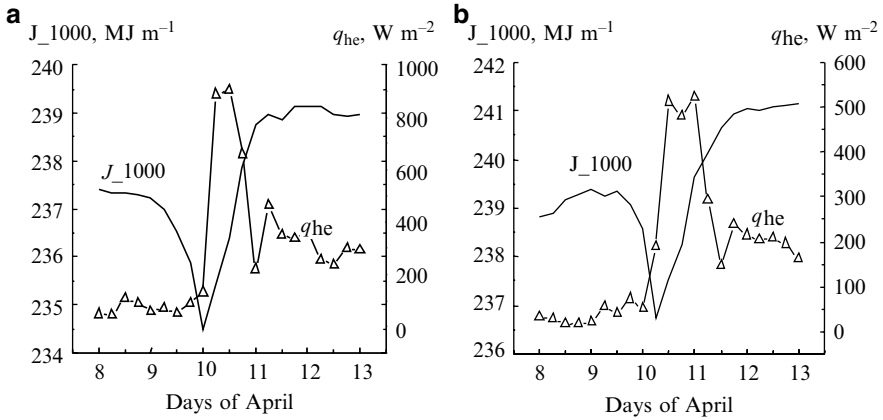
Fig. 2.12 Total heat fluxes q_{he} vs. the enthalpy J_1000 of the ABL during the passage of a cyclone (April 8–13, 1990) through the location of the (**a**) *Victor Bugaev* and (**b**) *Musson*

experiment ATLANTEX-90 in April 8–13, 1990. Figure 2.13 illustrates relations between the ABL enthalpy J and the SOA brightness temperature variations at the wavelengths 5.9 mm and 1.35 cm over this period.

One can see from Fig. 2.13 that synoptic variations of the enthalpy of the ABL stimulate an appreciable reaction of the SOA brightness temperature in the ranges of effect of atmospheric oxygen (5–6 mm) and water vapor (1.35 cm), which varies from 12 to 45 K, respectively; moreover, the response of the brightness temperature lags behind the enthalpy variation by 18–24 h. This property becomes especially apparent during the periods of a cyclonic activity of the atmosphere, when the ABL temperature and humidity are sharply and strongly varied.

For summarizing this stage of our investigations, one ought to keep in mind the following:

1. The data obtained confirm a close correlation between the synoptic variations of the atmospheric temperature and humidity, and an intensity of the ocean–atmosphere heat interaction, which were demonstrated earlier in Laihtman (1976) and Lebedeva 1991), for example.
2. Correlation between the SOA brightness temperature and an intensity of the surface vertical turbulent heat fluxes at the mid- and high latitudes of the North Atlantic, if formed, mainly due to the horizontal (*advective*) large-scale heat and water movements in the ABL; an influence of the vertical heat transfer on the SOA brightness temperature is much more less (in an order) in comparison with the advective factor.
3. Based on results of the analysis obtained in the experiment ATLANTEX-90, we concluded that the variations of temperature and humidity characteristics in the ABL caused by a large-scale horizontal heat and water transfer in the atmosphere *rule* over the vertical turbulent heat and water fluxes at the SOA interface as well as the intensity of natural MCW radiation of the system.
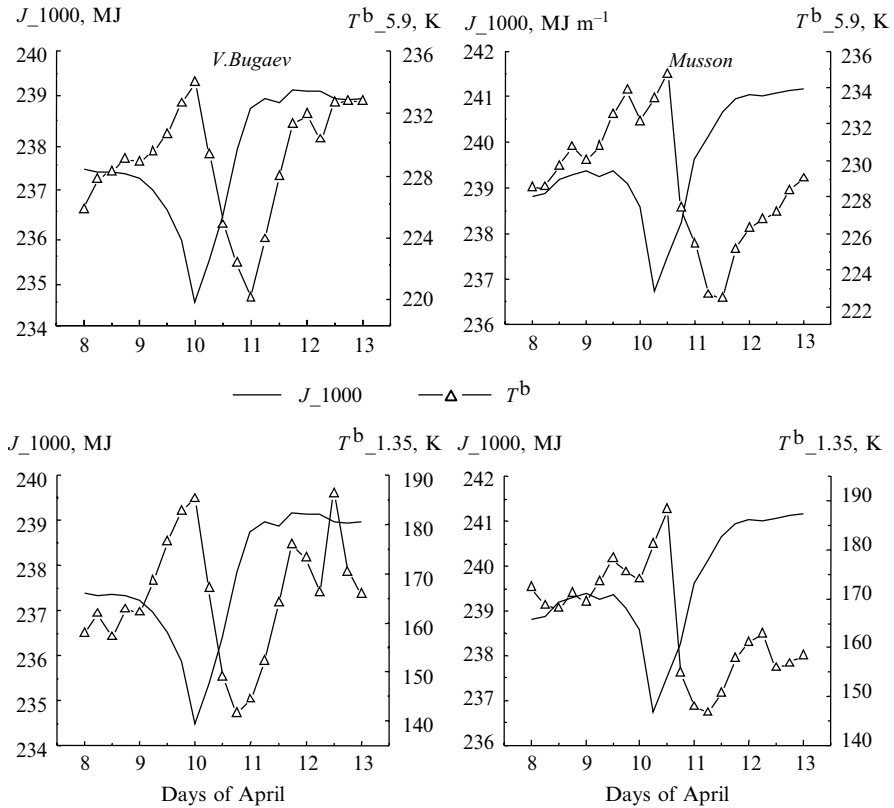
Fig. 2.13 Results of modeling the response of the SOA brightness temperature at the wavelengths 5.9 mm and 1.35 cm to variations of the ABL enthalpy J_1000 during the passage of a cyclone (April 8–13, 1990) through the places of locations of the R/Vs *V.Bugaev* and *Musson*

Moreover, to all appearances, the SOA brightness temperature formed in the atmospheric oxygen and water vapor resonance regions can be used not only for determining the near-surface heat fluxes, but also for estimating some characteristics of energy horizontal transfer in the ABL in the range of synoptic time scales.

2.3 Relations Between Monthly Mean Air–Sea Temperature Differences and SOA MCW and IR radiation

2.3.1 Statement of the Problem

The main objective of this study is modeling the seasonal dynamics of monthly mean characteristics of the SOA natural MCW and IR radiation and analyzing their correlations with seasonal dynamics of monthly mean differences between surface

(water) temperature of the ocean T_w and the near-surface atmosphere temperature T_a. As is known, the parameter $\Delta T = T_w - T_a$ directly determines the vertical turbulent fluxes of sensible and latent heat in the case of large-scale interaction of the ocean and atmosphere, as well as the average multiyear (climatic) values of ΔT in the North Atlantic (except its tropical zones) agree well with the average multiyear values of heat exchange between ocean and atmosphere. In the center of the study is the energy-active zone Gulf Stream, which is characterized by spacious oceanographic, meteorological, and other archives.

The following tasks are in a focus:

– Computing the MCW and IR temperatures of the SOA and their seasonal dynamics: (simulation of MCW and IR passive radiometric measurements from satellites with archival data of oceanographic and hydrometeorological measurements) in the Gulf Stream energy-active zone of the North Atlantic.
– Analysis of influence of the SOA parameters (with emphasizing the parameters T_w and T_a) on the MCW and IR radiation intensity at centimeters, millimeters, and infrareds in this area of the North Atlantic.
– Analysis of steadiness of relations between the MCW and IR radiation intensity in various pieces of spectrum and the parameter ΔT.
– Exposure of spectral pieces at centimeters, millimeters, and infrareds, which provide a top steadiness of the dependence "MCW radiation vs. parameter ΔT" and its interannual (seasonal) dynamics.

In the analysis were used the long-term data of oceanographic and meteorological measurements gathered in the fragment of Gulf Stream EAZO – the 5-degree square centered about the point (vessel station) with coordinates 38°N, 71°W – so called point *H* (HOTEL).

To compute the SOA radiation characteristics and their temporal dynamics at microwaves and infrareds we used the plane-layer model (2.12).

2.3.2 Approximations and Limitations Used

The analysis of the SOA radiation characteristics is made with the assumption that the ocean surface is calm (flat) and the atmosphere is cloudless. The relative frequency of these situations in SOA is around 50% (Shutko 1986). In addition, the results of special study show that the monthly mean values of brightness temperature of the SOA as well as the estimates of monthly mean parameters its system retrieved from satellite sensors (at microwaves) are practically inert to the wind speed, cloudiness, and precipitation intensity.

An intensity of the water surface radiation is computed within a wide range of its temperature variations in accordance with the well-known methods cited in Handbook (1977)) and Basharinov et al. (1974). Numerical estimates of the atmosphere attenuation γ are obtained with an account of the water vapor content (at microwaves and infrareds), molecular oxygen (at microwaves), and aerosol

(at infrareds) on the basis of theoretical (Zhevakin and Naumov 1964, 1965) and empirical (Arefjev 1991; Paramonova 1985) relationships.

In accordance with Arefjev (1991)), Paramonova (1985), and Zhevakin and Naumov (1964, 1965), the attenuation of natural emission in the atmosphere in the microwave and infrared ranges of wavelengths is caused mainly by its parameters as the air temperature T_a, humidity ρ, and pressure P as well as their vertical distribution. As the monthly mean parameters T_a, ρ, and P are considered in our study, the model of standard atmosphere (Xrgian 1978) is appropriate:

$$T_a(h) = T_a(0) \exp[-0.02h]; \qquad (2.15a)$$

$$P(h) = P(0) \exp[-0.125h]; \qquad (2.15b)$$

$$\rho(h) = r(0) \exp[-ah]. \qquad (2.15c)$$

Monthly mean values of the parameter a in (2.15c) can be determined from the monthly mean values of near-surface water vapor pressure $e(0)$ and integral water vapor content $Q = \int_0^H \rho(h)\,dh Q = \int_0^H \rho(h)$ in the atmosphere cited in Zhevakin and Naumov (1964) with an account of the next relationship between $e(0)$ (in mb) and $\rho(0)$ (in kg m^{-3}):

$$\rho(0) = 0.22\, e(0)/T_a(0). \qquad (2.16)$$

It follows from (2.15c) and (2.16):

$$a = 0.22\, e(0)\ /Q\, T_a(0),\ \text{km}^{-1}. \qquad (2.17)$$

The near-surface atmospheric pressure is taken as equal to its standard value $P(0) = 1,013$ mbar for all seasons, because the seasonal variations of $P(0)$ are of 10–15 hPa for the main active zones of the North Atlantic including its Gulf Stream zone (Handbook 1979). These variations are the cause of small variations of the line absorption of natural electromagnetic radiation, which does not exceed 0.5–0.7% of their averaged per year (climatic) absorption at the wavelength 1.35 cm and 1–1.5% in the IR band 8–12 mcm, respectively.

Let us note that variations of the near-surface air humidity yield the effect of tens of percents in seasonal variations of absorption at microwaves and infrareds.

The monthly mean parameters T_w, $T_a(0)$, $e(0)$, a, Q and $\rho(0)$ shown in Table 2.6 are used as the initial data for calculations of natural MCW and IR radiation in the Gulf Steam active zone for various seasons.

The data presented in Table 2.6 help us compute a vertical distribution of attenuation $\gamma(h)$ and intensity of radiation $I_a(h)$. The resulting values of brightness and radiation temperature are determined by integration of $\gamma(h)$ and $I_a(h)$ from $h = 0$ meters to $H = 10,000$ m.

2.3.3 Relations Between Natural Radiation and SOA Characteristics

We computed the monthly mean values of brightness temperature at wavelengths 3 mm–8.5 cm and radiation temperature at the window 8.5–14 mcm corresponding to monthly mean values of parameters T_w, $T_a(0)$, a, $\rho(0)$, and Q presented in Table 2.6. It follows from calculations that the SOA natural IR- and MCW radiation is most sensible to seasonal variations of the near-surface atmospheric temperature and humidity variations of the SOA, which are closely related to the SOA natural radiation intensity in the spectral interval 9–10 mcm, at the vicinity of the 5 mm - line of resonant absorption by molecular oxygen, and in the 1.35-line of resonant absorption by a water vapor as well as in nonresonant spectral interval 3–8 cm (see Fig. 2.14 illustrating these features at the microwaves).

Table 2.6 Monthly mean (climatic) temperature and humidity characteristics in the gulf stream active zone of the North Atlantic

Months	February	May	August	November
T_w (K)	286	291	298	293.5
$T_a(0)$ (K)	282.5	289	297	289.5
$e(0)$, mb	11	7	26	15
Q (g cm^{-2})	1.0	2.3	3.5	1.5
$\rho(0)$	8.6	12.9	19.2	11.4
a (km^{-1})	0.86	0.56	0.55	0.76
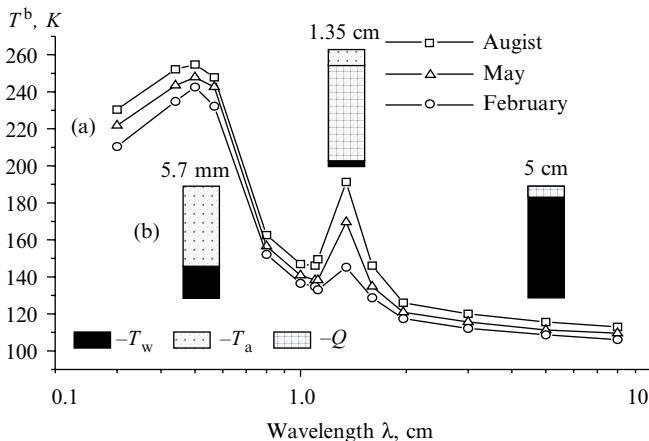
Fig. 2.14 Seasonal dynamics of monthly mean values of the brightness temperature in the Gulf Stream active zone (**a**) and the relative contribution of the parameters T_w, $T_a(0)$, and Q in the T^b variations (**b**)

This figure shows also the results of the linear regression analysis between the monthly mean values of the SOA brightness temperatures and parameters T_w, $T_a(0)$, and Q in a form of diagrams illustrating a relative contribution of variations of these parameters in variations of the parameter T^b at the wavelengths 5.7 mm, 1.35 cm, and 5 cm during the winter-summer period.

Let us note that the parameter Q is a more reliable factor governing the brightness temperature at the wavelength 1.35 cm in comparison with the parameter $\rho(0)$, as the parameter T^b depends not only on the near-surface air humidity, but also on its vertical distribution. That is why the integral water vapor content Q appears in Fig. 2.14 along with parameters T_w and $T_a(0)$. The results of a regression analysis clarify some important peculiarities of relations between MCW and IR radiation and the SOA parameters. For example, seasonal variations of an intensity of natural radiation in spectral intervals 10 mcm and 5 cm are well-correlated first of all with seasonal variations of the ocean surface temperature T_w. Parameter T_a shows its worth at the wavelengths 5.7 mm, and the parameter Q – in the line 1.35 cm of water vapor absorption; at these wavelengths, the values of T^b and T^t are increasing linearly with increasing parameters T_w, T_a, and Q. The coefficient of regression $\Delta T^b/\Delta T_w$ for the dependence "brightness temperature vs. water surface temperature" is about 0.4–0.45 K°C^{-1} at the wavelength 5 cm; the coefficient of regression $\Delta T^b/\Delta Q$ for the dependence "brightness temperature vs. integral vapor content of the atmosphere" at the wavelength 1.35 cm is varied from 14.4 K g^{-1}cm^{-2} between May and August to 17.3 K g^{-1}cm^{-2} between February and May. These results are in agreement with their well-known estimates obtained on the more short periods (hours, weeks) (Basharinov et al. 1974; Shutko 1986).

2.3.4 Correlation Between Monthly Mean Differences of the Ocean Surface and Atmosphere Near-Surface Temperatures and the SOA Natural Radiation

The fact that natural radiation of the SOA brings an information on the ocean surface temperature and the near-surface air temperature in appropriate spectral intervals suggests the idea of their usage for the determination of the difference between parameters T_w and T_a, which is the key factor of heat and water exchange in the ocean–atmosphere interface. In fact, the parameter T_w can be determined *directly* with the data of measurements of brightness temperature at the wavelength 5 cm or radiation temperature at the wavelength 10 mcm; estimates of the parameter T_a can be derived *directly* from the brightness temperature at the vicinity of the resonance line 5 mm or *indirectly* from the brightness temperature at the wavelength 1.35 cm (if to take into account a close correlation between parameters T_a and Q in a wide range of time scales shown in Chap. 1).

We examined the possibility of using the SOA intensity radiation at microwaves and infrareds for an analysis of seasonal dynamics of the monthly mean difference $\Delta T = T_w - T_a$ by means of studying a steadiness of relationships between this parameter

Table 2.7 Seasonal variations of monthly mean values of the parameter Δt and brightness (radiative) temperatures in the active zone Gulf Stream

Variations of initial characteristics	During periods (seasons)			
	February–May	May–August	August–November	November–February
$\Delta(\Delta T)$ (°C)	−1.5	−1	3	−0.5
ΔT^r(10 mcm) (K)	4.1	6.2	−3.2	−7.1
ΔT^b(5.7 mm) (K)	5.6	6.8	−6.4	−6
ΔT^b(1.35 cm) (K)	24	21.1	−34.9	−10.2
ΔT^b(5 cm) (K)	2.5	3.6	−2.5	−3.6

and various pairs of monthly mean values of $I(\lambda_1)$, $I(\lambda_2)$ for different combinations of λ_1 and λ_2 and the parameter ΔT for the Gulf Stream active zone. The initial for such examination values ΔT and estimates of seasonal variations of month mean brightness (radiation) temperatures are computed taking month mean values of parameters T_w, T_a, a, and $\rho(0)$ into account (Table 2.7)

On the basis of the data shown in Table 2.7, we analyzed the following regression:

$$\Delta_i(\Delta T) = k_1 \Delta T_{i1} + k_2\, \Delta T_{i2}; \, i = 1,...,4, \tag{2.18}$$

where the indices i_1, i_2 applied to brightness (radiation) contrasts mean one or another wavelength, and the index i applied to the parameter ΔT means one or another season of a year; it is supposed that the coefficients k_1, k_2 remain the same invariable of all seasons.

To evaluate an effectiveness of the procedure (2.18) of estimating the seasonal variations of ΔT, the next criteria are used:

1. The index k, which displays a steadiness of estimates of $\Delta_i(\Delta T)$ to errors of the values ΔT_{i1}, ΔT_{i2} determination:

$$k = (k_1 + k_2)^{1/2};$$

2. The discrepancy δT between the left-hand and right-hand and right-hand members of (3.18), that is, between real values of $\Delta_i(\Delta T)$ and their estimates:

$$\delta T = [\,1/4\, \Sigma\, \Delta_i - (k_1\, \Delta_{i1} + k_2\, \Delta_{i2})]^{1/2}; \, i = 1,...,4.$$

The results of computations of the criteria δT and k for several pairs of λ_1 and λ_2 are listed in Table 2.8.

As follows from Table 2.8, the parameter δT and, especially, k gets greatly increased if the spectral intervals λ_1 and λ_2 duplicate one another. For example, it is true for the case 3, as both wavelengths (10 mcm and 5 cm) bring similar information, mainly on the ocean surface temperature T_w and its seasonal variations.

An increase of the number of spectral intervals from 2 to 3 results in decrease of the value δT approximately in 3 times; at the same time, the coefficient k is increasing in 2–3 times. The minimum values of the criteria k are ensured if only one wavelength is used; however, the value of δT becomes unacceptable in this case.

Table 2.8 Values of the criteria k and δT for different cases of combining the wavelengths

Case	λ_1 and λ_2	δT (°C)	k (°C K^{-1})
1	10 mcm and 5.7 mm	0.1	1.18
2	10 mcm and 1.35 cm	0.9	0.24
3	10 mcm and 5 cm	0.33	4.2
4	5.7 mm and 1.35 cm	0.22	0.35
5	5.7 mm and 5 cm	0.39	2.86
6	1.35 cm and 5 cm	0.25	0.46

For example, for $\lambda = 10$ mcm, $\delta T = 3.1$°C and $k = 0.16$, and for $\lambda = 1.35$ cm, $\delta T = 1.4$°C and $k = 0.067$.

The best results (minimum values of k and δT) ensure the pairs of λ_1 and λ_2, which *include the wavelength* 1.35 cm: 10 mcm and 1.35 cm (case 2), 5.7 mm and 1.35 cm (case 4), 1.35 cm and 5 cm (case 6). Here, as typical for modern radiometers values of errors ΔT_{i1}, ΔT_{i2}, it is possible to amount the accuracy of the parameter δT estimates to 0.25–0.3°C and, therefore, to derive the reliable estimates of seasonal variations of the monthly mean differences ΔT, which are varied from 0.5 to 3°C in the EAZO Gulf Stream.

And more results of our study show that it is sufficient to use merely a pair of wavelengths to estimate the parameter ΔT and its seasonal variations with a use for oceanologist's and climatologist's accuracy, in spite of the fact that the SOA radiation characteristics depend not only on the parameters T_w and T_a, but also on the air humidity. This fact, which is substantial for understanding the capabilities of remote diagnostics of the SOA interface at microwaves and infrareds, can be justified solely by close correlation between monthly mean temperature and humidity characteristics of the atmosphere appearing in this zone and in the middle and high latitudes generally.

2.4 Brightness Temperature as the Characteristic of Seasonal and Interannual Dynamics of the Ocean–Atmosphere Heat Interaction

2.4.1 T_w, T_a – loops as Characteristics of Heat Exchange Between the Ocean and Atmosphere

Here, we state one approach of the utilization of the data of long-term MCW radiometric measurements settled on (described in Lappo et al. (1990)) the method of determination of integral (averaged per year) sensible and latent fluxes at the SOA interface, which is prevailing in *climatic* studies. The method is based on the fact discovered by authors that a magnitude of integral heat flux depends not only on

values of monthly mean water surface and air near-surface temperatures, but on forestalling (lag) one of these with respect to another during a year cycle. We ought to keep in mind the fact that parameters T_w and T_a are adapting one to another over a 1-year and more long periods; their average values during these periods are practically equal. In the *seasonal* time scales, when intending to estimate an intensity of the ocean–atmosphere heat exchange and the character of this process in various situations (either a heat influx is directed from the ocean to atmosphere or from the atmosphere to ocean), we certainly require to take into account the degree of match (dismatch) of these parameters (Lappo et al. 1990). The interannual variations of monthly mean parameters T_w and T_a can be visually presented in the form of specific trajectories – (T_w, T_a) loops in the two-dimensional system of coordinates (see Fig. 2.15). Namely, an availability of the time shift between the evolutions of the parameters T_w and T_a predetermines the folded kind of their visual presentation.

It was shown that such geometric characteristics as the loop squares and their orientations, the degree of distinctions of their forms from the rectangular ones, etc. can be served as the quantitative characteristics of intensity of heat processes in the SOA interface.

Taking into account a close correlation between the SOA own (oceanographic, meteorological, and aerologic characteristics) and its MCW and IR radiation characteristics, we can expect that this method is effective in the case when we will use
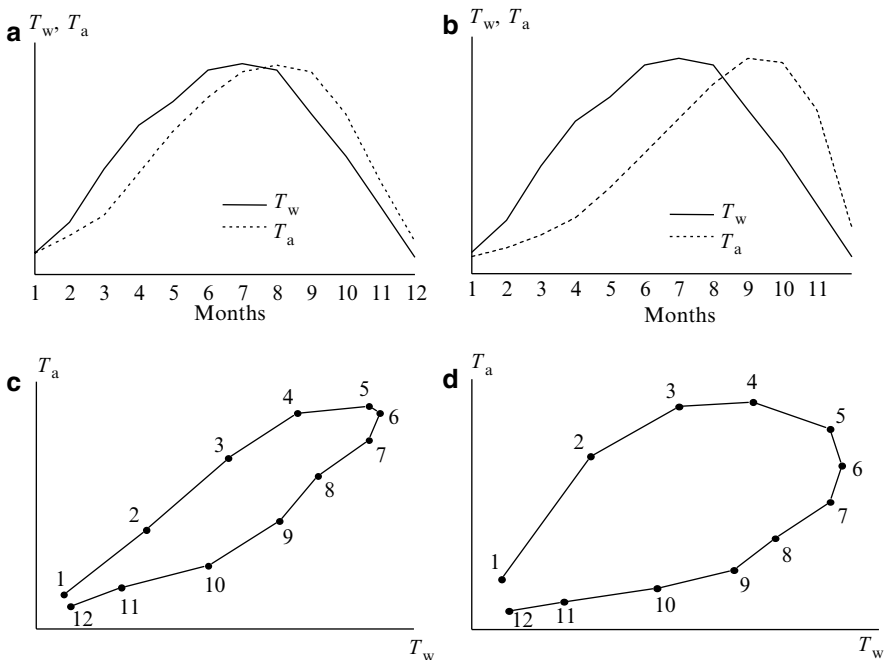
Fig. 2.15 Annual evolutions of monthly mean parameters T_w and T_a (**a**, **b**) and their phase trajectories (**c**, **d**) the figures denotes the months of year

in place of parameters T_w and T_a suitable values of brightness (radiation) temperatures of the SOA for estimating an intensity of heat interchanges between the ocean and atmosphere in different areas of the World ocean and estimate the annual heat fluxes and their intraannual variability.

2.4.2   Ways to Use the Brightness Temperature Loops for Estimation of Annual Heat Fluxes

So, due to a sensitivity of the SOA natural MCW and IR radiation to variations of the oceanic surface and atmospheric near-surface atmospheric temperature, we can construct some analog of the processes existent in the system interface of heat processes in the SOA interface, that is, to build the radiation images of the annual T_w, T_a – cycles using as initial data, for example, the brightness temperature in the spectral interval 3–8 cm, where the highest possible values of sensitivity of the parameter T^b to variations of the parameter T_w is observed, and the brightness temperature at the wavelength 1.35 cm, which is a considerable source of information on the atmospheric temperature and humidity characteristics.

In comparison with traditional methods of estimating the annual heat fluxes based on the separated determination of the parameters T_w, T_a as the input values used in the bulk-formulas, the peculiarity of this approach consists in a more high stability of the estimates sought under effect of accidental errors. In this case, the final estimates of heat fluxes is based not only on the selected (monthly mean) samples, but assimilates their seasonal dynamics as a whole, that is, the possibility of accumulation of these data is used. If the data of measurements of the SOA brightness temperature are compared to the values of heat fluxes gathered a few times in a year in reference zones of the World ocean, we can successfully estimate the annual heat fluxes and their intraannual variability.

We studied the possibilities of MCW radiometric methods of determination of the annual sensible heat fluxes by way of comparing the characteristics of the brightness temperature annual loops computed with the climatic values of the SST, the atmospheric near-surface, and integral humidity in the Norwegian, Newfoundland, and Gulf Stream active zones of the North Atlantic taken from Handbook (1977)) and Tuller (1968)) (see Fig. 2.16 with the Newfoundland and Gulf Stream EAZOs taken as the examples).

The calculations were made with the radiation model (2.8) for the wavelengths 1.35 and 3.4 cm, which are traditionally used in meteorological and oceanographic satellites; it is seen from these results that the ratio between the loop squares for these EAZOs is of 1: 1.25: 2.33. The results of analysis of climatic (archival) data show:

1. The ratio between annual fluxes of sensible heat in the Newfoundland and Norwegian active zones is equal to 1.08 (estimations of the State Oceanographic Institute – SOI), to 1.16 (the Main Geophysical Observatory), and to 1.41 (the Institute of the Water Problems – IWP).
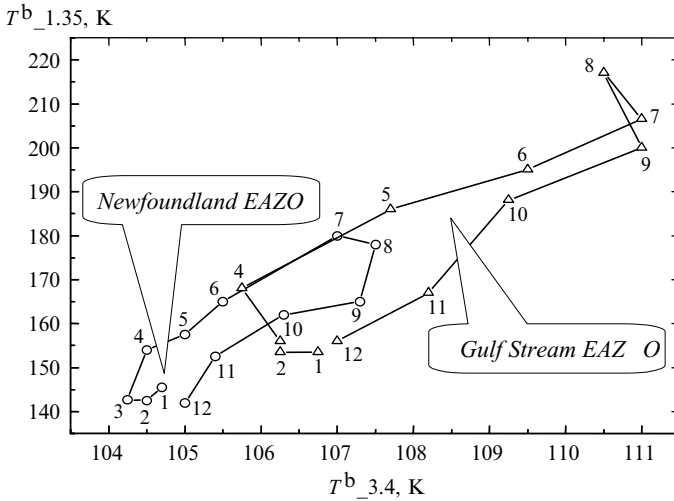
Fig. 2.16 Seasonal evolutions of the SOA monthly mean brightness temperatures at the wavelengths 1.35 and 3.4 cm in the Newfoundland and Gulf Stream active zones of the North Atlantic: figures – the months of the year cycle, counted from the January

Table 2.9 Estimates of the annual heat fluxes in active zones of the North Atlantic

	Heat fluxes (W m^{-2})			
Author (year)	Norwegian EAZO	Newfoundland EAZO	Gulf Stream EAZO	Tropical EAZO
Budyko (1962))	140	230	285	170
Bunker (1976)	150	240	380	165
Mintz (1979)	110	235	220	180
Lappo et al. (1990)	200	245	385	185
Birman et al. (1983)	70	120	185	155
Strokina (1989)	90	235	240	170
Grassl et al. (2000)	120	120	200	150

2. The ratio between annual fluxes of sensible heat between Gulf Stream and Norwegian active zones is varied from 1.24 (SOI) to 1.59 (IWP).

Excessive values of the annual sensible heat flux (a square of the $T^b\_1.35$-$T^b\_3.4$ loop) in the Gulf Stream EAZO can be explained by the specific of this oceanic area, namely by dominating the component of a latent heat in comparison with a sensible heat as a result of intensive evaporations from the water surface.

Let us note that the estimates of annual heat fluxes made by oceanologists strongly differ from one to another versions (see Table 2.9); it gives rise to some problems in validation of results of the MCW radiometric sensing the heat processes in the SOA interface.

2.5 Use of Satellite MCW Radiometric Methods to Determine the Role of Energy-Active Zones in the North Atlantic in Forming the Weather Conditions in the ETR

2.5.1 Initial Point

The concept of energy-active zones of the oceans (EAZOs) due to academician Marchuk (1979, 1989) and the problems of modeling short-period climatic changes and of early estimations of weather anomalies are currently occupying many researches. For example, Strokina et al. (1983) identified a significant link between Spring/Summer temperature and precipitation in the main agricultural regions of the Russia and changes in the water heat content (enthalpy) in a number of EAZOs of the North Atlantic over the previous winter and winter-spring periods. In Andrianova (1986)), based on joint analysis of a series of sea surface temperature (SST) and the near-surface air temperature at individual points of the European territories of Russia (ETR), it was shown that the SST anomalies in the regions of Gulf Stream and Newfoundland are manifest in the form of large-scale changes in the air temperature over the ETR after 2–3 months. The research in Vazhnik and Chistyakova (1989) confirms the existence of active areas in the North Atlantic and shows that it is possible theoretically to forecast anomalies of the winter (January) air temperature over the Western Part of ETR 2 months beforehand. The important role of EAZO in relation to the development of weather trends and short-period variations of the climate is also confirmed by the results of research expeditions carried out within the framework of the RAZREZY program (Marchuk, 1989). Remote, and in particular, satellites methods of studying the physical processes in the Earth's weather (climatic) system have a special value (Dymnikov et al. 1984; Becker and Seguin 1985; Malkevich, 1986; Kozoderov 1989). Significant experience in the use of national and international satellite facilities has been recognized when applying it to the following:

- Determination of meteorological parameters of the atmosphere
- Retrieval of the ocean surface temperature
- Monitoring of the state of the oceanic surface using the MCW and IR passive radiometric methods
- Analysis of synoptic and mesoscale properties of hydrophysical fields in the ocean suing radar and high-resolution optical and IR scanners
- Estimation of the radiation balance of the SOA in the IR band

Numerous results have confirmed also the effectiveness of using satellite passive radiometric means to determine some climatic-mean characteristics of the system "land covers-atmosphere" from space at microwaves.

2.5.2   Our Approach

To analyze the effect of the EAZO on the weather conditions over the adjacent continents to these areas, we associated the latter with parameters such as the air temperature, the form and the quantity of clouds and the soil moisture content, or with the deviations of these from the monthly mean norms (Strokina 1983; Andrianova 1986; Vazhnik and Chistyakova 1989; Nikolaev 1981). As a generalized parameter characterizing the balance of heat and humidity, we will use the so-called radiation index of dryness R = Pinc/Pevap, which is the ratio of the heat incident on a given area of the earth surface (Pinc) to the amount of heat required to evaporate the precipitation falling in this area over a specific period (Pevap) introduced long ago in Grigor`ev and Budyko (1956). As the theoretical and experimental results show, the MCW and IR radiometric methods can provide us the reliable information on the soil humidity, the temperatures of the atmosphere, and of the land surface and enable us to reliably recognize the precipitation zones.

It was the especially important observation made in Reutov and Shutko (1987) and Reutov (1989) that an intensity of natural MCW radiation of the land surface for specific scales of spatial and temporal averaging can serve as a *direct* (natural) measure of the parameter R. The physical uniformity of this parameter and the enthalpy of the oceanic upper layer Q_Σ is the reason to carry out an analysis of these characteristics as having a similar heat and energy nature and depending on the processes of heat transfer between the underlying surface and atmosphere. This fact means that the choice of the value of radiation index of dryness R as the parameter describing the reaction of atmospheric processes over continents to the effects of EAZOs is promising, in particular, in studying the influence of the North Atlantic EAZO on the weather conditions of the ETR.

We compared the variations (from month to month) of the average multiyear values of the parameter R for the ETR and the intensity of the heat exchange at the points "M" (Norwegian EAZO) and "E" (Gulf Stream EAZO) in the North Atlantic (Grankov and Shutko 1992, 1997). In this comparison we considered both components of the heat exchange between the ocean and the atmosphere, namely, the vertical turbulent fluxes of sensible heat and the so-called heat loss (latent heat) due to evaporation (which is significant for the point "E"); the necessary data are taken from Nikolaev (1981)). The estimates of the radiation index (in arbitrary units) were obtained by calculating the relationship between the amount of heat in the air and the loss of heat due to evaporation (thawing) of the precipitation, taking into account data about the monthly mean air temperature and the precipitation intensity given in Handbook (1964). The mean values of this index for the ETR and some other regions were determined from partial values for the towns Murmansk, Leningrad (St. Petersburg), Kiev, Kirov (Vyatka), Sverdlovsk (Ekaterinburg), and Moscow. The results obtained for the point "E" shown at Fig. 2.17 confirm that the variations of monthly mean values of the parameter R in these territories with a delay of 2–3 months are correlated with changes in the monthly mean heat of a heat
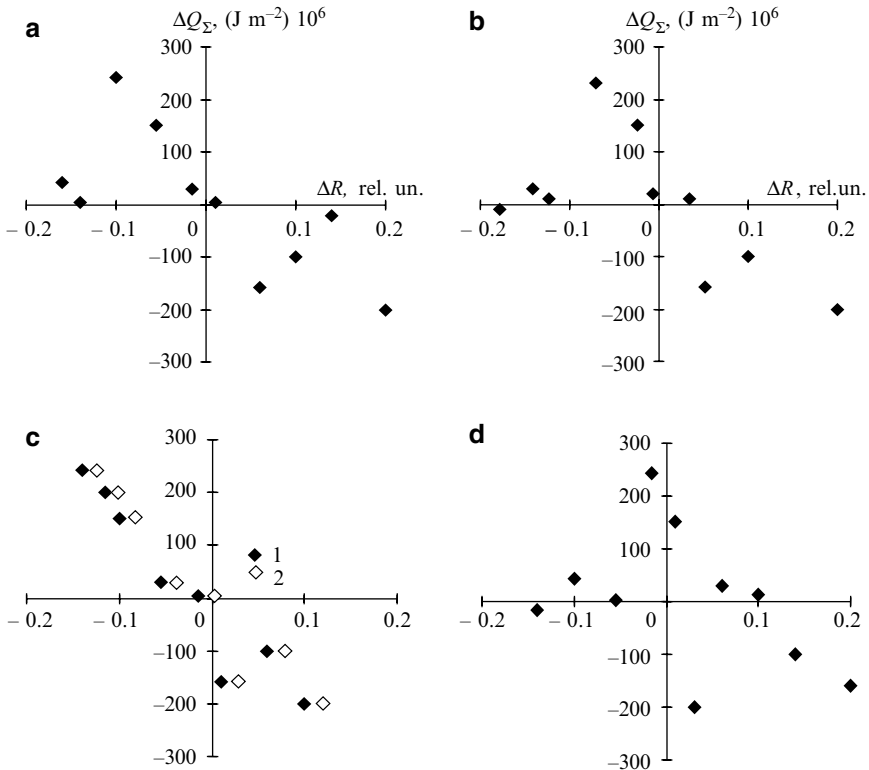
Fig. 2.17 Comparison of the variations of monthly mean values of the oceanic heat content in the upper oceanic layer at the point "E" ΔQ_Σ and the radiation index of dryness ΔR (in relative units) for conditions: (**a**) variations of ΔR synchronous with that of ΔQ_Σ; (**b**) ΔR is 1 month behind ΔQ_Σ; (**c**) 2 months behind (1) and 3 months behind (2); and (**d**) ΔR is 1 month ahead of ΔQ_Σ

content of the oceanic upper layer exchanges in the given area of the North Atlantic. There is a less strict correlation between the value ΔQ_Σ and the variations of the air temperature ΔT_a, which only reflects the component of the radiation index of dryness associated with transformations of the flux of sensible heat in the atmosphere and does not take into account the latent heat associated with precipitation. At the same time, the results of the atmospheric circulation and their comparative analysis show that it is possible to use the difference between the monthly values of the oceanic surface and the near-surface air temperatures as equivalent to the intensity of the heat exchange processes at the point "E" in the North Atlantic in studies of their effects on variations of the weather characteristics over the ETR (Fig. 2.18).

We observed also the influence of the heat properties of the ocean at the point "M" of the North Atlantic on the radiation index of dryness of the ETR; in this case the time delay between the parameters ΔQ_Σ and ΔR is minimal due to their geographical closeness to the ETR. Thus, we can test a *separate* idea of influence of the energy active zones in the oceans on the weather characteristics of the *adjacent*
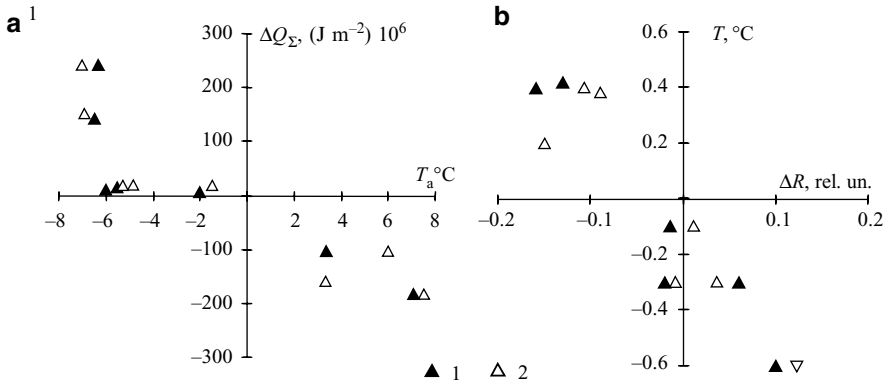
Fig. 2.18 Comparison of the variations of monthly mean values of: (**a**) an intensity of heat content in the oceanic upper layer ΔQ_{Σ} at the point "E" (excluding the winter months) and the averaged over the ETR air temperature ΔT_a; and (**b**) the difference between the oceanic surface and the atmospheric near-surface temperatures ΔT and radiation index of dryness ΔR (in relative units) for conditions that the weather changes over the ETR are (1) 2 months and (2) 3 months later than the ΔQ_{Σ} variations

continents for various systems such as the "Gulf Stream outflow in the Norwegian sea/the North Europe territories," the "Kuroshio current source/the East Asia territories," etc. It is hard to propose that these phenomena might be useful as the long-term predictors of weather changes in these territories, but we assume their usefulness when analyzing the sources of their current (synoptic and seasonal) developments in these systems.

So it seems to be perspective the using of satellite MCW and IR means and methods in studies of the influence of heat processes in the North Atlantic EAZOs on the radiation index of dryness at the territory of ETR as a whole as well as at some of its adjoining points as the Ekaterinburg (trans-Ural area), Kiev (Ukraine). Let us note that both processes are accessible for the MCW radiometric measurements in the millimeter and centimeter range of wavelengths (related to the parameter ΔQ_{Σ}) and at the decimeter range of wavelengths (related to the parameter ΔR).

This conception can be entirely realized using various satellite systems with moderate spatial resolution comparable with the sizes of EAZOs (of 300–500 km) and considerable time averaging during of 30–40 days.

2.6 Conclusion

An influence of the oceanic water surface temperature T_w on the SOA brightness temperature is the passive factor in comparison with the near-surface air temperature and integral water vapor content of the atmosphere observed in the experiments NEWFOUEX-88 and ATLANTEX-90 in the range of synoptic time scales. This fact possibly is not evident for oceanologists and climatologists in their traditional

understanding of the role of using the remote sensing methods, when only the partial parameters of the SOA interface are used in retrieving the heat fluxes in the ocean–atmosphere interface with the well-known procedures such as the bulk-formulas. Such result can be justified by an intensive variability of the atmospheric parameters T_a, e, and Q, as well as their close correlation determined by the processes of the horizontal air movements in the near-surface and the boundary layers masses typical for middle and high latitudes. This effect excites the brightness contrasts at the synoptic time scales exceeding in ten times the contrasts produced by variations of the parameter T_w because the influence of the vertical heat transfer on the MCW radiation characteristics is weaker in comparison with the effect of the horizontal heat transfer on the atmosphere.

The significant and unique effect observed in these tasks is a high sensitivity of the SOA brightness temperature at the wavelength 1.35 cm to variations of the atmospheric parameters determining the processes of heat transfer through the ocean–atmosphere boundary.

References

Andrianova OR (1986) The connection between thermal anomalies in the Northen Atlantric and in the Europenian territory of the USSR. Meteorol Gidrol 7:114–116 In Russian

Arefjev VN (1991) Molecular absorption of emission in the window of relative transparency of the atmosphere 8–13 mcm (review). Fiz Atm Okeana 27:1187–1225 In Russian

Basharinov AE, Gurvich AS, Egorov ST (1974) Radio emission of the planet Earth. Nauka, Moscow In Russian

Becker F, Seguin B (1985) Determination of surface parameters and fluxes for climate studies from space observations. Methods, results, and problems. Adv Space Res 6:299–317

Birman BA, Larin DA, Pozdnyakova TG (1983) Some questions of climatology of heat echanges in energy active zones of the World ocean. Meteorol Gidrol 5:79–86 In Russian

Budyko MI (1962) The Earth heat balance atlas AN SSSR (in Russian)

Bunker AF (1976) Computations of surface energy flux and annual sea-air interaction cycles of the North Atlantic ocean. Mon Wea Rev 96:1122–1140

Dymnikov VP, Korotaev GK, Ya Galin V (1984) Atmosphere, ocean, space – "Razrezy" program. VINITI, Moscow In Russian

Grankov AG, Resnjanskii JuD (1998) Modeling the response of the ocean-atmosphere natural radiation system to the pertrubation of a thermal equilibrium at the interface. Russian Meteorology and Hydrology, Allerton Press 11:57–65

Grankov AG, Shutko AM (1992) Use of remote radiophysical methods to determine the role of energy-active zones of the ocean in the development of the weather on the continents. Sov J Remote Sens 9:926–941

Grankov AG., Shutko AM (1997) Use of the methods of microwave and infrared radiometry for studying the role of active zones of the world ocean in forming the weather conditions at continents. In: Donelan MA, Hui WH, Plant WJ (ed) The air-sea interface (radio and acoustics sensing, turbulence and wave dynamics), Miami, pp 593–598

Grassl H, Jost V, Schulz J et al (2000) The Hamburg ocean-atmosphere parameters and fluxes from satellite data (HOAPS): a climatological atlas of satellite-derived air-sea interaction parameters over the world oceans. Report No. 312. MPI, Hamburg

Grigor`ev AA, Budyko MI (1956) A periodic mechanism for geographical zoning. Doklady AN SSSR, 110:129–132

Gulev SK, Kolinko AV, Lappo SS (1994) Synoptic interaction between the ocean and atmosphere in middle latitudes. Gidrometeoizdat, St. Petersburg In Russian

Handbook (1964) Atlas of the physical geography of the World AN SSR and GUGiK, Moscow (in Russian)

Handbook (1977) Atlas of the oceans: Atlantic and Indian oceans. MO SSSR, Moscow (in Russian)

Handbook (1979) Averaged month, 10 and 5-day periods values of the air water and temperature, their difference and wind speed in selected regions of the North Atlantic (1953–1974 years). VNIIGMI-MZD, Obninsk (in Russian)

Kozoderov VV (1989) Energetics of the Earth`s climatic system Issled. Zemli iz kosmosa 5:3–13 In Russian

Laihtman DA (1976) Dynamical meteorology. Gidrometeoizdat, Leningrad In Russian

Lappo SS, Gulev SK, Rozhdestvenskii AE (1990) Large-scale heat interaction in the ocean–atmosphere system and energy-active zones in the world ocean. Gidrometeoizdat, Leningrad In Russian

Lebedeva EL (1991) Integral water vapor content of the atmosphere as the characteristic of air-sea interaction in the Newfoundland energy active zone. Trudy Glavnoi Geofizicheskoi Observatorii, Leningrad 535:32–45 (in Russian)

Malkevich MS (1986) Main results of remote sensing of the ocean-atmosphere system from satellites and the study of heat and moisture exchange in the system. Atmosphere, Ocean, Space -"Razrezy" Program, VINITI, Moscow 7:145–165 (in Russian)

Marchuk GI (1979) Modeling of climate changes and long-range weather forecasting. Meteorol Gidrol 7:25–36 In Russian

Marchuk GI (ed) (1989) Scientific programme to study the influence of energy-active zones of the oceans on climatic fluctuations ("Razrezy" Program). Gidrometeoizdat, Moscow In Russian

Mintz Y (1979) Simulation of the oceanic general circulation. GARP Publ Ser 2:607–687

Nikolaev Ju V (1981) The role of the large-scale interaction of the ocean and the atmosphere in the development of weather anomalies. Gidrometeoizdat, Leningrad In Russian

Paramonova NN (1985) Comparison of results of new laboratory measurements of emission absorption in water vapor in the window 8–12 mcm with data of natural experiments. Trudy Glavnoi Geofizicheskoi Observatorii, Leningrad 496:79–84 In Russian

Perevedentsev Ju P (1984) Circulation and energy processes in the atmosphere. Kazan University, Kazan In Russian

Pinus NZ (1982) Available potential energy in the atmosphere and it transformation in the kinetic energy. Meteorol Gidrol 4:106–116 In Russian

Reutov EA (1989) On intercorrelation of microwave and IR radiation of natural objects with their state. Issled Zemli iz kosmosa 1:70–76 In Russian

Reutov EA, Shutko AM (1987) On correlation of radiobrightness temperature with the radiative index of dryness. Issled Zemli iz kosmosa 6:42–48 In Russian

Shutko AM (1986) Microwave radiometry of water surface and soils. Science, Moscow In Russian

Strokina LA (1989) Heat balance of the oceans surface (handbook). Gidrometeoizdat, Leningrad In Russian

Strokina LA, Chuvashina IE, Yudin MI (1983) Changes in the heat content of water in the North Atlantic as an indicator of processes with long-term consequences. Meteorol Gidrol 4:67–75 In Russian

Tuller ST (1968) World distribution of mean monthly and annual precipitable water. Monthly Weather Rev 96:785–797

Vazhnik TP, Chistyakova EA (1989) A method for forecasting the air-sea anomalies in the Northern Atlantic and the European territory of the USSR in western Siberia and North Kazhakstan using the water temperature in active zones of the North Atlantic Search Earth from Space), Tr. GidrometCenter, 303:127–134 (in Russian)

Xrgian (1978) Fysics of the atmosphere, vol.1, Leningrad (in Russian)

Zhevakin SA, Naumov AP (1964) Absorption of centimeter and millimeter radiowaves in water vapor of the atmosphere. Radiotekhnika i Elektronica 9:1327–1337 In Russian

Zhevakin SA, Naumov AP (1965) On determining the coefficient of absorption of centimeter radiowaves in atmospheric oxygen. Radiotekhnika i Elektronica 10:987–996 In Russian

Chapter 3
Interconnection Between the Brightness Temperature and an Intensity of the Heat Ocean–Atmosphere Interaction: Experimental Results

3.1 Assimilation of Satellite-Derived Microwave Radiometric Data in Parameterizations of Heat Exchange Between the Ocean and Atmosphere (Based on the Atlantex-90 Experiment)

3.1.1 How it is Possible to Use the Parameter Q in Estimating the Synoptic Variations of Parameters e and T_a in Midlatitudes

Earlier, using the data of experiments NEWFOUEX-88 and ATLANTEX-90, we discovered close correlation between total water vapor content Q in the atmosphere and its near-surface temperature T_a and humidity (vapor pressure e) in the synoptic range of time scales.

Now, let us try to answer the question: is it possible to use parameter Q instead of parameters T_a and e in the formulas of Global Bulk Aerodynamic Method to estimate a synoptic variability of sensible and latent heat fluxes at the ocean–atmosphere boundary.

Answer to this question can be searched on the basis of data from combined hydrological, meteorological, and aerologic observations conducted on the R/V *Volna* of the State Oceanographic Institute in April 1990 in the North Atlantic Newfoundland EAZO within the framework of the ATLANTEX-90 experiment. The research vessel was located in the eastern branch of the cold Labrador Current, 40 miles from a hydrological front formed by the Labrador Current and a warm quasi-stationary Gulf Stream anticyclonic vortex. The vortex leads to the regeneration of cyclones and determines a strong synoptic variability of oceanic and atmospheric parameters in this region (Gulev et al. 1994). Thus, the amplitudes of the near-surface temperature and humidity and of the total water vapor content of the atmosphere during the passage of a cyclone typical of this region and season (April 15–19) are respectively 9.9°C, 4.7 hPa, and 3.5 g cm⁻².

From the extensive set of data accumulated over the whole period of measurements from the R/V *Volna* (24 February–15 May 1990), we selected data only for

the stationary (April) phase of the experiment (April 4–21, 1990), which differed from the other phases by the following peculiarities:

(a) The highest frequency and regularity of hydrological, meteorological and, especially, aerologic measurements in that period
(b) The possibility of studying the temporal dynamics of oceanic and atmospheric parameters due to a stationary position of the vessel (48°N and 46°W in the North Atlantic)

From the April data, the following parameters were selected for further analysis:

– Hourly values of sea surface temperature T_w, near-surface air temperature T_a, humidity (vapor pressure) e, and wind speed V derived from hydrological and meteorological measurements
– Results of aerologic measurements of total atmospheric vapor content Q with periodicity 6-h
– Hourly estimates of turbulent fluxes of heat q_h and vapor q_e calculated at the State Oceanographic Institute through traditional parameterizations (Guidelines 1981) from hourly measurements of T_w, T_a, V, and e

    The above-listed data form the basis for analysis of the relationships between synoptic variations of total atmospheric water vapor content, temperature and humidity of the near-surface air, and fluxes of sensible and latent heat at the ocean–atmosphere interface in the vicinity of the R/V *Volna* in the ATLANTEX-90 stationary phase.

3.1.2   Useful Parameterizations for This Approach

To answer the question whether the total atmospheric water vapor content can be used instead of parameters T_a and e for analysis of synoptic variability of sensible and latent heat fluxes, the original (taken from archival materials of the stationary phase of the experiment) values of q_h and q_e are calculated by standard methods (Guidelines 1981) from the R/V *Volna* hydrological and meteorological measurements with results of independent measurements of parameter Q.

$$q^*_h = c_0 + c_1 T_w V + c_2 T_a V; \qquad (3.1)$$

$$q^*_h = c_0 + c_1 T_w V + c_2 Q V, \qquad (3.2)$$

where T_w, T_a, V, and Q are data of standard measurements of water surface temperature, the near-surface air temperature and wind speed, and the integral water vapor content of the atmosphere averaged over every 24 and 6 h, respectively, during 18 days (April 4–21); the coefficients c_0, c_1, and c_2 are determined using the least-squares method by minimizing the discrepancy (residual) d between the original values of fluxes q_h and their estimates q^*_h for 24-h and 6-h averaging.

The analogical parameterization was examined for the fluxes of latent heat q_e

$$q_e^* = c_0 + c_1 \, T_w V + c_2 \, eV; \tag{3.3}$$

$$q_e^* = c_0 + c_1 T_w \, V + c_2 \, QV, \tag{3.4}$$

As an example, Fig. 3.1 shows average values of sensible heat fluxes q_h for every 24 h and also their approximate estimates q_h^*.

Let us note that parameterizations (3.1) and (3.3) include the same components that are used in traditional bulk-formulas for calculations of sensible and latent heat fluxes in a wide range of space and time scales and have a similar form, except that c_0, c_1, c_2 are invariable, while the coefficients in the bulk parameterizations generally depend on the near-surface wind speed. Parameterizations (3.2) and (3.4) follow from parameterizations (3.1) and (3.3) after the near-surface temperature T_a and (vapor pressure e) is replaced by Q; therefore, they contain only those components of the SOA that are reliably recorded by methods of satellite MCW and IR radiometry.

As seen from Figs. 3.1 and 3.2, parameterizations (3.1) and (3.3) provide a rather accurate approximation of the mean daily sensible and latent fluxes in the ATLANTEX-90 stationary phase; it is worthy to note that their efficiency is confirmed by measurement data obtained from the R/V *Volna* in other phases of the experiment, in March and May. However, the main result seen in Figs. 3.1 and 3.2 is that q_h and q_e are closely connected with q_h^* and q_e^*, calculated from (3.2) and (3.4), which use total vapor content of the atmosphere as a characteristic of sensible and latent heat fluxes. This result is the quantitative substantiation of the relationships between atmospheric vapor total content and the intensity of the ocean–atmosphere heat exchange in the synoptic range of time scales, studied in Lebedeva (1991).
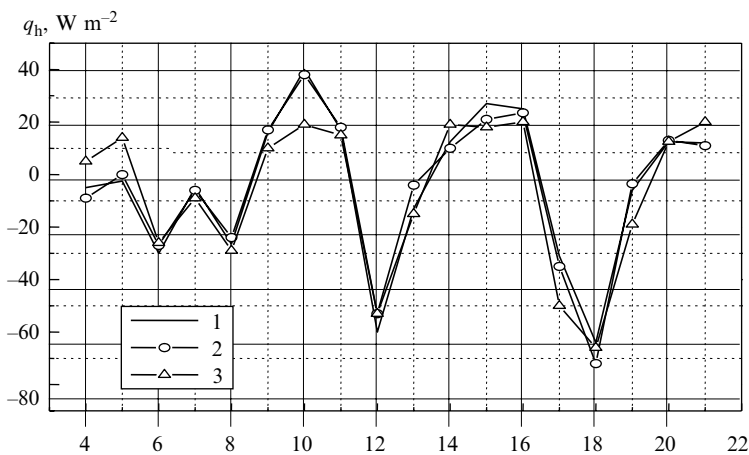
Fig. 3.1 Original (archival) values of sensible heat fluxes (1) and their approximations (2, 3) calculated from parameterizations (3.1) and (3.3), respectively
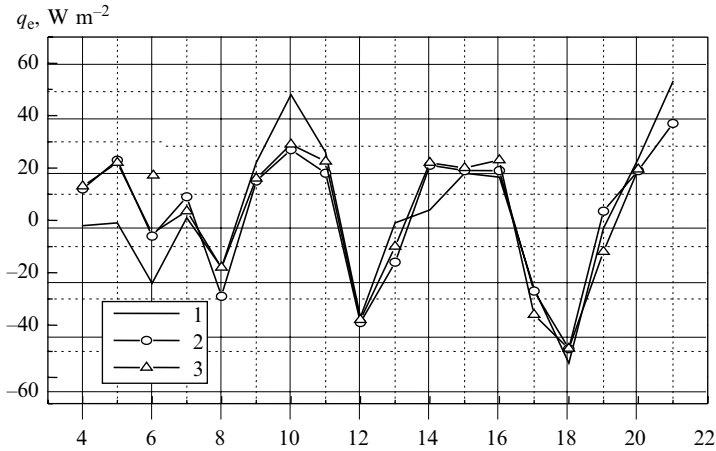
Fig. 3.2 Original (archival) values of latent heat fluxes (1) and their approximations (2, 3) calculated from parameterizations (3.3) and (3.4), respectively

More comprehensive results of analysis of the efficiency of the above-mentioned and other parameterizations of synoptic fluxes of sensible and latent heat in the ATLANTEX-90 stationary phase are given in Table 3.1, which contains the values of the residual d and of correlation coefficient r between q_h and q_h^*, q_e and q_e^*, and also the coefficients c_0, c_1, c_2 for various time averaging of standard measurement data.

The calculation results confirm the efficiency of parameterizations (3.1) and (3.3), which have the largest r and smallest d values (except for a one-parameter formula for moisture exchange $q_e(e)$ competitive with formula (3.3)).

Data in Table 3.1 show that the temperature and humidity of the near-surface atmosphere in bulk parameterizations can be replaced by total atmospheric vapor content. Thus, the residual in approximations of sensible heat fluxes q_h by formula (3.2) is 10–13 W m^{-2}, while the amplitude of q_h (Δq_h) variations attains 100 W m^{-2} with 24-h averaging and 160 W m^{-2} with 6-h averaging. The approximation of latent heat flux by formula (3.4) yields the following values: $d = 12$ W m^{-2}, $\Delta q_e = 105$ W m^{-2} with 24-h averaging and $d = 15$ W m^{-2}, $\Delta q_h = 205$ W m^{-2} with 6-h averaging. The quantity $\Delta q/d$, a valid signal/noise ratio, does not decrease upon transition from 24-h to 6-h averaging, which may be explained by the stability of the relationship not only between mean daily variations of Q and T_a, but also between their more dynamic (diurnal) variations.

Data in Table 3.1 also show that total atmospheric vapor content can be used most effectively as a characteristic of the heat and moisture exchange between the ocean and atmosphere when it is combined with sea surface temperature T_w and near-surface wind speed V: "truncated" one- and two-parameter modifications of (3.2) and (3.4) of the form of q_h, $e(Q)$, and $q_{h,e}(T_w,Q)$ have the similar values of the correlation coefficient r and larger values of the residual d between q_h and q_h^* and q_e and q_e^*.

Table 3.1 Sensible (q_h) and latent (q_e) heat approximations with 6-h (numerator) and 24-h (denominator) averaging for different parameterizations of heat and moisture exchange between ocean and atmosphere

Parameterizations	c_0	c_1	c_2	r	d
$q_h^* = c_0 + c_1 T_w + c_2 T_a V$	1.61/−0.84	1.53/1.64	−1.36/−1.36	0.99/0.99	4.16/4.09
$q_h^* = c_0 + c_1 (T_w − T_a) V$	3.24/1.99	1.35/1.34	–	0.99/0.99	4.23/4.21
$q_h^* = c_0 + c_1 T_w V + c_2 Q V$	22.7/17.9	0.61/1.45	−0.02/−0.02	0.91/0.93	13.0/10.4
$q_h^* = c_0 + c_1 T_w V + c_2 e V$	27.0/27.4	1.99/1.98	−0.93/−0.94	0.89/0.91	14.0/11.6
$q_h^* = c_0 + c_1 T_w + c_2 Q$	24.2/25.6	8.30/12.3	−0.23/−0.27	0.76/0.85	20.0/14.6
$q_h^* = c_0 + c_1 T_a$	12.3/12.0	−13.0/−12.8	–	0.88/0.90	14.6/12.4
$q_h^* = c_0 + c_1 Q$	36.4/43.8	−0.24/−0.28	–	0.76/0.84	20.3/15.3
$q_h^* = c_0 + c_1 T_w$	−30.6/−39.1	20.2/26.9	–	0.29/0.37	29.8/26.0
$q_e^* = c_0 + c_1 T_w V + c_2 e V$	25.7/27.1	2.70/2.64	−0.91/−0.93	0.86/0.89	15.4/1.3
$q_e^* = c_0 + c_1 T_w V + c_2 T_a V$	1.36/0.31	2.17/2.14	−1.29/−1.28	0.94/0.93	10.4/9.73
$q_e^* = c_0 + c_1 T_w V + c_2 Q V$	21.6/17.8	1.35/2.04	−0.02/−0.02	0.87/0.89	14.7/12.2
$q_e^* = c_0 + c_1 T_w + c_2 Q$	31.2/32.0	8.71/12.2	−0.23/−0.26	0.79/0.85	18.6/14.1
$q_e^* = c_0 + c_1 T_w$	17.6/1.7	−11.2/−11.3	–	0.78/0.82	18.7/15.7
$q_e^* = c_0 + c_1 Q$	43.9/49.9	−0.24/0.27	–	0.78/0.84	18.9/14.8
$q_e^* = c_0 + c_1 e$	122.0/118.0	−19.2/−18.6	–	0.92/0.94	11.9/9.5

Thus, analysis of data from hydrological, meteorological, and aerologic measurements made aboard the R/V *Volna* in the Newfoundland EAZO suggested that bulk parameterizations used for calculating vertical turbulent fluxes of sensible and latent heat over the ocean can be reconstructed in the form of combinations of only those parameters of the ocean–atmosphere system that are directly related to satellite-derived characteristics of MCW and IR natural radiation of the system. The reconstruction is based on a close relation between temperature and humidity of the near-surface layer observed in the ATLANTEX-90 stationary phase (April 4–21, 1990) in the synoptic range of time scales.

3.2 Experimental Studies of Interrelation Between the Brightness Temperature and Synoptic Heat and Impulse Fluxes (Based on the NEWFOUEX-88 and ATLANTEX-90 Experiments)

3.2.1 SSM/I Radiometer of the DMSP Satellites

The multichannel radiometer SSM/I (Special Sensor Microwave/Imager) is one of the best satellite passive microwave radiometric systems operated in the last 13 years within the framework of Defense Meteorological Satellite Program – DMSP), designed for the long-term monitoring of the Earth to provide US Forces with

Table 3.2 Main parameters of the SSM/I radiometer

Frequency (GHz)	19.35	22.235	37.0	85.5
Wavelength (cm)	1.55	1.35	0.81	0.35
Polarization (V/H)[a]	V, H	V	V, H	V, H
Symbol of channels used	19.35V(H)	22.2V	37V(H)	85.5V(H)
Spatial resolution (km)	43×69	40×60	29×37	13×15
Sensitivity (K)	0.7	0.7	0.4	0.8

[a]*V* vertical polarization, *H* horizontal polarization

global meteorological, oceanographic, and solar-geophysical information (Kramer 1994) (in December 1992, the DMSP data were declassified and become available for the civil and scientific community). The operative satellites of the DMSP series have a solar-synchronous low circular orbit close to the polar tilted by $98.8°$ with an altitude of about 850 km and period of 102 min (14.2 circuits per day). Presently, several satellites of this series (F-10, F-11, F-12, F-13, F-14, and F-15) are actively operating in space for last few years.

The radiometer SSM/I of the satellite F-08, which is out of operation since December 1991, is of a particular interest in our investigations because it was the only satellite microwave radiometric means of the Earth observation in 1988 and 1990 years during the wide-scale experiments NEWFOUEX-88 and ATLANTEX-90. This device was designed for the global and synoptic sounding the atmospheric liquid water content in clouds (parameter W), precipitation intensity I, water vapor integral content (parameter Q) wind speed (parameter V), and different land and ice cover parameters. This is a scanning seven-channel four-frequency system under the angle of $52°$ at the horizontal and vertical polarizations (see its parameters in Table 3.2) for measuring the SOA brightness temperature in a view band of 1,400 km providing global coverage of the Earth in 3 days and incomplete coverage in a day (Hollinger et al. 1990).

The description of the data of ship-borne and satellite-derived passive micro-wave radiometric measurements used in the analysis of the correlation between the SOA brightness temperature and the boundary heat fluxes at the stationary phases of the NEWFOUEX-88 and ATLANTEX-90 experiments is presented in Table 3.3.

A unique archive of long-term satellite data was obtained with the help of the radiometer SSM/I in the NASA Marshal Center (MSFC, specifically – in its DAAC). To determine the brightness temperatures with the SSM/I device, its telemetric data (forming the SSM/I archive) were transformed for each channel into the antenna temperatures using a priori known *antenna-feeder-radiometer* tract parameters with a help of the absolute calibration principle. Then the antenna temperatures measured directly by satellite radiometers were converted in the SOA brightness temperatures through a parameterization of the so-called equation of smoothing. Both stages were passed with the algorithms developed by Wentz (1991).

Table 3.3 Description of ship-borne and satellite-derived microwave radiometric measurements used at the stationary phases of the NEWFOUEX-88 and ATLANTEX-90 experiments

Type	Sources	Makeup	Volume	Purposes
Meteorological observations	R/Vs *V.Bugaev, Musson,* and *Volna*	Ocean surface temperature, near-surface wind speed	More than 2,000 observations with 1-h resolution	Determination of heat, moisture, and momentum fluxes; evaluation of the ocean surface microwave radiation characteristics
Aerologic observations	R/Vs *V.Bugaev, Musson,* and *Volna*	Air temperature, humidity, pressure within 10–16,000 m at 20 levels	More than 400 observations with an interval of 6 h	Determination of the integral water vapor content of the atmosphere; evaluation of the atmospheric microwave radiation characteristics
Satellite measurements	The SSM/I radiometer of the F-08 satellite (DMSP)	Brightness temperature frequencies 19.3, 37, 22.2, and 85.5 GHz for two types of polarization	More than 120 sessions of measurements with an interval of about 24 h	Validation of the modeling results

3.2.2 Comparison of the SSM/I-Derived and Evaluated Synoptic Variations of the SOA Brightness Temperatures

We compared the simulated SOA brightness temperatures evaluated from the vertical observations (toward the nadir) in oceanic areas where the R/Vs *V.Bugaev*, *Musson*, and *Volna* resided with simultaneous microwave radiometric measurement data derived from the SSM/I radiometer of the F-08 satellite during the stationary phases of NEWFOUEX-88 and ATLANTEX-90 experiments (Grankov and Mil'shin 1999). For this purpose, we analyzed data of the MSFC archive and selected some its fragments corresponding to surveys made in the areas of location of these vessels during March 3–23, 1988, and April 4–21, 1990. It was established then that the corresponding survey sessions fall on the morning (between 8:00 and 9:00, Greenwich time) and on the evening (between 21:00 and 22:30, Greenwich time), and the average interval between sessions is about 24 h.

Figure 3.3 compares the SOA brightness temperatures evaluated at the wavelength 1.35 cm with those obtained from satellite measurements. The temporal resolution of evaluated estimates (4 times a day) follows from the frequency of aerologic measurements, and the temporal resolution of the satellite measurements (about once a day) is governed by the frequency of satellite surveys.

Let us note that the theoretical estimates of the parameter T^b were obtained for a nadir-looking radiometer, whereas the SSM/I radiometer provides the brightness temperature measurements at the angle of $52°$. This is a reason to observe essential differences (of tens K) between *absolute* values of evaluated and measured brightness temperature for the RVs *V.Bugaev*, *Musson*, and *Volna*; at the same time, the correlation coefficient r between their *relative* variations ranges from 0.89 to 0.91. For areas where these weather research vessels were resided, the mismatch d (rms difference) between the evaluated and measured brightness temperatures ranges between 3 and 5 K, i.e., reaches 5−10% of the magnitude of the parameter T^b_1.35 variations. With the use of additional measurements at the wavelength 0.81 cm for vertical and horizontal polarizations (these data predominantly give information on the liquid water content in the clouds), the quantity d reduces to 2−3 K and the correlation coefficient r increases to 0.94−0.95; one can observe a good similarity of simulated and measured brightness temperatures in this case (see Fig. 3.4).

Formally, this result follows from the fact that the evaluation of the brightness temperatures is carried out from a model with three degrees of freedom instead of a model with one degree of freedom. A possible physical interpretation lies in the improvement of the signal-to-noise ratio in the channel 22V of the SSM/I radiometer due to the channels 37V, 37H (here, the signal received from the satellite is meant to be the brightness temperature variations caused by variations in the atmospheric water vapor content, and the noise is meant to be the brightness temperature variations caused by variations of the atmospheric cloudiness characteristics).

The relationships between the brightness temperature evaluated at 1.6 cm and that measured with the SSM/I radiometer at 1.55 cm are characterized by approximately the same values of the correlation coefficient and mismatch (discrepancy).
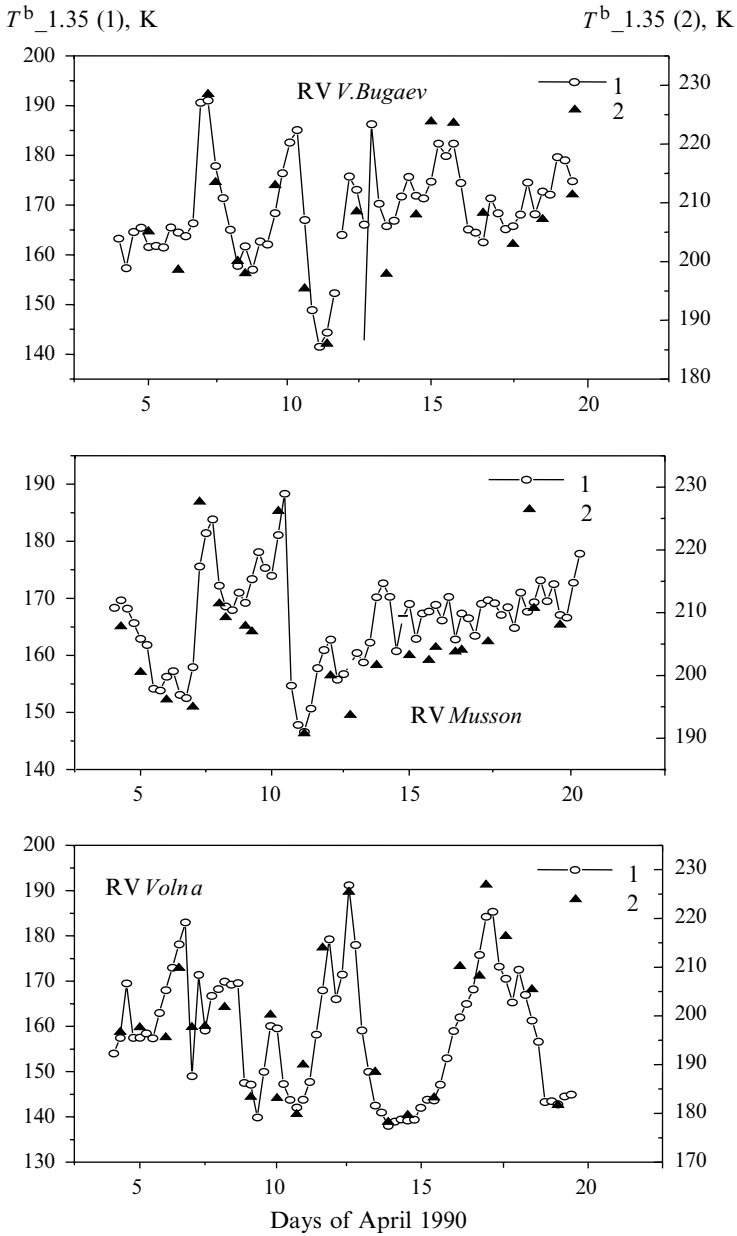
Fig. 3.3 Comparison of (1) the evaluated ocean–atmosphere brightness temperature (temporal spacing 24 h) for the resonance line of the water vapor at 1.35 cm during April 4–21, 1990

T^{b}_1.35/(1.35V +0.81V,H), K
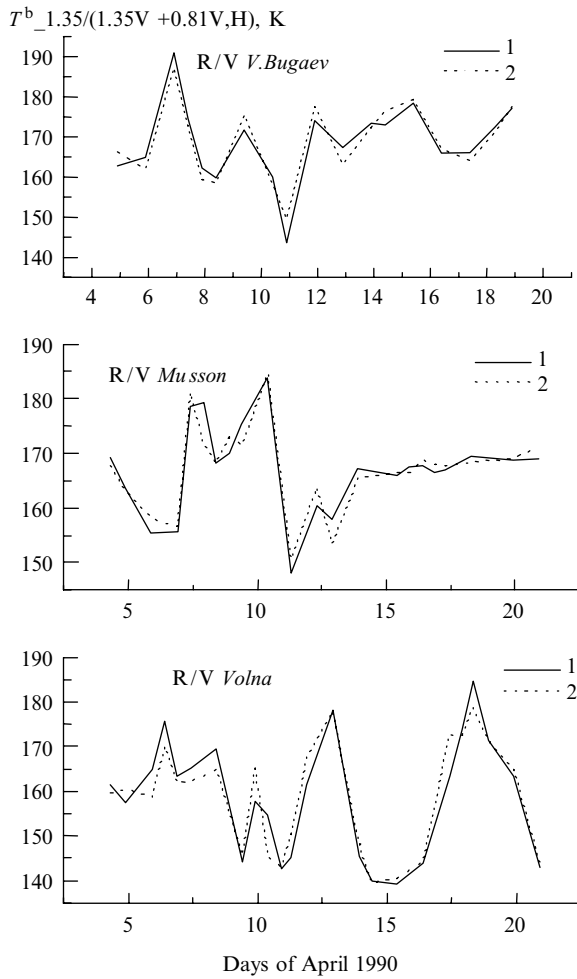
Fig. 3.4 Comparison of (1) the evaluated ocean–atmosphere brightness temperature at 1.35 cm and (2) the estimates from brightness temperatures measured by the SSM/I radiometer at wavelengths 1.35 and 1.55 cm during April 4–21, 1990 (temporal spacing 24 h)

Thus, there is a good agreement between theoretical and experimental estimates of the brightness temperature of the SOA natural microwave radiation during the stationary phases of the NEWFOUEX-88 and ATLANTEX-90 experiments.

Besides, as follows from results of the analysis made, the intensity of the brightness temperature variations (30–50 K) is much more than its minimal values (1−3 K) resoluted by the SSM/I radiometer. So this device can be served as an effective tool used for an analysis of the SOA heat interaction in the synoptic range of time scales.

3.2.3   Relations of the SSM/I-Derived Brightness Temperatures with the Near-Surface Fluxes of Heat and Impulse

The response of natural microwave radiation to variations of the heat fluxes at the SOA interface is most prominent during the passage of the midlatitude cyclones. For example, the cyclone of April 8–13, 1990 caused variations in the total heat fluxes of more than 800 $W\,m^{-2}$ for the R/V *V.Bugaev*, 500 $W\,m^{-2}$ for the R/V *Musson*, and about 2,000 $W\,m^{-2}$ for the R/V *Volna* (experiment ATLANTEX-90) (Gulev et al. 1994).

We analyzed relations of the SSM/I-derived SOA brightness temperature measured by various channels and the near-surface heat and momentum (impulse) fluxes observed in the stationary phases of the ATLANTEX-90 and NEWFOUEX-88 experiments. It was shown, for weak cloudiness, the brightness temperature in channel 22V and the brightness temperatures in channels 19V and 19H are good qualitative characteristics of the heat and momentum fluxes, respectively. In the general case, however, it is necessary to use the additional data of the measurements of channels 37V and 37H, which allow for the effect of cloudiness. Figures 3.5 and 3.6 show the results of a comparison of the ship-borne estimates of the total fluxes of heat q_{he} and momentum q_v recorded at the stationary phase of the ATLANTEX-90 experiment with their satellite estimates obtained as linear combinations of the brightness temperature values measured at the wavelengths 1.35 cm (channel 22V) and 0.81 cm (37V, and 37H). These combinations are constructed in such a way to ensure the minimum *rms* differences (mismatch) with the original values of q_{he} and q_v. Although the character of ocean–atmosphere heat at the places of the R/Vs *V. Bugaev*, *Musson*, and *Volna* is quantitatively and even qualitatively different, the estimates made afloat and aboard the satellites are in a good agreement.

The correlation coefficients of heat fluxes and their estimates are as high as $r=0.85$ for the R/V *V.Bugaev*, $r=0.73$ for the R/V *Musson*, and $r=0.84$ for the R/V *Volna*. The corresponding correlation coefficients for the momentum fluxes are 0.87, 0.81, and 0.84, respectively. The ratio of mismatch between the original fluxes and their satellite estimates to the maximum variations of fluxes varies from 12% (R/V *Volna*) to 19% (R/V *Musson*) for the parameter q_{he} and from 13% (R/V *Musson*) to 18% (R/V *V.Bugaev*) for the parameter q_v.

Figure 3.7 shows the results of applying this technique to the data of synchronous measurements from the satellite F-08 and weather research vessels *V.Bugaev* and *Musson* in the stationary phase of the NEWFOUEX-88 experiment. The correlation coefficients of heat fluxes and their estimates are as high as $r=0.85$ for the R/V *V.Bugaev* and $r=0.91$ for the R/V *Musson*.

The total heat fluxes estimated afloat at higher latitudes, at the point M (66°N, 2°E) of the Norwegian-Greenland EAZO (the data distributed by the Scientific Computing Division of the National Center for Atmospheric Research (NCAR) were submitted by courteously of Joerg Schulz, Germany) are also closely correlated with the satellite estimates made by linear regressions applied to the data obtained simultaneously from channels 22V, 37V, 37H, and 19V of the F-08 SSM/I radiometer in April 1988 (Fig. 3.8a).
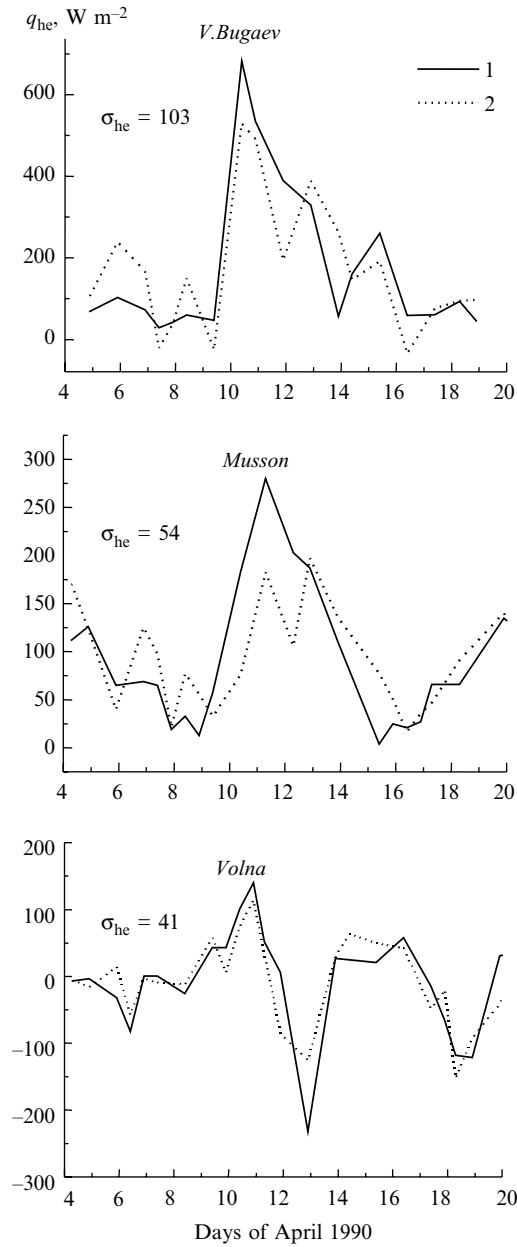
Fig. 3.5 Comparison of total heat fluxes q_{he} parameterized from vessel measurements (1) and their estimates (2) derived from the SSM/I channels 22V (1.35 cm), 37V, and 37H (0.81 cm). Experiment ATLANTEX-90
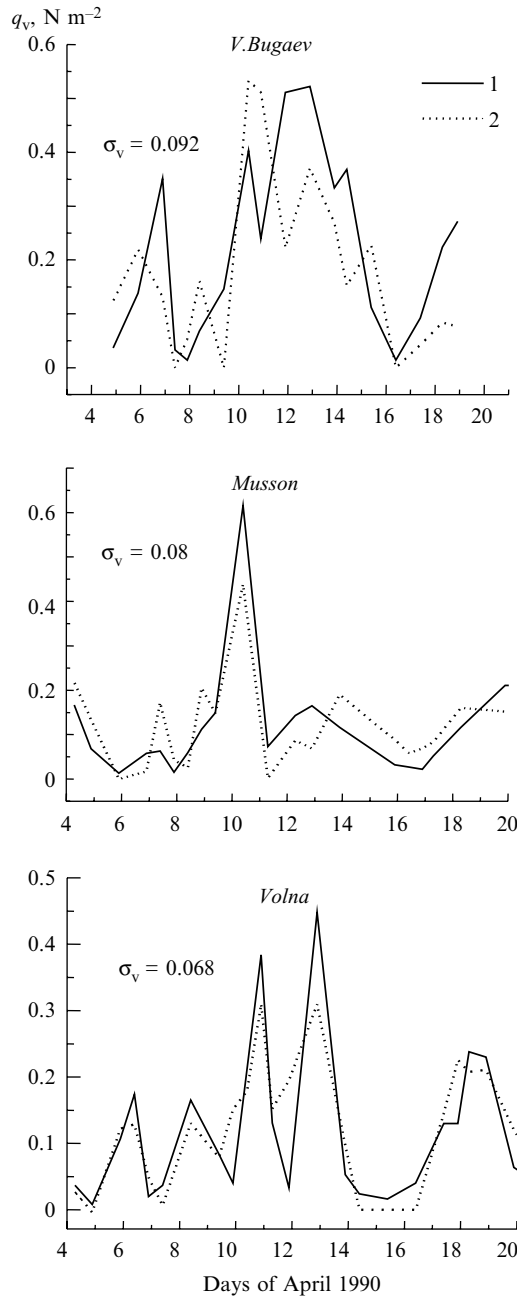
Fig. 3.6 Comparison of impulse fluxes q_v parameterized from vessel measurements (1) and their estimates (2) derived from the SSM/I channels 19V, and 19H (1.55 cm), 37V, and 37H (0.81 cm). Experiment ATLANTEX-90
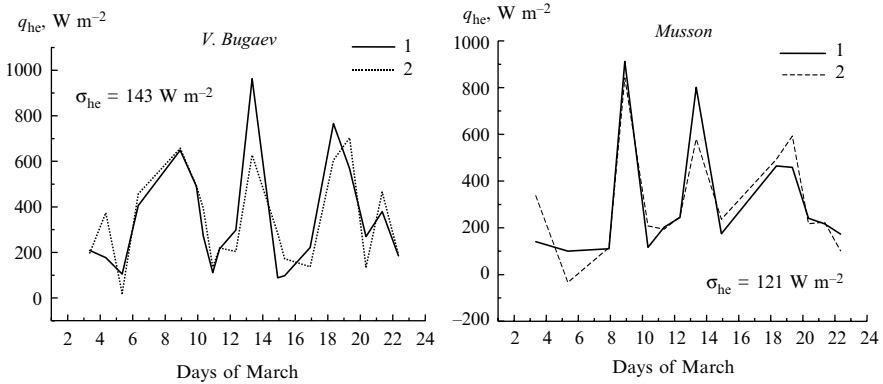
Fig. 3.7 Comparison of total heat fluxes q_{he} parameterized from vessel measurements (1) and their estimates (2) derived from the SSM/I channels 22V (1.35 cm), 1.55V, and 1.55H (19 GHz). Experiment NEWFOUEX-88

3.2.4 Stability of the Relationships Between the Vessel and Their Satellite Estimates

The stability of relations between the total heat fluxes and their satellite microwave radiometric estimates constructed by linear regressions applied to the data from the channels 22V, 37V, H, and 19V of the F-08 SSM/I radiometer is readily apparent from comparing the parameters q_{he} and q_{he}^* that were determined with a 2-year shift in time (i.e., during the NEWFOUEX-88 and ATLANTEX-90 stationary phases) in nearly the same areas of the Newfoundland EAZO (Fig. 3.9).

In our opinion, the following reasons add to the mismatch occurring in these experiments between direct and satellite estimates of the boundary heat and momentum fluxes and hamper the stability of interrelations between characteristics of the SOA natural microwave radiation and parameters q_{he} and q_v:

1. The areas where the R/Vs *V.Bugaev*, *Musson*, and *Volna* resided are characterzed by significant horizontal gradients of heat and momentum fluxes. For example, judging from the data (Gulev et al. 1994), in the area where the RV *V.Bugaev* resided and which is closest to the subpolar hydrologic front, the horizontal gradient of the total heat flux is as high as 2–4 W m^{-2}. As a result, the ambiguity in the parameters q_{he} can be 30–200 W m^{-2}, because the field of view of radiometer receiving antenna covers an area whose linear size can reach 15–50 km (see Fig. 3.10).
2. Ship measurements are shifted in time (to 30 min) relative to satellite measurements, which can introduce an additional error into the results of comparison; to our estimates, this error can reach 20 W m^{-2} for the parameter q_{he} and 0.03 N m^{-2} for the parameter q_v (see Fig. 3.11).
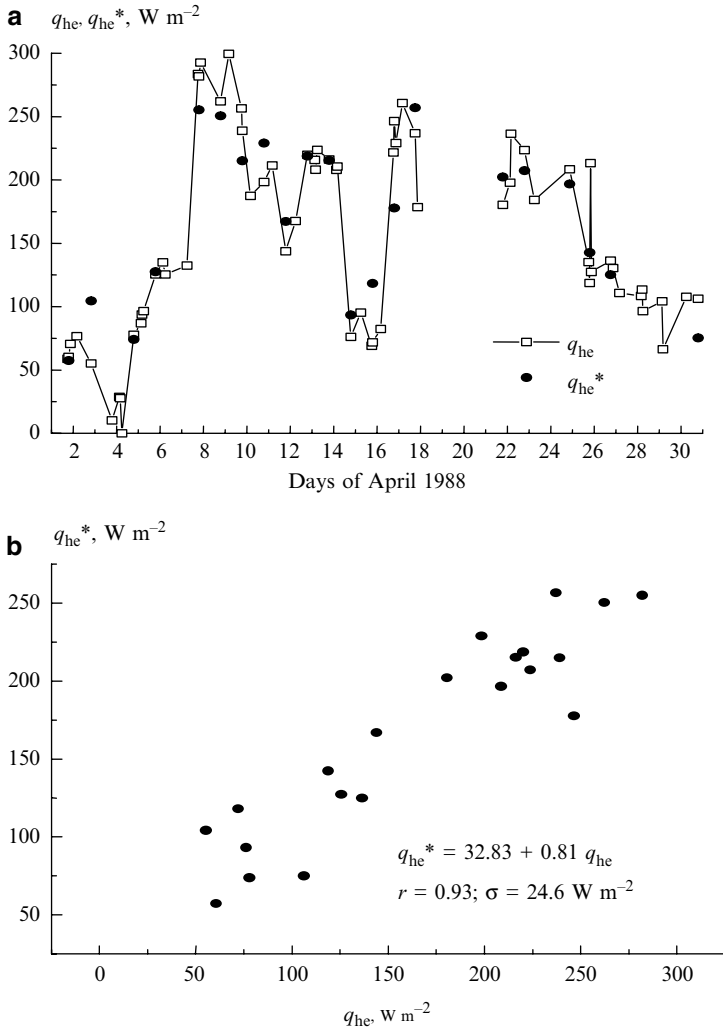
Fig. 3.8 Total heat fluxes parameterized from measurements of the weather ship M q_{he} and (**a**) satellite-derived estimates q_{he}^* and results their comparison (**b**) in April 1988: r coefficient of correlation; σ rms of mismatch

3. The cyclones typical in the Newfoundland EAZO midlatitude cause a time delay (of 6–12 h) of the SOA brightness temperature response to the heat flux variations. It is the reason that this factor is accounted for when comparing the direct and satellite estimates of parameter q_{he}.

Additionally, the relative error of the bulk-formulas used by oceanologists and meteorologists for calculations of the heat and momentum fluxes from *direct* measurements of parameter T_w, V, and T_a measures 10–30% (Gulev 1997; Blanc 1987).
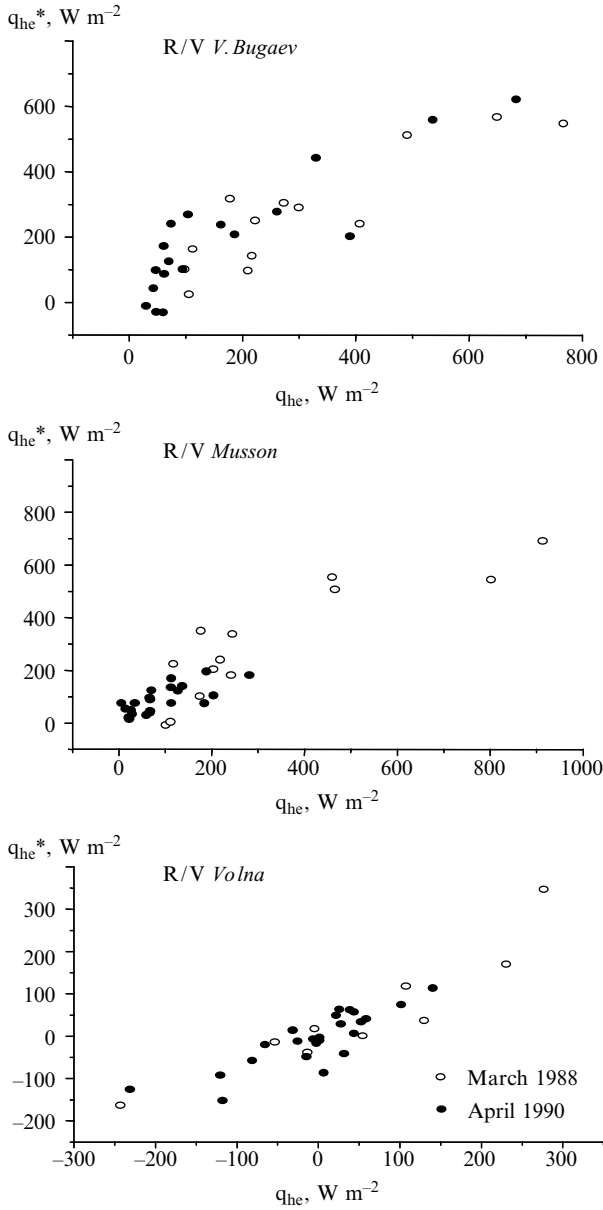
Fig. 3.9 Results of comparison the data of direct measurements the total heat fluxes q_{he} and their satellite estimates $q_{he}*$ resided to the regions of the R/Vs *V.Bugaev*, *Musson*, and *Volna* at the stationary phases of the experiments NEWOUEX-88 and ATLANTEX-90

Fig. 3.10 Results of comparison
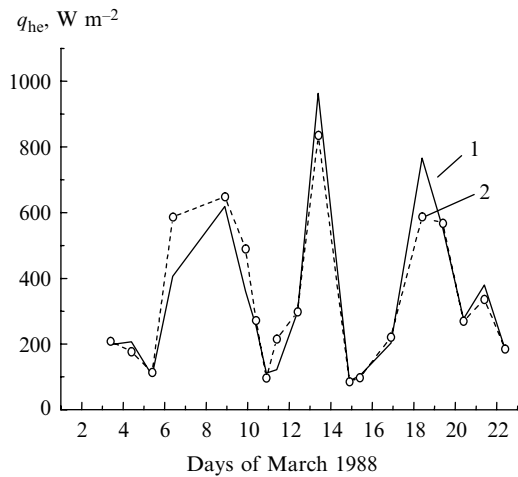the data of direct measurements the
total heat fluxes q_{he} and their
satellite estimates $q_{he}*$ with $0.5 \times 0.5°$
(1) and $1 \times 1°$ (2) spatial resolution.
Experiment NEWFOUEX-88, vessel
Volna
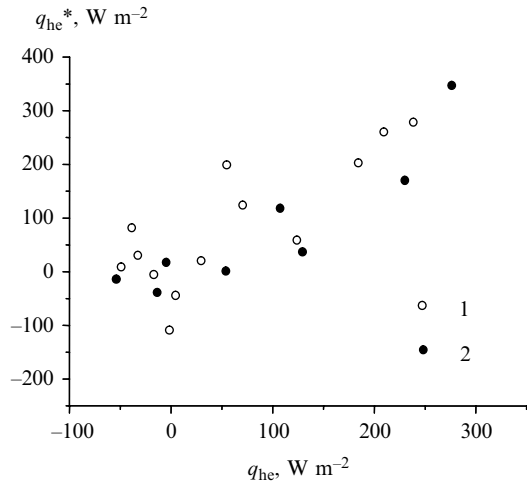
Fig. 3.11 Results of comparison the
data of direct measurements the total
heat fluxes (1) and those (2) shifted
in 1 h. Experiment NEWFOUEX-88,
vessel *V.Bugaev*

3.3 Experimental Studies of Interrelation Between the Brightness Temperature and SOA Parameters in Front Zones

3.3.1 Synoptic Variability of the SOA Parameters and Its Brightness Temperature in the Region of the Subpolar Hydrological Front

Studying the dynamics and energy of the subpolar hydrological front (SHF) in the North Atlantic, which separate the cold Labrador Current and the warm Gulf Stream, is of key importance in investigating the North Atlantic climate (WCRP:CLIVAR Initial Implementation Plan 1998). The SHF is a unique source of generation (regeneration) of the midlatitude cyclones. Thus, according to the NEWFOUEX-88 data, seven frontal cyclones were generated in March–April 1988 in the SHF area whose mean lifetime was 3–5 days. This area of the Atlantic gets subjected to intensive cyclonic impacts for about 50% of the time accompanied by substantial variations in the atmospheric temperature and humidity fields and in the characteristics of the energy exchange with the sea surface (Gulev et al. 1994).

We analyzed the synoptic variability of oceanographic and meteorological parameters of the SOA as well as its natural radiation characteristics at microwaves in the region of the SHF using data of observations from R/Vs *V.Bugaev*, *Musson*, and *Volna* at the stationary phases of the NEWFOUEX-88 and ATLANTEX-90 experiments (see Fig. 3.12) and data of simultaneous measurements from the radiometer SSM/I (satellite F-08).

Below, some results of the study of the HSF with passive microwave radiometric method at the stationary phase of the NEWFOUEX experiment (March 3–23, 1988) are presented.

The oceanic area was studied in this period by a strong variability of the near-surface air temperature T_a and humidity e and wind speed V, as well as the fluxes of sensible q_h and latent q_e heat and momentum q_v. This is confirmed by Table 3.4.

Such strong variability of the SOA parameters in the SHF areas, in areas where the RVs *V.Bugaev*, *Musson*, and *Volna* were resided and observed simultaneously by the radiometer SSM/I from the satellite F-08, initiates the appropriate brightness temperature contrasts (see Table 3.5).

3.3.2 Features of the Atmospheric Dynamics Observed in the Region of the SHF

The satellite images received by different SSM/I channels give an idea of such SHF characteristics as the sizes and the position of a frontal area in the synoptic range of time scales. As an example, Fig. 3.13 shows the black-and-white half-tint
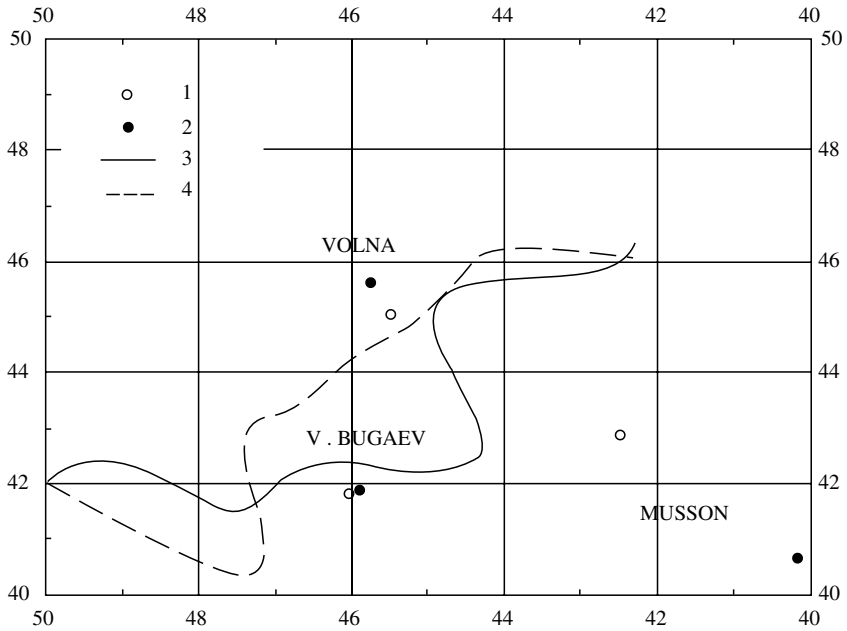
Fig. 3.12 Locations of the vessels *V.Bugaev*, *Musson*, and *Volna* during the stationary phases of the experiments NEWFOUEX-88 (1) and ATLANTEX-90 (2) as related to the subpolar hydrological front in the March 1998 (3) and April 1990 (4) (Gulev et al. 1994). The numerals along the axes are the latitude and longitude

Table 3.4 Extreme values of the SOA parameters

Parameter	Measurement unit	V.Bugaev min	max	Musson min	max	Volna min	max
T_a	°C	6.4	17.6	2.8	17.8	−2.2	13.3
e	hPa	5.8	18.1	4.4	18.2	2.9	14.6
V	m s^{-1}	0.6	25.2	0.8	26.6	0.6	27.7
q_h	W m^{-2}	−35	455	−19	601	−270	480
q_e	W m^{-2}	3	1,208	42	1,232	255	574
q_v	N m^{-2}	0.1	1.3	0.1	1.6	0.05	1.9

Table 3.5 Brightness temperature contrasts (in kelvins)

SSM/I channel	85H	37V	37H	22V	19V	19H
V.Bugaev	46.6	26.8	56.3	33.6	25.1	45.7
Musson	72	33.6	78.8	40.4	29.5	62.8
Volna	78.2	33.6	67.5	37.9	24.3	45.8
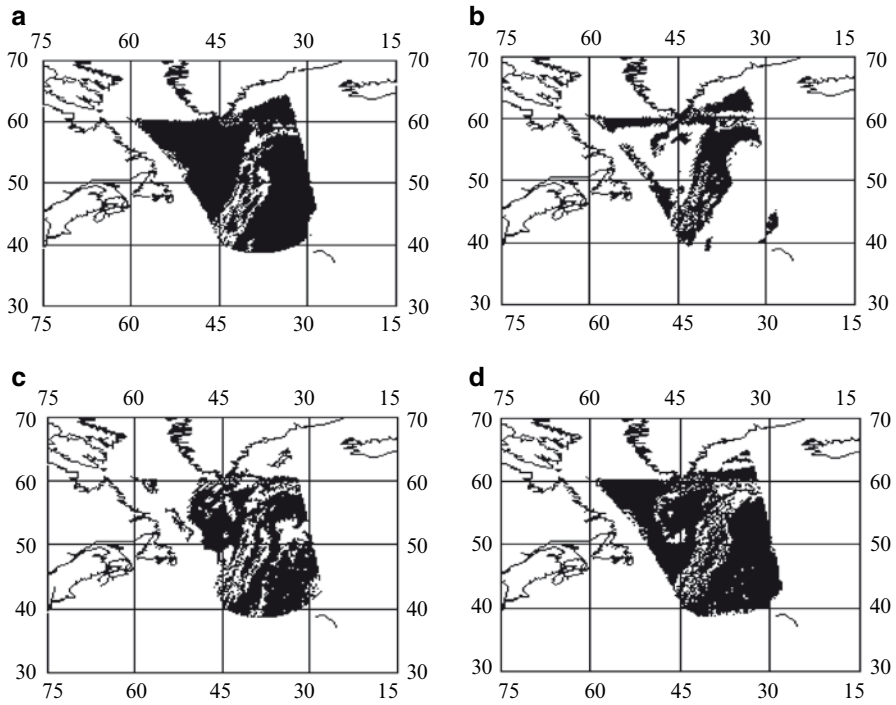
Fig. 3.13 Spatial distribution of the SOA brightness temperature in the area of the SHF at 08:00 local time on March 6, 1988 from the data of different SSM/I channels: (**a**) 19V in a range of brightness temperature variations of 175–220 K; (**b**) 37V in a range of 200–250 K; (**c**) 19H in a range of 125–190 K; and (**d**) 37H (150–230 K). The numbers along the axes are the degrees of latitude and longitude

illustrations of spatial brightness temperature distribution (scan fragments measured with the radiometer SSM/I channels 19V,H and 37V) in the SHF area during an intensive cyclone of March 6, 1988 (brightness temperature rises in going from darker to lighter tones). It follows from the quantitative analysis that the spatial brightness temperature contrasts can be of 45–50 K at the vertical polarization and of 65–80 K at the horizontal one, depending on frequency. These contrasts are localized within the extended and narrow ocean area of 500–700 km wide, which corresponds to the SHF position.

Synoptic variability of atmospheric parameters, namely the wind speed in the near-surface V, the integral water vapor content Q, and the liquid water content W (in the absence of precipitation), makes great contribution to the brightness temperature variations in the operating SSM/I frequency (wavelengths) range. Figure 3.14 illustrates the example of recovering spatial variations in the above parameters with the SSM/I data from F-08 in the SHF area (the growth of the parameters V, Q, and W is accompanied by the transition from darker to lighter tones).
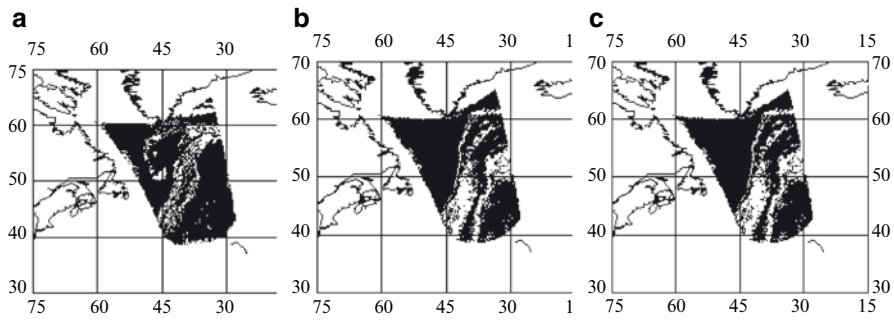
Fig. 3.14 Satellite microwave estimates of (**a**) near-surface wind speed V, (**b**) integral water vapor content of the atmosphere Q, and (**c**) liquid water content of the clouds W in the area of the HSF at 8:00 local time on March 6, 1988. The range of V, Q, W is 8−32 m s^{-1}, 0.6−2.6 g cm^{-2}, and 0−1 kg m^{-2}. The numbers along the axes are the degrees of latitude and longitude

In this case, the algorithms (Alishouse et al. 1990a, b; Goodberlet et al. 1990) are based on the regression analysis of the interrelation between the long-term series of SOA brightness temperatures and the direct V, Q, and W measurement data in different physical and geographical zones of the World Ocean. It follows from the analysis that the satellite V, Q, and W estimates vary from 8 to 32 m s^{-1}, from 0.6 to 2.6 g cm^{-2}, and from 0 to 1 kg m^{-2}, respectively. Of note is that the pattern of the spatial V and Q distribution (unlike the W distribution) obtained from the SSM/I data corresponds to the generally accepted notions of frontal zones in the ocean and atmosphere, which suppose the availability of two contiguous areas differing substantially in their parameters and separated by a sharp boundary.

The MCW measurements from F-08 give some idea of the intensity of the horizontal circulations of the atmosphere, in particular, of the dynamics of cyclone development with diurnal resolution. Such is, for example, the brightness temperature of the SOA in the channel 22V of the radiometer SSM/I, which mainly characterizes the integral water vapor content of the atmosphere, clearly responded to the cyclone development in the SHF area in the morning hours of March 6–7, 1988 (Fig. 3.14).

The comparison of Fig. 3.14a and b allows the conclusion to be made that the atmospheric front was shifting at that time toward the Azores with a rate of approximately 30 km h^{-1} (Fig. 3.15).

The potential of the assessment of spatial and temporal contrasts of vertical turbulent fluxes of total (sensible and latent) heat and impulse at the sea–air interface in the SHF is based on the radiometric SSM/I data from the F-08 satellite and direct measurement data from R/Vs *V.Bugaev* and *Volna* participating in the NEWFOUEX-88 experiment. The technique was used of satellite SHF sections crossing both vessels simultaneously. The idea of sections was earlier used in the vessel investigations in the energy active oceanic zones under the RAZREZY program (Marchuk 1989). The regression coefficients between the brightness temperature
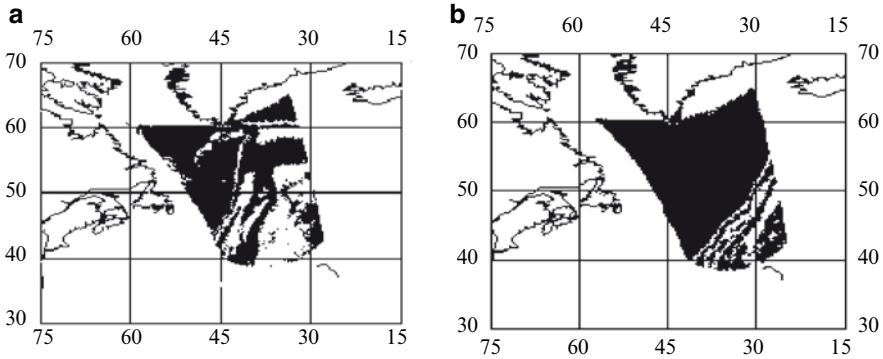
Fig. 3.15 Spatial distribution sea–air brightness temperature in the SSM/I channel 22V in the area of the HSF in the range of its variation from 190 to 240 K: (**a**) 8:00 local time on March 6, 1988 and (**b**) 08:00 local time on March 7, 1988. The numbers along the axes are the degrees of latitude and longitude

measured in different radiometric channels and the intensity of vertical turbulent fluxes of total heat q_{he} and impulse q_v at the SOA interface calculated from the weather research vessels in the period of 3–23 March were determined. Then the local regression ratios were used to retrieve the variations in the heat and impulse along the satellite SHF sections. Fig. 3.16 shows results of retrieving these variations for the satellite section crossing the R/Vs *V.Bugaev* and *Volna* in the morning and evening of 6 March.

This illustration demonstrates the effect, i.e., the q_{he} and q_v variations (related to the effect of atmosphere cyclonic activity) in the warm SHF area formed by the southern periphery of the Gulf Stream.

3.3.3   Interrelation of the Brightness Temperature and Wind Direction in the Region of the SHF

A distinguishing feature of the SHF is that the SOA heat exchange characteristics here and in adjacent areas depend not only on the intensity, but also on the direction of the air mass transfer relative to the front. Table 3.6 presents (Gulev et al. 1994) data on the heat fluxes at the SOA interface for different directions of the horizontal air-mass transfer counted clockwise from the north. The ranges selected correspond to the monthly mean directions of transfer along and across the front.

One can see that q_h and q_e are maximal at all points of observations at northwesterly winds. To the north of the SHF (R/V *Volna*) at southeastern winds, when the air assimilated the heat and moisture over the warm oceanic area (R/Vs *V.Bugaev and Musson*) is transferred toward the cold surface, favorable conditions for phase transitions arise in the near-surface atmospheric layer. Due to moisture condensation,
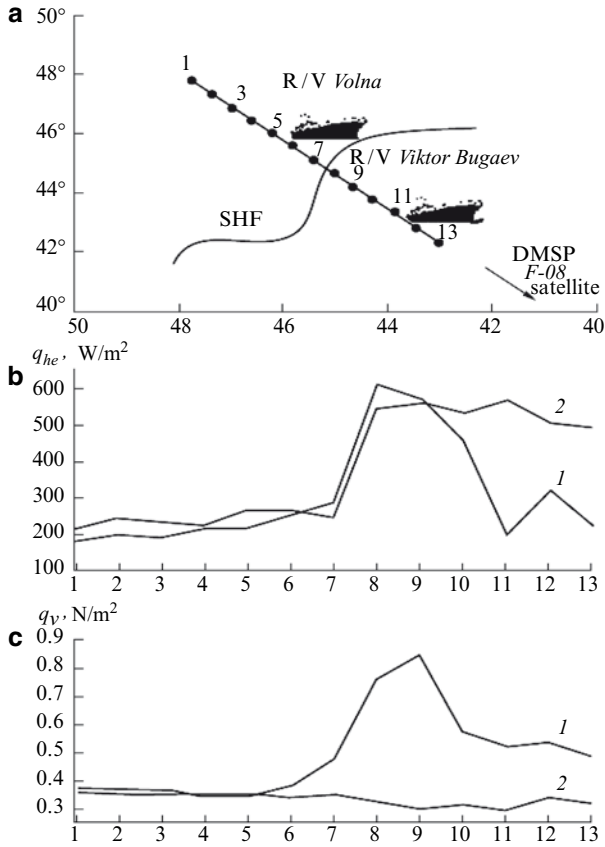
Fig. 3.16 Chart scheme of (**a**) the section of the SHF over the subsatellite path F-08 crossing the R/Vs *Volna* and *V.Bugaev* on March 6, 1988 and variations of (**b**) heat fluxes q_{he} and (**c**) impulse q_v fluxes: (1) 08:00, (2) 22:00 this day. Points indicate the satellite samples, *N* subsatellite path number

Table 3.6 Mean values of sensible q_h and latent q_e heat fluxes (in W m^{-2}) at different wind directions at stationary phase of NEWFOUEX-88

φ (deg)	V.Bugaev		Musson		Volna	
	q_h	q_e	q_h	q_e	q_h	q_e
30–90	30	104.4	42.3	90.9	10.8	4.5
90–210	39.3	213.2	69.4	256.9	−35.6	−16.5
210–270	83.3	301.1	100.2	313.5	65.3	109
270–300	131.7	319.4	141.4	271.7	92.7	111.3

the air to the north of the front is heated, and heat fluxes are directed from the atmosphere to the ocean. Therefore, atmospheric synoptic processes in this case play the role of one of the mechanisms of the heat and moisture transfer across the front from the warm to the cold part of the ocean.

We also estimated in details an influence of the near-surface wind speed and its direction on synoptic variability of meteorological parameters, total heat (sensible and latent fluxes), and the SOA brightness temperature at the stationary phase of the ATLANTEX-90 experiment in cold oceanic waters in the area of the R/V *Volna*, located at a distance about 200 km from the SHF. Results of regression analysis of the relationships between these parameters demonstrate that a variability of the near-surface air temperature and humidity is determined by a combined effect of wind speed and direction, characterized quantitatively by a projection of the wind vector V_n onto the normal passing through the R/V *Volna* to the curve describing the position of the SHF. Linear regression analysis of the relationships between T_a and V_n, e and V_n parameters in the range of the angle φ from 290 to 340° was carried out taking into account the approximate data on the SHF position in April 1990, presented in Gulev et al. (1994). It was found that the largest values of the correlation coefficients in these relationships correspond to $\varphi = 330°$. Figure 3.17 illustrates a relation between hourly samples of sheep measurements of the near-surface air temperature and humidity and V_n in the period April 4–21, 1990.

Figure 3.18 compares variations of the total heat fluxes q_{he} and the brightness temperature T_b measured in the SSM/I channel 22V with variations of the parameter V_n at $\varphi = 330°$.

A well-marked connection is found between variations of q_{he} and V_n ($r = 0.79$). As V_n increases, discrepancies between the heat characteristics of the ocean and atmosphere grow, and consequently, the total heat fluxes increase. The brightness temperature of the SOA natural MCW radiation measured by the SSM/I channel 22V is closely related to the intensity of heat and moisture exchange at the system interface. Its value increases with the increase in temperature and humidity of the atmosphere. The minimum of brightness temperature and maximum of heat fluxes on April 9–11 are caused by the transfer of cold dry air from the northwest, which leads to the formation of positive total heat fluxes directed from the ocean to atmosphere. On the contrary, on April 13, the southeasterly winds blowing from the warm Gulf Stream caused a heating of the atmospheric layers in the area of the R/V *Volna*. This heating produced the heat fluxes directed from the atmosphere to the ocean and simultaneously resulted in an increase of the SOA brightness temperature.

It is also found that there is a close connection between the mean daily values of total heat fluxes and brightness temperature measured from F-08 approximately once in 24 h and mean daily values throughout the stationary phase of the ATLANTEX-90 experiment (Fig. 3.19).

Regression analysis was made of the relationships between variations of q_{he}, T_b, and V_n. The value of the latter was determined on the assumption that the angle of the normal to the SHF boundary passing through the R/V *Volna* was kept constant in the period from April 4 to 21, 1999 ($\varphi = 330°$). Under this condition, the variations of V_n are caused only by variations of wind speed and direction with respect to the normal. The values of correlation coefficients between q_{he} and V_n, T_b, and V_n are 0.85 and −0.73, respectively.

Thus, the data of the combined ship and satellite analysis of the SHF suggest that there is a close connection between the brightness temperature of the SOA in cold frontal waters and the intensity and direction of the air-mass transfer from the
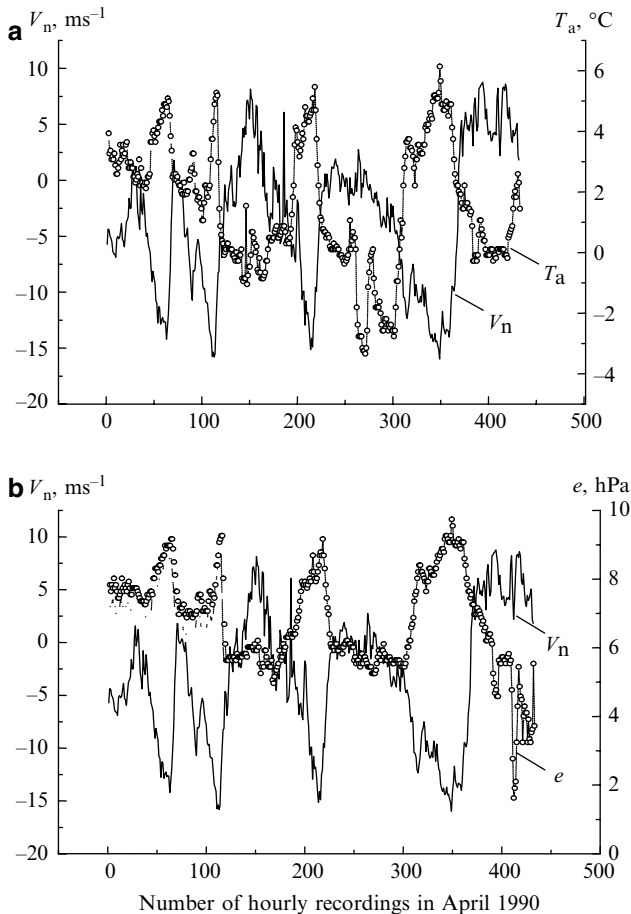
Fig. 3.17 Results of combined analysis of hourly samples of (**a**) V_n and T_a; (**b**) V_n and e at the stationary phase of ATLANTEX-90 (R/V *Volna*, April 4–21, 1990). Correlation coefficient (**a**) $r=0.7$; (**b**) $r=-0.81$

opposite warm oceanic areas determining the heat characteristic of the cold areas. This result points to a potential possibility of using satellite microwave radiometric measurements to estimate the influence of the heat and moisture transfer across the front on the intensity of the ocean–atmosphere heat interaction in the Newfoundland and, possibly, in other energy-active zones.

3.4   Conclusion

The relations between the system ocean–atmosphere natural microwave radiation with the processes of heat interchanges in the system are most indicative at the synoptic range of time scales; the following regularities are observed in this case:
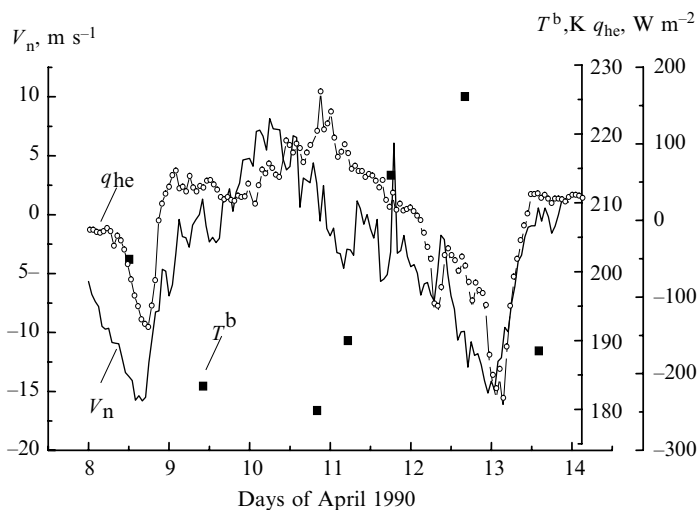
Fig. 3.18 Response of the SOA brightness temperature T^b at the wavelength 1.35 cm and total heat fluxes q_{he} to variations of V_n during the passage of a cyclone, R/V *Volna*, April 8–13, 1990
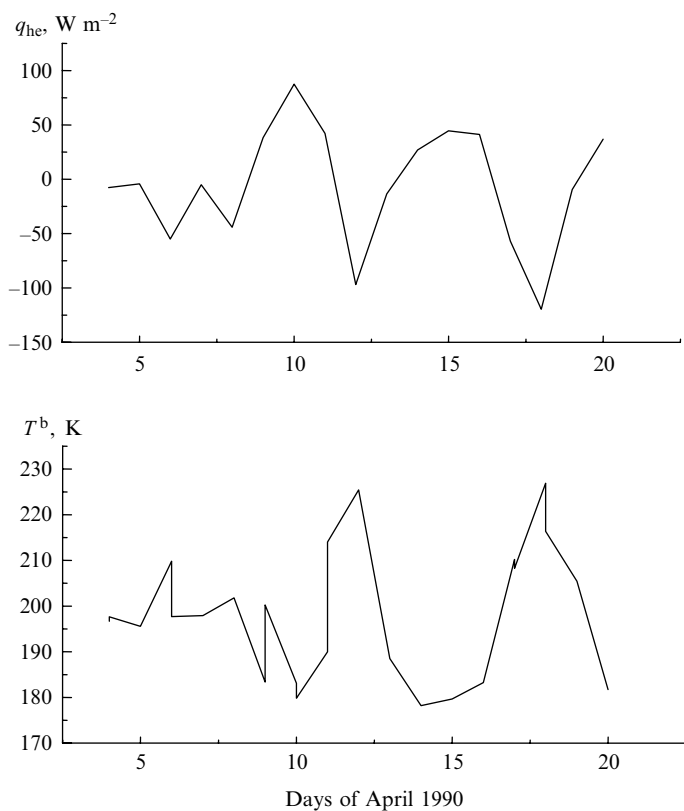
Fig. 3.19 Variations of the daily values of the parameter q_{he} and the SSM/I-derived parameter T^b during the stationary phase of ATLANTEX-90 (the R/V *Volna* position)

- Parameterizations used for calculating the vertical turbulent fluxes of sensible and latent heat over the ocean can be reconstructed in the form of combinations of only those parameters of the ocean–atmosphere system that are directly related to satellite-derived characteristics
- A good agreement between theoretical and experimental (satellite) estimates of the brightness temperature of the system ocean atmosphere natural microwave radiation and the results of their processing is observed in the mid- and north latitudes of the North Atlantic
- An influence of the near-surface wind speed and its direction on synoptic variability of meteorological parameters, total heat (sensible and latent fluxes), and the system ocean–atmosphere brightness temperature over the Subpolar Hydrological Front in the North Atlantic has been discovered

References

Gulev SK, Kolinko AV, Lappo SS (1994) Synoptic interaction between the ocean and atmosphere in middle latitudes. Gidrometeoizdat, St. Petersburg In Russian

Guidelines (1981) Calculation of turbulent fluxes of heat, moisture, and the momentum fluxes over the ocean. GGO, Leningrad In Russian

Lebedeva EL (1991) Integral water vapor content of the atmosphere as the characteristic of air-sea interaction in the Newfoundland energy active zone. Trudy Glavnoi Geofizicheskoi Observatorii, Leningrad 535:32–45 (in Russian)

Kramer HJ (1994) Observation of the Earth and environment. Survey of missions and sensors, 2nd edn. Springer, Berlin

Hollinger PH, Peirce JL, Poe GA (1990) SSM instrument evaluation. IEEE Trans Geosci Rem Sens 28:781–790

Wentz FJ (1991) User's manual SSM/I antenna temperature tapes (Revision 1). RSS Technical Report, Santa Rose

Grankov AG, Mil'shin AA (1999) Interrelation between the microwave radiation of the ocean-atmosphere system and the boundary heat and momentum fluxes. Izvestiya, Atmos Oceanic Phys 35:570–577 In Russian

Gulev SK (1997) Long-term variability of sea-air heat transfer in the North Atlantic Ocean. Int J Clim 15:825–852

Blanc TV (1987) Accuracy of bulk-method-determined flux, stability, and sea surface roughness. J Geophys Res 92:3867–3876

WCRP:CLIVAR Initial Implementation Plan (1998) (CLIVAR Scientific Steering Group). World Meteorological Organization, Geneva

Alishouse JC, Snyder SA, Vongsatorn J, Ferrado RR (1990a) Determination of oceanic total precipitable water from the SSM/I. J Geophys Res 28:811–816

Alishouse JC, Snyder JB, Westwater ER et al (1990b) Determination of cloud liquid water content using the SSM/I. J Geophys Res 28:817–821

Goodberlet MA, Swift CT, Wilkerson JC (1990) Ocean surface wind speed measurements of the Special Sensor Microwave/Imager (SSM/I). IEEE Trans Geosci Remote Sens 28:823–828

Marchuk GI (ed) (1989) Scientific programme to study the influence of energy-active zones of the oceans on climatic fluctuations ("Razrezy" Program). Gidrometeoizdat, Moscow In Russian

Chapter 4
Results of Studies of Heat and Dynamic Air–Sea Interactions with Passive Microwave Radiometric Methods at the Seasonal and Climatic Scales

4.1 Satellite-Derived Estimates of Monthly Mean Integral Parameters of the Atmosphere and Near-Surface Wind Speed

4.1.1 Monthly Mean Brightness Temperatures Observed with the SSM/I Radiometer Over the Energy-Active Zones of the North Atlantic at the Seasonal Scales

The satellite microwave radiometric methods can be used as an effective tool for an exposure of the most changeable SOA parameters forming the processes of air–sea interaction such as the near-surface wind speed V, and total water vapor content Q and characterized by a strong changeability of their current (hourly, daily) values. On the basis of the results of measurements from the radiometer SSM/I of satellite F-08 carried out in January, February, July, and August of 1994 (taken from the archive of the *Remote Sensing Laboratory, California*), we have retrieved the monthly mean values of parameters V, Q, and W in selected points of the North Atlantic. These points coincide with locations of the so-called weather stations, named as ALPHA (**A**), BRAVO (**B**), CHARLIE (**C**), DELTA (**D**), ECHO (**E**), HOTEL (**H**), INDIA (**I**), JULIETT (**J**), KILO (**K**), LIMA (**L**), and MIKE (**M**). Some of these points are related to the Norwegian, Newfoundland, and Gulf Stream energy active zones (EAZOs) characterized by most values of intensity of air–sea heat interaction (see Fig. 4.1).

Most of them are related to the area of the Gulf Stream and North-Atlantic currents where appreciable values of the air–sea temperature differences and their changeability are observed (see Fig. 4.2).

Number of satellite orbits suitable for the points shown above is varied from 17 to 34 per month; this frequency of spatial observations provides determination of the monthly mean surface parameters V, Q, and W with suitable oceanologists and meteorologists accuracy.

One can see from the results of the SSM/I data in various EAZOs where the appreciable monthly mean brightness temperature contrasts are observed between

Fig. 4.1 Location of vessel weather stations in the North Atlantic
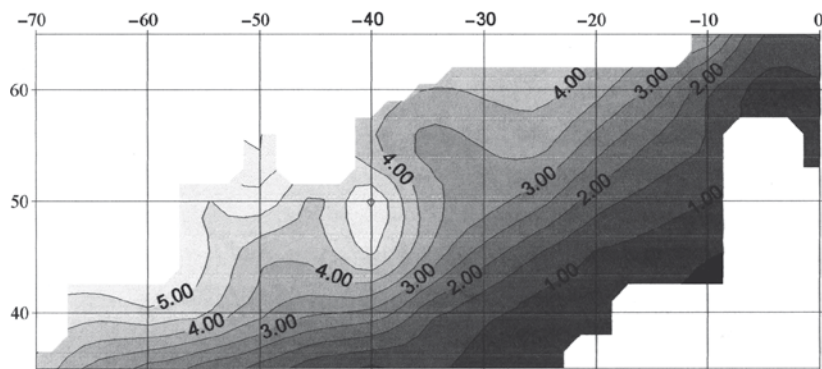
Fig. 4.2 Spatial distribution of the climatic air and sea temperature differences in the area of Gulf Stream and North-Atlantic currents. The numbers along the axes are the degrees of latitude and longitude

February and August, 1994 (see Table 4.1). Let us note that this work was conducted in the frame of the NASA and Roscosmos contract during 1996–1998 and printed later in Grankov and Gulev (1996).

For example, in the point H, belonging to the Gulf Stream EAZO, the seasonal variations of the SOA monthly mean brightness temperatures in the range of millimeter and centimeter wavelength are varied from 16 to 45 K; in the point **M** (the Norwegian EAZO), these contrasts are about 13 K. Such level of the brightness temperature contrasts with respect to a sensitivity of the SSM/I device and the errors of its calibration is a background for an analysis of seasonal dynamics of the air–sea interaction.

Table 4.1 Monthly mean brightness temperatures of the SOA (in Kelvins) observed in active points of the North Atlantic in February and August 1994

	85V	85H	37V	37H	22V	19V	19H
In February 1994							
A	234.5	196.5	201.4	147.8	188.2	177.0	112.1
B	232.1	192.5	200.9	147.5	184.7	175.7	110.4
C	237.3	201.1	202.2	149.3	189.9	177.1	113.0
D	242.4	213.2	207.7	160.1	198.9	183.8	123.4
E	250.3	221.1	206.2	154.1	210.6	186.6	126.0
H	239.4	198.4	201.0	144.1	193.9	178.3	111.9
I	238.0	200.5	202.8	150.6	192.3	178.7	115.3
J	240.1	206.5	204.3	153.3	196.8	180.7	118.8
K	245.0	214.9	206.3	156.3	202.5	183.2	122.6
L	238.8	204.9	203.9	153.1	194.4	179.8	117.6
M	236.9	197.7	201.7	145.7	187.8	175.9	108.8
In August 1994							
A	250.2	220.6	207.5	153.4	204.6	182.4	119.3
B	249.9	222.7	211.8	163.0	210.1	186.8	128.2
C	252.3	223.3	207.9	154.0	207.7	184.0	122.0
D	259.8	235.6	214.1	163.1	225.2	195.6	137.9
E	267.0	244.9	216.0	162.0	235.0	201.1	142.8
H	264.3	242.7	216.9	165.7	234.5	201.6	145.1
I	249.2	215.2	205.0	147.7	203.1	181.5	116.5
J	251.9	223.3	208.2	155.0	209.2	185.1	123.4
K	258.4	234.2	211.7	159.1	219.1	190.7	130.6
L	249.9	217.7	205.7	150.0	205.1	182.6	118.9
M	247.3	210.9	203.6	145.3	201.9	180.4	114.8

4.1.2 *Monthly Mean SOA Parameters Retrieved with the SSM/I Radiometer over the Energy-Active Zones of the North Atlantic and Their Accuracy*

Using algorithms (Alishouse et al. 1990a; Goodberlet et al. 1990) approved with the data of durational satellite and direct measurements in various physical and geographical areas of the World ocean, we have obtained the daily estimates of the near-surface wind speed V, total water vapor content of the atmosphere Q, and integral water content of the clouds W in the above listed points of the North Atlantic. On the basis of these results, we have estimated the monthly mean values of the parameters V, Q, and W as well as their variability for different scales of spatial averaging the brightness temperatures measured by the radiometer SSM/I; Tables 4.2 and 4.3 show some results of this analysis for the points **A**…**M** of the North Atlantic.

For validation of satellite microwave radiometric estimates of the monthly mean wind speed and total content of the water vapor of the atmosphere, we attached the

Table 4.2 Microwave radiometric estimates of monthly mean wind speed and their *rms* values

Points	Mean	*rms*	Mean	*rms*	Mean	*rms*
(without any corrections on the precipitations effect)						
A	17.9	3.86	17.8	3.71	18.0	3.67
B	18.7	4.16	18.4	3.22	18.6	3.15
C	17.1	3.70	16.6	3.83	16.3	3.87
D	19.7	4.99	18.9	5.34	18.9	5.39
E	14.9	3.16	15.1	3.04	15.0	2.89
H	14.6	4.09	14.7	4.13	14.9	3.99
I	17.7	4.17	17.5	4.22	17.6	4.21
J	17.4	–	17.0	4.00	17.9	3.91
K	16.3	4.02	16.6	3.38	16.7	4.62
L	18.0	4.32	18.2	4.41	18.4	4.50
M	15.4	–	15.6	–	15.2	3.25
(with an account of influence of precipitations)						
A	17.7	3.30	17.7	3.67	17.8	3.70
B	18.9	3.60	18.2	3.22	18.5	3.50
C	16.2	3.70	16.5	3.60	16.8	3.50
D	18.9	4.40	18.7	4.00	17.7	4.30
E	14.8	2.90	14.6	2.50	14.0	2.70
H	14.5	4.30	14.0	4.20	14.6	4.00
I	17.2	3.70	17.2	4.13	17.2	4.12
J	16.9	–	16.4	4.45	17.1	3.81
K	15.8	3.57	15.8	3.87	15.8	3.92
L	17.2	3.85	17.3	3.91	17.2	3.87
M	14.9	3.21	14.9	3.22	15.0	3.11
	5 x 5⁰		2.5×2.5°		1×1°	

data of the archive comprehensive ocean and atmosphere data set (COADS) and the National Centers for Environmental Prediction/National Center for Atmospheric Research (NCEP/NCAR) at the seasonal time scales (between February and August months). The NCEP/NCAR archive includes results of long-term observations in such areas of study as oceanography, weather and climate, hydrology and glaciology, biogeochemistry, etc. (Kalnay et al. 1996).

We have established that a discrepancy between the satellite and direct data is: $0.2-0.4 \ \mathrm{g \, cm^{-2}}$ for the parameter Q in the range of its variations $0.5 < Q < 4 \ \mathrm{g \, cm^{-2}}$, $2-3 \ \mathrm{m \, s^{-1}}$ for the parameter V in the range of its variations $0 < V < 10 \ \mathrm{m \, s^{-1}}$, and $3-5 \ \mathrm{m \, s^{-1}}$, if $V > 10 \ \mathrm{m \, s^{-1}}$.

It follows from Tables 4.2 and 4.3 that: (1) the SSM/I estimates of the monthly mean near-surface wind speed and total water vapor of the atmosphere are slightly dependent on the spatial averaging the satellite data; and (2) in the range of time and spatial resolution suitable for the SSM/I device, the atmospheric cloudiness and precipitations do not influence essentially an accuracy of microwave radiometric estimates of the near-surface wind speed V and total water vapor content Q.

Table 4.3 Microwave radiometric estimates of monthly mean the total vapor content of the atmosphere monthly mean wind speed and their *rms* values

Points	Mean	*rms*	Mean	*rms*	Mean	*rms*
(without any corrections on the precipitations and cloudiness effect)						
A	0.74	0.16	0.73	0.16	0.74	0.17
B	0.62	0,16	0.60	0.13	0.59	0.13
C	0.81	0.18	0.81	0.18	0.10	0.09
D	1.09	0.70	1.00	0.60	0.90	0.3
E	1.90	0.54	1.92	0.55	1.70	0.70
H	1.12	0.46	1.11	0.43	1.12	0.30
I	0.90	0.19	0.80	0.70	0.88	0.70
J	1.13	–	1.18	–	–	–
K	1.38	0.42	1.40	0.44	1.39	0.44
L	0.98	0.25	0.98	0.22	0.98	0.21
M	0.77	–0	0.80	–	–	–
(with an account of cloudiness and precipitations)						
A	0.72	0.16	0.73	0.16	0.74	0.17
B	0.61	0.14	0.60	0.13	0.59	0.13
C	0.80	0.17	0.81	0.18	0.81	0.19
D	1.00	0.38	1.00	0.36	0.99	0.33
E	1.88	0.53	1.90	0.54	1.96	0.57
H	1.08	0.42	1.09	0.41	1.10	0.42
I	0.87	0.16	0.87	0.15	0.87	0.15
J	1.09	–	1.16	–	1.08	0.27
K	1.31	0.38	1.31	0.40	1.31	0.41
L	0.93	0.20	0.93	0.19	0.92	0.18
M	0.74	0.16	0.74	0.16	0.75	0.14
	$5\times5°$		$2.5\times2.5°$		$1\times1°$	

4.2 Estimates of Monthly Mean Heat Fluxes in the North Atlantic Using Data of the Satellite F-08 (DMSP)

4.2.1 Validation of the Monthly Mean Heat Fluxes Estimated from Satellites with Archival Data in Active Zones of the North Atlantic

Average monthly averaged sensible and latent heat fluxes were estimated on the basis of satellite measurements and compared to the estimated heat fluxes taken from the climatic archives COADS and current (1994) data from the archives NCEP/NCAR (Grankov et al. 1999).

Satellite passive microwave radiometric data are used for the determination of the near-surface wind speed V and total water vapor content of the atmosphere Q, whose monthly mean values Q clearly correlate with those of the near-surface air humidity

(water vapor pressure) e and temperature T_a. The relationships between monthly mean values of Q and e parameters are calculated by analyzing 49 oceanic aerologic stations during 17 years (Liu 1988). We used these data as well as the results of systematization for an extensive series of atmospheric humidity observations (Matweev Ju and Soldatov 1982) to estimate some local regressions for the determination of water vapor pressure e in the near-surface atmosphere in the formula (1.2) for the calculation of monthly mean latent heat fluxes q_e. The monthly mean values of the near-surface air temperature T_a necessary for the calculation of sensible heat fluxes q_h by the formula (1.1) can be determined from monthly mean values of the near-surface air humidity e with the help of the regression relationships between the T_a and e parameters using the archival data of VNII GMI (All-Russian Research Hydrometeorological Institute, Obninsk) averaged over the period 1957–1990 (the archives of Birman).

The monthly mean SST values (T_w) necessary for the calculations of sensible heat fluxes q_h are borrowed from the archives of oceanographic and hydrometeorological data COADS in the form of a average many-year values, which can be explained by the following two circumstances: (1) the channels for the SST determination are absent as such in the SSM/I radiometer, whose data are used for approbation of this algorithm; (2) the interannual variability of monthly mean SST values is substantially lower than their intra-annual (seasonal) variability, the analysis of which is the basic purpose.

In order to calculate the monthly mean heat fluxes q_h and q_e the parameterizations, (1.1) and (1.2) are used. Here, the monthly mean values of T_w, T_a, e, and V parameters serve as initial values. Such an approach yields results close to those obtained by a more rigorous method for the calculation of heat fluxes, taking into account the synoptic variability of these parameters of the SOA.

The average (monthly mean) values of sensible and latent heat fluxes were assessed in January, February, July, and August 1994 for 16 regions of the North Atlantic, for which the most representative archives of oceanological and meteorological data are available. The assessments for 11 areas of the North Atlantic weather stations **A**, **B**, **C**, **D**, **E**, **H**, **I**, **J**, **K**, **L**, and **M** for January 1994 are presented in Fig. 4.3 with the help of example. Many of these stations are confined to the energy-active zones, such as Norwegian, Newfoundland, and the Gulf Stream, which are characterized by the highest intensity of thermal interaction between the ocean and atmosphere. The number of satellite orbits falling on the mentioned regions of the North Atlantic varies from 17 to 34 per month and ensures a quite satisfactory (according to measures accepted in the oceanology) quality of the heat fluxes estimations (Taylor 1984).

4.2.2   Some Conclusions

So, the results of comparison of the SSM/I estimations of the monthly mean sensible and latent heat fluxes averaged in the squares 2.5 by 2.5° with the COADS and NCEP/NCAR archival data are quite satisfactory.

In our opinion, the main reasons for the discrepancy between the satellite and direct measurement data observed are as follows:
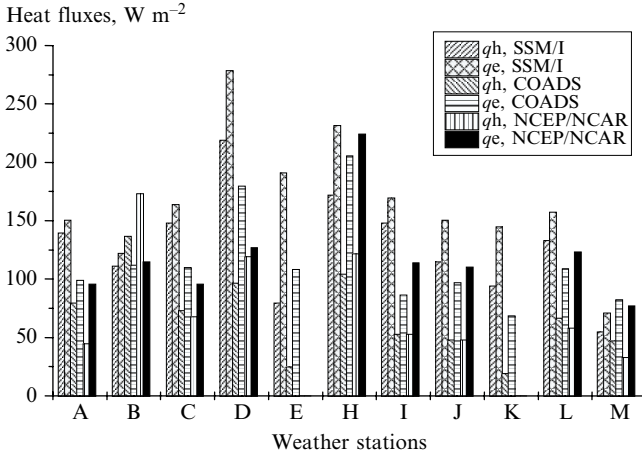
Fig. 4.3 Comparison of satellite derived (SSM/I) and archival (COADS and NCEP/NCAR) estimates of the monthly mean sensible q_h and latent q_e heat fluxes attached to various weather stations in the North Atlantic in February 1994 with spatial averaging $2.5 \times 2.5°$

– the errors in calculating heat fluxes from the monthly mean parameters V and Q, but not from its current (hourly, daily) values
– ignoring the spatial and seasonal variability of some parameters of the bulk-parameterizations such as the coefficients of heat (C_T) and moisture (C_V) interchange between ocean and atmosphere errors in calculations

Moreover, there exist considerable differences between various archival data that characterized the spatial and temporal variability of the monthly mean sensible and latent heat fluxes in the North Atlantic; these differences attain 50 and sometimes even 100% (Lappo et al. 1990).

It is also seen from the results of the analysis made that the satellite passive microwave radiometric estimates of the monthly mean heat fluxes, as well as their most dynamic components in the form of monthly mean values of wind speed and total water vapor content in the atmosphere, are weakly changed in transition from 1° to 5° squares.

4.3 Satellite-Derived Estimates of Multiyear (Climatic) Variability of the Surface Heat Fluxes in Active Zones of the North Atlantic

4.3.1 Areas of Interests in the North Atlantic

The use of satellite passive microwave radiometric methods in climatic studies has become a realistic and unique idea only after launching the NIMBUS 7 satellite (1978) with the radiometer scanning multichannel microwave radiometer (SMMR)

on the board, which operated for about 9 years. From 1987 year the DMSP satellite series (1987) equipped with the devices Special Sensor Microwave/Imager (SMM/I), the SSM/T-1 (Atmospheric Temperature Profiler), and the SSM/T-2 (Atmospheric Water Vapor Profiler) are operating. In addition to this, the satellites EOS Aqua (2002) data with the radiometer advanced microwave scanning radiometer (AMSR-E) data and the data satellites of the METEOR-3 M series with the radiometer module of temperature and humidity sensing of the atmosphere (MTVZA) provide us a unique possibility to study the *decadal* processes of the ocean-atmosphere heat and dynamic interaction over periods of 30 years steadily. These tools can be used in the frame of the programs climate variability and predictability (CLIVAR) (CLIVAR Implemantion Plan 1998) and other prominent projects.

Here, we present some estimates of usefulness of the SSM/I data collected during the DMSP satellite missions to evaluate the long-term dynamics of a large-scale heat fluxes at the boundary of SOA and its most significant components, such as the wind speed V, integral water vapor of the atmosphere Q, and precipitation R.

The Norwegian, Newfoundland, and Gulf Stream energy-active zones of the North Atlantic including their local parts related to the oceanic weather stations **M** (66°N, 2°E), **D** (44°N, 41°W), and **H** (38°N, 71°W) were considered as the areas of our paramount interests. These zones situated in a course of the Gulf Stream and North Atlantic current exert appreciable influence on the weather conditions of the Europe and European part of Russia (see Fig. 4.4).

For examination of the feasibility of determining the heat fluxes and their main components to efficient accuracy using DMSP SSM/I measurements, we used the data measurements from the satellites F-08, F10–F13 during the period January 1988–December 1996 (these data are available from the Goddard Distributed Active Archive Center (DAAC) of NASA Marshall Space Flight). The initial telemetry signals (more than 200-Gigabyte datasets in formats SSM and HDF) were converted into antenna, then into brightness temperatures by applying the special calibration procedure described in Wentz (1991). The next step was to evolve from the global data sets the fragments appropriate to the Norwegian, Newfoundland,
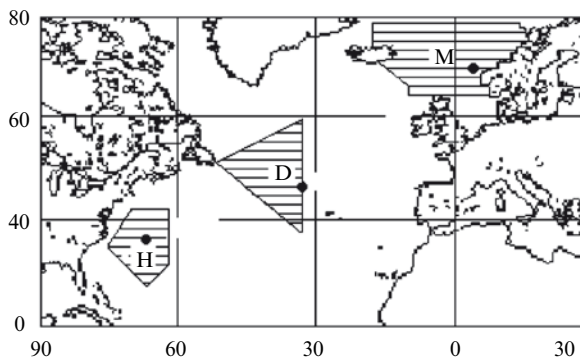
Fig. 4.4 Location of Norwegian, Newfoundland, and Gulf Stream active zones and the ocean weather stations MIKE (**M**), DELTA (**D**), HOTEL (**H**)

and Gulf Stream active zones of the North Atlantic. Then, the sequences of current (daily) and month mean SSM/I brightness temperatures over the period 1988–1994 were developed for those satellite orbits that are passing through more local areas (squares 0.5 by 0.5°) covering the points **M**, **D**, and **H**.

4.3.2 Potential of the Radiometer SMM/I in Retrieving the Parameters *V, Q, W* and Estimating the Interannual Variability of Their Monthly Mean Values

Figure 4.5 illustrates variations of the monthly mean parameters *V*, *Q*, and *R* in the point **M** in the Norwegian EAZO, which were retrieved from the SSM/I data with algorithms (Alishouse et al. 1990b; Goodberlet et al. 1990; Ferraro and Marks 1995). These algorithms are based on the regressions between the SOA brightness temperatures and the parameters *V*, *Q*, *R* accumulated during long-continued synchronous satellite and in situ measurements in different physical and geographical zones of the Earth; the discrepancy between the estimates of the parameters *V*, *Q*, and *R* is of 2 m s^{-1}, 0.02 g cm^{-2}, and 5 mm h^{-1}, accordingly. The time interval of January 1988–July 1988 has been omitted as the initial data were inaccessible for their processing in these series.

We analyzed the possibilities of using the radiometer SSM/I for studying the interannual variations of the parameters *V*, *Q*, *R* during the 1988–1998s (see Fig. 4.6).

From here, we see a good compliance between a climatic satellite-derived microwave radiometric estimates of the monthly mean wind speed at the centimeters averaged during the 1988–1998 period and the data collected in the point **M** by traditional means in the Obninsk Center during 1953–1974 years (Handbook 1979); their correlation is varied from 0.84 to 0.88. On the basis of the archival NCEP/NCAR data, we discovered that the differences between the satellite and direct estimates (in terms of their absolute values) are of 3–4 m s^{-1}.

Besides, the satellite microwave radiometric estimates of the monthly mean integral water vapor content of the atmosphere are slightly differed from the NCEP/NCAR estimates. To our opinion, this fact is evoked by an active use of the satellite microwave radiometric data in the archive NCEP/NCAR in latest years, when satellite data (especially the data of the SSM/I radiometer) naturally enlarged the arsenal of traditional (vessel, meteorological, and aerologic) means.

We analyzed the intraannual (seasonal) contrasts of monthly mean SSM/I brightness temperatures of the SOA during 10-year period in the points **M**, **D**, and **H** (see Table 4.4).

One can observe from the illustration appreciable year-to-year variations of seasonal contrasts of the monthly mean brightness temperature in the points **M**, **D**, and **H**; this gives us a good basis for an analysis of interannual dynamics of large-scale air–sea interaction characteristics with the data of the SSM/I long-term measurements.
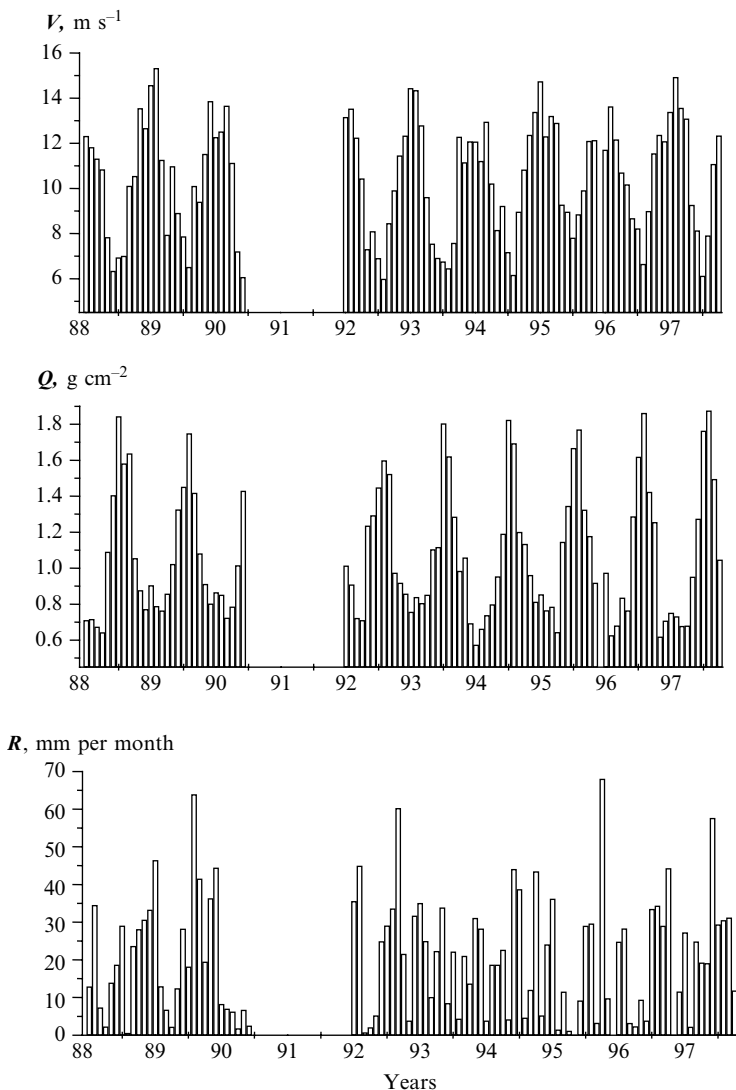
Fig. 4.5 Seasonal and annual variability of the monthly mean parameters V, Q, and R in the point **M** of the North Atlantic derived from the radiometer SSM/I (the time interval January 1988–July 1988 has been omitted as the initial data were inaccessible for their processing in these series)

We compared the seasonal trends of monthly mean SSM/I brightness temperature of the SOA in points **M**, **D**, and **H** averaged over the period 1988–1999 and their interannual variations during this time interval. Figure 4.7 demonstrates these results for the SSM/I channel 22 V (the wavelength 1.35 cm) which, as stated above, are the most informative at the analysis of air–sea interaction in the synoptic range of time intervals.
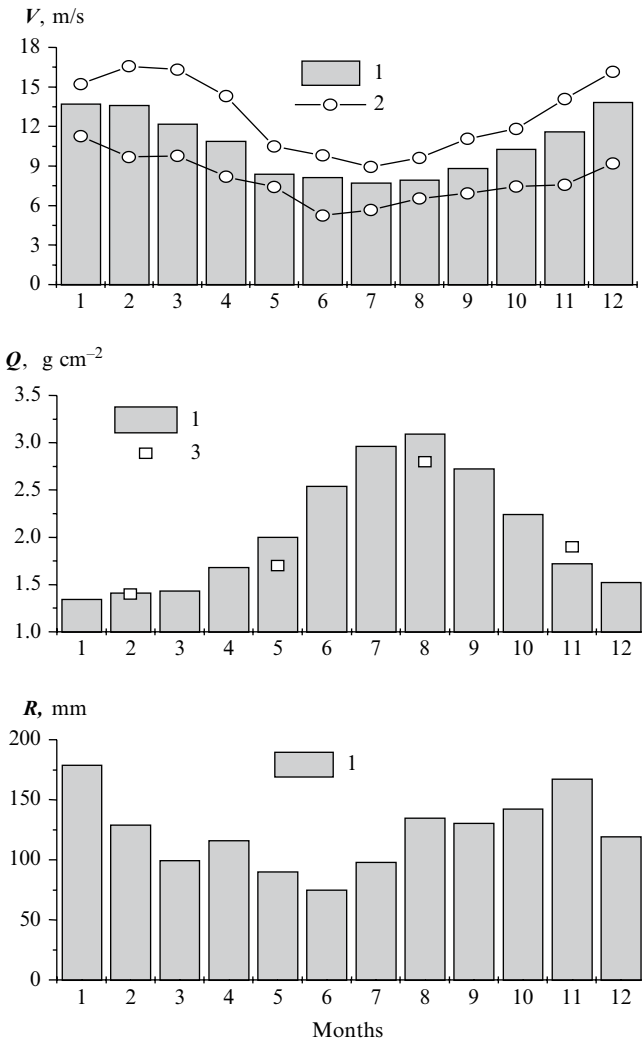
Fig. 4.6 Seasonal dynamics of monthly mean parameters V, Q, and R due to the ten-year measurements of the radiometer SSM/I in the Newfoundland EAZO: 1 – SSM/I, 2 – extreme values from (Handbook 1979), 3 – (Snopkov 1981).

Taking into account a strong correlation between brightness temperature at the wavelength 1.35 cm and the parameters of heat exchange processes in the air–sea interface at synoptic and seasonal time scales, we can expect that the data of long-term measurements from the SSM/I device (or similar devices) will be useful in studies of these processes at climatic scales. Possibly, an analysis of relations between seasonal and climatic components of the brightness temperature variability will help explain the peculiarities of the SOA behavior as a climatic system in various oceanic regions.

Table 4.4 Intra-annual contrasts of the monthly mean brightness temperature values (in Kelvins) in the points **M**, **D**, and **H** for various channels of the SSM/I device

Years	SSM/I channels						
	85V	85H	37V	37H	22V	19V	19H
Point **M**							
1988	8.7	14.6	4.9	80	11.9	6.1	9.4
1989	–	19.7	5.3	11.0	14.4	5.6	10.1
1990	–	28.1	8.7	13.2	19.3	9.3	13.9
1992	13.2	24.9	8.1	11.7	15.9	8.5	13.1
1994	6.5	12.7	3.5	8.2	14.1	6.0	7.1
1996	16.2	34.6	37.8	29.1	22.8	47.6	23.2
1997	16.0	25.3	7.6	12.0	18.8	8.8	13.0
1998	14.9	29.1	7.6	12.6	20.9	9.2	14.2
Point **D**							
1988	11.8	21.8	6.6	9.3	14.3	8.7	12.6
1989	–	23.3	6.3	10.8	23.6	9.1	12.4
1990	–	30.7	9.8	12.7	29.7	15.6	22.1
1992	10.3	28.3	11.7	23.2	20.6	13.0	22.6
1994	13.3	23.8	8.3	11.3	21.6	11.6	17.8
1996	19.2	20.0	12.1	34.2	24.2	18.8	45.1
1997	18.0	36.0	10.3	20.9	27.5	13.5	21.2
1998	18.3	26.6	7.5	14.7	29.6	12.8	19.4
Point **H**							
1988	12.4	22.2	5.8	8.5	19.2	9.4	14.9
1989	–	26.2	7.2	16.2	33.5	19.5	25.5
1990	–	37.2	13.5	20.5	35.4	20.2	31.3
1992	16.1	32.0	11.1	17.8	28.6	6.7	25.7
1994	21.1	44.2	16.6	27.0	36.8	25.3	36.5
1996	16.3	19.0	10.7	19.1	27.9	15.2	24.3
1997	18.5	33.0	10.0	19.7	31.1	16.7	24.6
1998	21.2	40.5	10.7	20.0	33.7	20.0	29.1

4.3.3 Brightness Temperature as the Direct Characteristic of Heat Interaction in the Climatic Time Scales

We have revealed that the SSM/I-derived brightness temperatures of the SOA are responsive to intra- and interannual variations of sensible, latent, and total heat fluxes in the points **M**, **D**, and **H** (rather, in areas 0.5 by 0.5° covering these points and being in line with the SSM/I spatial resolution). For example, Fig. 4.8 demonstrates a noticeable relation between long-term variability of monthly mean total heat flux and SSM/I brightness temperature at the wavelength 1.35 cm measured in the channel 22 V of the radiometer (available gaps in the brightness temperature
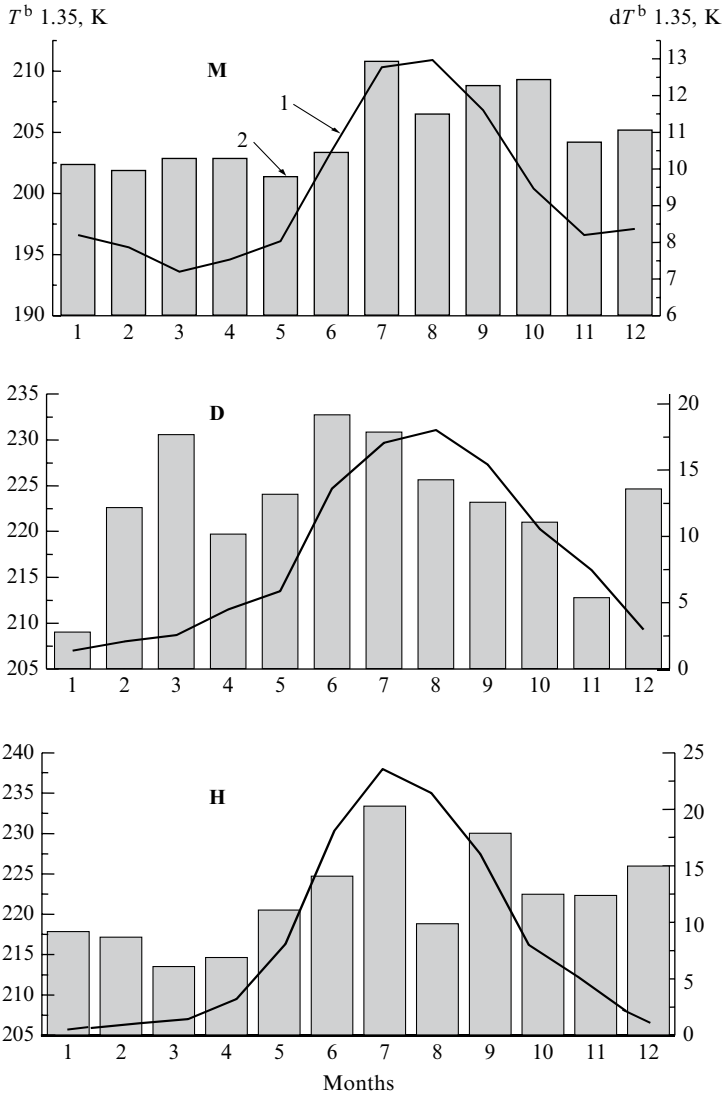
Fig. 4.7 Seasonal trends of monthly mean SSM/I brightness temperature at the wavelength 1.35 cm averaged over the period 1988–1999 (1) and their interannual variations during this time interval (2) in points **M**, **D**, and **H**

data are caused by troubles in processing of initial SSM/I data). Figure 4.9 shows some results of comparison between the total heat fluxes and their estimates represented as a linear combination of brightness temperatures T^b_22 V, T^b_1.55 V, and T^b_1.55H.

Therefore, it has become possible to determine a total heat flux as a linear combination of SSM/I brightness temperatures. The use of another SSM/I channels (besides
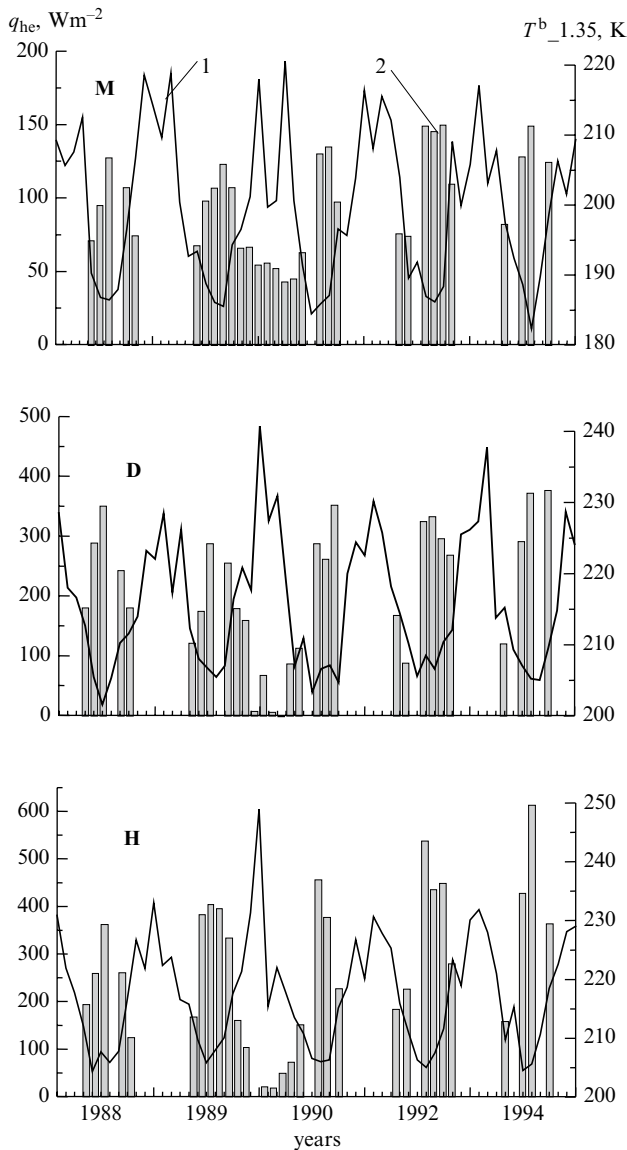
Fig. 4.8 Comparison of monthly mean heat fluxes q_{he} (1) and brightness temperature $T^b\_1.35$ (2) in the points **M**, **D**, **H** during 1988–1994

the channel 22 V) is helpful for corrections of heat flux estimates subjected to an influence of the atmospheric liquid water and near-surface wind speed variations.

The results obtained display the feasibility of determining the climatic heat flux in the ocean-atmosphere interface based on the data of *meteorological* sensing of the atmosphere.
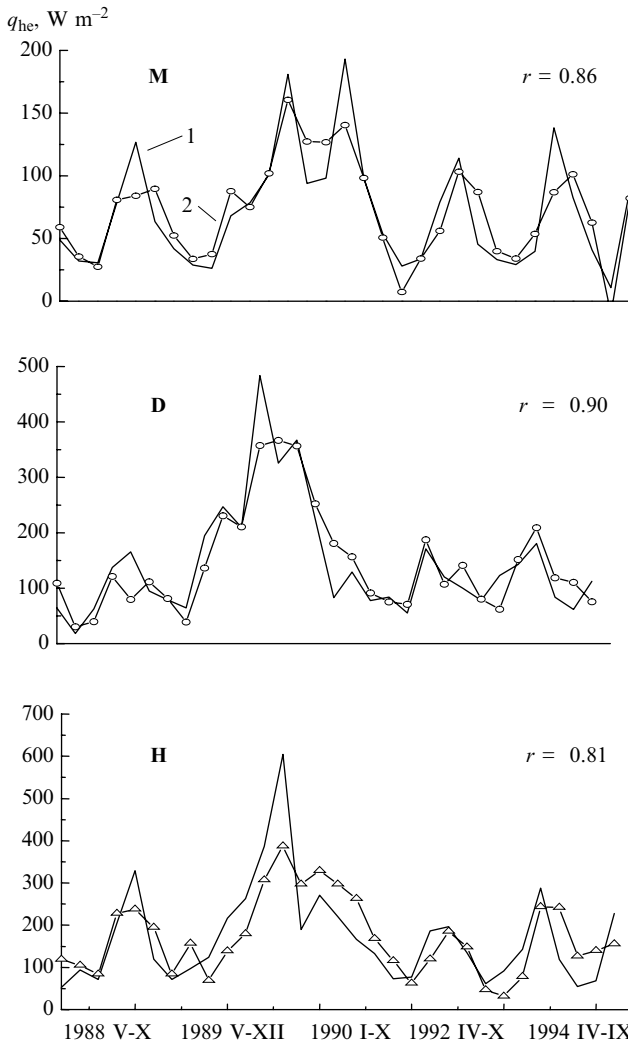
Fig. 4.9 Correlation of monthly mean heat fluxes q_{he} (1) with their SSM/I-derived estimates (2) in the points **M**, **D**, **H** during 1988–1994 (r coefficient of correlation)

This question has occurred to us while studying the contribution of different parameters of the ocean and atmosphere on relations between brightness temperature and heat fluxes in the *synoptic* range of time scales (Grankov et al. 2000). We observed in this case a negligible effect of the water surface temperature on these relations by more considerable heat inertia of the ocean against the atmosphere. But why this peculiarity is extending over climatic scales is the urgent question; its solution is substantial when we analyze the following problems: (a) what are the original factors in processes of large-scale air–sea heat interaction (from the scientific

point of view); and (b) to what extent the meteorological satellites are effective in the studies of these processes (as the practical aspect).

4.4   Conclusion

Long-term measurements from the DMSP SSM/I devices allow the estimation of the monthly mean values of most changeable SOA parameters, which are forming the air–sea heat interaction at seasonal and climatic time scales such as the monthly mean wind speed and integral water vapor content in the atmosphere, and which current values cannot be evaluated with ordinary reference data.

The satellite estimates of the monthly mean estimates of the wind speed and atmosphere integral water vapor content are slightly dependent on the spatial averaging (within the squares varied from 1×1 to $5 \times 5°$); the cloudiness and precipitation do not influence essentially an accuracy of these parameters estimation.

A strong correlation between monthly mean values of the SOA brightness temperature at the resonant line of a water vapor absorption in the atmosphere (1.35 cm) and the surface vertical turbulent heat fluxes in some areas of the North Atlantic over a period of years has been discovered.

References

Alishouse JC, Snyder SA, Vongsatorn J, Ferrado RR (1990a) Determination of oceanic total precipitable water from the SSM/I. J Geophys Res 28:811–816

Alishouse JC, Snyder JB, Westwater ER et al (1990b) Determination of cloud liquid water content using the SSM/I. J Geophys Res 28:817–821

Ferraro RR, Marks GF (1995) The development of the SSM/I rain rate retrieval algorithms using ground based radar measurements. J Atmos Oceanic Tech 12:755–770

Goodberlet MA, Swift CT, Wilkerson JC (1990) Ocean surface wind speed measurements of the Special Sensor Microwave/Imager (SSM/I). IEEE Trans Geosc Remote Sens 28:823–828

Grankov AG, Gulev SK (1996) Use of the radiometric measurements from the "Priroda-Mir" (Alpha) station for estimating seasonal and synoptic vertical fluxes of heat and water over oceans, earth and basins. In: NASA/RSA Science and Technical Advisory Council research

Grankov AG, Mil'shin AA, Petrenko BZ (1999) Natural microwave radiation as a characteristic of the ocean-atmosphere heat interaction on seasonal and synoptic time scales. Dokl Acad Nauk 367:680–683 In Russian

Grankov AG, Mil`shin AA, Novichikhin EP (2000) Interconnection between the brightness temperature and the intensity of the thermal ocean-atmosphere interaction (Based on the data Atlantex-90 experiment). Earth Obs Rem Sens 16:457–467

Handbook (1979) Averaged month, 10 and 5-day periods values of the air water and temperature, their difference and wind speed in selected regions of the North Atlantic (1953–1974 years). VNII GMI, Obninsk (in Russian)

Kalnay E, Kanamitsu M, Kistler R et al (1996) The NCEP/NCAR Reanalysis Project. Bull Am Meteorol Soc 77:437–471

Lappo SS, Gulev SK, Rozhdestvenskii AE (1990) Large-scale heat interaction in the ocean–atmosphere system and energy-active zones in the world ocean. Gidrometeoizdat, Leningrad (in Russian)

Liu WT (1988) Moisture and latent flux variabilities in the tropical Pacific derived from satellite data. J Geophys Res 93:6749–6760

Matweev Ju L, Soldatov SA (1982) Water content of the atmosphere. Trudy VNII GMI 94:36–42 (in Russian)

Snopkov VG (1981) On seasonal variations of the water vapor content over the Atlantic. In: Atmosphere circulation and its interaction with the ocean in the tropical and subtropical latitudes of the Atlantic Nauka, Moscow (in Russian)

Taylor PK (1984) The determination of surface fluxes of heat and water by satellite radiometry and in situ measurements. In: Gautier C, Fleux M (eds) Large-scale oceanographic experiments and satellites. Reidel, Dordrecht, pp 223–246

Wentz FJ (1991) User's manual SSM/I antenna temperature tapes (Revision 1). RSS Technical Report, Santa Rose

Chapter 5
Effectiveness of the Satellite MCW Radiometric Means of Studying the Air–Sea Interaction

5.1 Present-Day and Perspective Satellite Passive MCW Radiometric and Other Means of the Earth Remote Sensing and Their Potential

5.1.1 Prehistory and General Information

When studying the global ocean and its main climate-forming factors, a reach arsenal of instrumentation in optical, infrared, and microwave electromagnetic ranges is used. In accordance with the requirements of the Global System of Climate Observations (Kondrat`ev et al. 1992) to the characteristics of means of remote sensing from satellites such as a spatial and temporal resolution, survey coverage and its duration, an accuracy of determination of geophysical parameters, the polar space platforms are most suitable. Some types of polar platforms as well as the orbital parameters are presented in Table 5.1; the low-latitude satellite TRRM and the PROTEUS satellite are the exceptions in this series.

The idea of using the MCW radiometric methods in climatic studies became a realistic one in 1978 after the launch of the Nimbus-7 multichannel scanning radiometer SMMR, which operated for about 9 years. On the basis of the data of its measurements, the archive of the antenna temperatures (the SMMR level 1A data set) in NASA Goddard Space Flight Center (GSFC) has been created. Later, these data have been calibrated and processed in the form of brightness temperatures (the SMMR level 1B data set) in Jet Propulsion Laboratory (JPL) in the frame of the program EOS (Earth observing system) Pathfinder Program, and archived in NASA Marshall Space Flight Center Distributed Active Archive Center with the 8-mm magnetic tapes – about 70 GB of information (Njoku et al. 1995).

Since 1987, the operative meteorological satellites DMSP with the radiometers SSM/I, SSM/T, and SSM/T-2 are successfully functioning; the original measurement data and results of their processing are accumulated and stored in several USA scientific centers (Dubach 1988; Defense Meteorological Satellite Program, DMSP 1997). Thus, because of efforts of specialists of NASA, NOAA, and USA Defense

Ministry, the unique possibility to conduct the climatic studies of the ocean with the methods of MCW radiometry over periods of 30 years is appearing.

5.1.2   MCW Radiometer SMMR of the Nimbus-7 Satellite

The radiometer SMMR (scanning multichannel microwave radiometer) was operated on the board the Seasat and Nimbus 7 satellites, launched in June 28 and October 24, 1978, respectively. Later, in October 10, a functioning of the Seasat satellite has been violated; the Nimbus-7 SMMR Radiometer operated about 9 years. This device served as the source of information on ocean surface temperature, near-surface wind speed, rain rate, integral water vapor content of the atmosphere, cloud liquid water content, the soil moisture, and snow and ice covers characteristics (Njoku 1982).

The SMMR had six separated receivers, a single antenna and a calibration subsystem. Two radiometers measured the signals at the frequency 37 GHz on the vertical (V) and horizontal (H) polarizations. Other receivers operated at the frequencies 6.6, 10.69, 18.0, and 21.0 GHz on V- and H-polarizations. The antenna system of radiometer provided the conical scanning under the angle 42° from the nadir in the sector of azimuth angles ±25°, ensuring the survey width of 780 km. The satellite had the circular orbit with inclination 99.2°, the height about 995 km, and the periodicity of survey 104.16 min, i.e., 13.8 revolutions per every 24 h. A global Earth coverage was obtained during 6 days. In August 1987, the antenna scanning mechanism has lost its functions, but the radiometer was working during the next 1-year period in the nonscanning (the tracer) regime.

5.1.3   DMSP MCW Radiometric Complex

The visible place in the row of modern satellite MCW passive radiometric means is the radiometer developed and used till now in the frame of the satellite meteorological program of the Defense Meteorological Satellite Program (DMSP). This program was designed at that time and now for a long-term Earth monitoring to obtain the meteorological, oceanographic, and the Sun activity information over the oceans (Hollinger et al. 1990; Defense Meteorological Satellite Program, DMSP 1997).

The DMSP satellites have an inclination of 98.8° and the height of the 850 km with the periodicity of 102 min (14.2 revolutions per 24 h). The global coverage of the Earth is accomplished after 3 days, and the partial one – every 24 h; the sub satellite tracks are repeated every 16 days. Main orbital parameters of the DMSP satellites are shown in Table 5.1. At present, six satellites of the DMSP series are functioning – F-12, F-13, F-14, F-15, F-16, and F-17, which have a leaving time of about 4 years. The first-born satellite in this series was the satellite F-08, whose measurements (meaning the places and dates of their conducting) have been coincided with the vessel measurements fulfilled during the experiments NEWFOUEXS-88 and ATLANTEX-90.

Table 5.1 Parameters of the satellite circular orbits

Satellite	Data of launch	Inclination (°)	Height (km)	Period (min)	Local time of the equator crossing
Nimbus-7	October 1978	99.2	955	104.16	–
DMSP F-08	June 1987	98.8	833	102.0	6.12
DMSP F-10	December 1990	98.8	740–853	100.5	19.42
DMSP F-11	November 1991	98.8	841–878	101.9	18.11
DMSP F-12	August 1994	98.9	844–851	102.0	21.22
DMSP F-13	March 1995	98.8	844–856	102.0	17.42
DMSP F-14	April 1997	98.8	850	102.0	19.08
TRMM	November 1997	35	400	92.5	–
DMSP F-15	October 1998	98.8	850	102.0	20.42
Meteor-3M, No. 1	December 2001	99.65	1,024	105.5	09.15
EOS-Aqua	May 2002	98.2	705	99	13.15–13.45
ADEOS-II	2002	98.6	797	101	10.00
DMSP F-16	October 2003	98.9	843–853	101.9	21.05
Sich-1	December 2004	99.64	1,024	105.53	10.30 (16.30)
DMSP F-17	November 2006	98.8	841–855	102.0	–
NPOESS	2009–2011	98.7	833	–	5:30 (13:30)
PROTEUS	November 2009	98.4	763	100	06:00
MKA-FKI No. 1	2010	82.5	650–664	–	–
Meteor-M, No. 1	2009	98.068	830	101.3	–

Table 5.2 Composition of the DMSP satellites

Device	F-08	F-10	F-11	F-12	F-13	F-14	F-15	F-16	F-17
OLS	–	x	x	x	x	x	x	x	x
SSM/I	x	x	x	x	x	x	x	–	–
SSM/T	–	x	x	x	x	x	x	–	–
SSM/T2	–	–	x	x	–	x	x	–	–
SSI/ES-2,3	–	x	x	x	x	x	x	x	x
SSJ/4,5	–	x	x	x	x	x	x	x	x
SSB/X-2	–	x	x	x	x	x	x	–	–
SSM	–	–	–	x	x	x	x	–	–
SSZ	–	–	–	–	x	–	–	–	–
SSMIS	–	–	–	–	–	–	–	x	x
SSULI	–	–	–	–	–	–	–	x	x
SSUSI	–	–	–	–	–	–	–	x	x
SSF	–	–	–	–	–	–	–	x	x

The following abbreviations are used in the table 5.2 (operational linescan system) – the scanner operating in the visible and IR range of electromagnetic wavelengths: SSM/I – special sensor microwave/imager, SSM/T – atmospheric temperature profiler, SSM/T2 – atmospheric water vapor profiler, SSI/ES-2, 3 – Special sensor ionospheric plasma drift/scintillation meter, SSJ/4,5 – precipitating plasma monitor, SSB/X-2 – gamma ray particle detector, SSM – special sensor magnetometer,

SSULI – ultraviolet limb imager, SSUSI – ultraviolet spectrographic imager and Nadir airglow photometer, and SSF – laser threat warning sensor.

5.1.4 SSM/I – Special Sensor Microwave/Imager

This radiometer was designed for global and local remote sensing the cloud integral liquid water, the intensity of rainfalls, the integral water vapor content in the atmosphere over the ocean, the near-surface wind speed, sea ice characteristics, and the moisture and temperature characteristics of the soil surface (Special Sensor Microwave Imager (SSM/I) User's Interpretation Guide 2000).

The antenna system of radiometer provides the conical scanning under the angle 45° from the nadir in the sector of azimuth angles ±52°, ensuring the survey width of 1,400 km.

The measurements are carrying out with the 7-channel, 4-frequency channel MCW radiometric system (see Table 5.3) (Hollinger et al. 1990).

5.1.5 SSM/T – Atmospheric Temperature Profiler

This device is the 7-channel MCW sounder, which was designed for global and synoptic analysis of the troposphere and bottom stratosphere layers (Defense Meteorological Satellite Program, DMSP 1997). Its seven frequency channels are arranged in the band of the radiowave absorption in the molecular oxygen at the frequencies 50.50, 53.20, 54.35, 54.90, 58.40, 58.825, and 59.40 GHz.

Outer calibration of the radiometer is processed with two etalons: as the first one, the galactic MCW natural radiation (~2.7 K) is used; the second pole is an artificial hot target attached to the SSM/T input circuits.

First, the SSM/T-1 was launched in space with the satellite Block 5D in 1978 (Njoku 1982).

5.1.6 SSM/T-2 – Atmospheric Water Vapor

The radiometer SSM/T-2 is a scanning fifth channel system of passive MCW radiometric sensing of the atmospheric bottom layers profiler (Falcone et al. 1992; Tadepalli 1994).

Table 5.3 Parameters of the SSM/I radiometer

Frequency (GHz)	19.35	22.235	37.0	85.5
Polarization (V/H)	V, H	V	V, H	V, H
Sensitivity (K)	0.5	0.7	0.4	0.8
Spatial resolution (km)	69×43	60×40	37×29	15×13
Survey width (km)	1,400			

It has three spectral channels centralized round the frequency 183.31 GHz (the line of absorption in the water vapor) and the channels 91 and 150 GHz.

The SSM/T-2 device has the swath width about 1,500 km and provides the Earth overview every 24 h (about 14 circles).

5.1.7   SSMIS – Special Sensor Microwave Imager/Sounder

At present, a new generation of the MCW radiometers is used on the board of the DMSP F16 and F17, which are designed for monitoring the system ocean–atmosphere and combine the functions as the scanner and the sounder (Special Sensor Microwave Imager and Sounder, SSMIS 2007). The channel parameters of this device are illustrated in Table 5.4.

The SSMIS collects microwave energy from the Earth's surface and atmosphere with a rotating 61-cm parabolic reflector. This reflector focuses the energy on an assembly consisting of six feedhorns, which provide the initial frequency multiplexing for the 24 channels. The reflector and the six feedhorns rotate with the entire sensor canister. Located at the top of the canister are a cold calibration reflector and a warm calibration source, which do not rotate with the canister. The feedhorns view a fixed cold calibration reflector and a fixed warm calibration source for each revolution of the sensor. These calibration data are used to convert the sensor output to absolute radiometric brightness temperatures. At the nominal orbital height of 833km, SSMIS produces a swath width on the ground of 1,707 km with 12.5 km scene spacing. The achieved swath width applies uniformly to all channels of the SSMIS. The 1.9 s interscan period provides along-track sample spacing (12.5 km) equivalent to the along-scan spacing.

5.1.8   TRMM Complex

The satellite TRMM (tropical rainfall measuring mission) developed in the frame of a joint America/Japan program was designed for regular synoptic information on the tropical rainfalls as one of appreciable weather and climate forming factors (Kondrat`ev et al. 1992; Remote Sensing 1998). This satellite has been launched in 1997; its main parameters are shown in Table 5.1.

The central task of the program was the extraction of information about the monthly mean estimates of precipitation and vertical profiles of latent heat in the atmosphere over the periods not less than 3 years. Remote sensing devices were placed on the board – the MCW-radiometer TMI (TRMM Microwave Imager); the meteorological radar (precipitation radar) with an electronic scanning at the frequency 13.8 GHz, the 5-channel scanning radiometer VIRS operated in the visible and IR-electromagnetic ranges, is similar to the NOAA AVHRR-3 radi-

Table 5.4 Channel characteristics of SSMIS sensor

Channel	Center frequency (GHz)	3-db width[c] (MHz)	Frequency stability (MHz)	Polarization[d]	Sensitivity[b] (K)	Sampling interval[a] (km)
1	50.3	380	10	V	0.34	37.5
2	52.8	389	10	V	0.32	37.5
3	53.596	380	10	V	0.33	37.5
4	54.4	383	10	V	0.33	37.5
5	55.5	391	10	V	0.34	37.5
6	57.29	330	10	RCP	0.41	37.5
7	59.4	239	10	RCP	0.40	37.5
8	150	1,642 (2)	200	H	0.89	12.5
9	183.31+/−6.6	1,526 (2)	200	H	0.97	12.5
10	183.31+/−3	1,019 (2)	200	H	0.67	12.5
11	183.31+/−1	513 (2)	200	H	0.81	12.5
12	19.35	355	75	H	0.33	25
13	19.35	357	75	V	0.31	25
14	22.235	401	75	V	0.43	25
15	37	1,616	75	H	0.25	25
16	37	1,545	75	V	0.20	25
17	91.655	1,418 (2)	100	V	0.33	12.5
18	91.655	1,411 (2)	100	H	0.32	12.5
19	63.283248+/−0.285271	1.35 (2)	0.08	RCP	2.7	75
20	60.792668+/−0.357892	1.35 (2)	0.08	RCP	2.7	75
21	60.792668+/−0.357892 +/−0.002	1.3 (4)	0.08	RCP	1.9	75
22	60.792668+/−0.357892 +/−0.0055	2.6 (4)	0.12	RCP	1.3	75
23	60.792668+/−0.357892 +/−0.016	7.35 (4)	0.34	RCP	0.8	75
24	60.792668+/−0.357892 +/−0.050	26.6 (4)	0.84	RCP	0.9	37.5

[a]Sampling refers to along scan direction based on 833 km spacecraft altitude
[b]Sensitivity for instrument temperature 0°C and calibration target 260 K with integration times of 8.4 ms for channels 12–16; 12.6 ms for channels 1–7, 24; and 25.2 ms for channels 19–23 and 4.2 ms for channels 8–11, 17–18
[c]In brackets number of subbands is indicated in individual 3-db width
[d]RCP denotes right-hand circular polarization, *V (H)* vertical (horizontal) polarization

ometer; the sensor of the cloud brightness LIS (lighting imaging sensor) and the sensor of the radiation balance characteristics CERES (radiation budget instrument). The TMI device is 5-channel scanning MCW radiometer operated at the frequencies ranged from 10 to 91 GHz with the spatial resolution varied from 5 to 23 km in the swath of 520 km.

5.1.9 Meteor-3M No. 1 Complex

The satellites of the Meteor-3M series have the polar, sunsynchronous, circular orbit (see orbital parameters in Table 5.1). At the satellite Meteor-3M No. 1 launched in December, 2001, the multispectral optical and infrared instrumentation, the ozonometric spectrometer SAGE-III, the MCW radiometric scanning radiometer MTVZA, and some other sensors were installed. The satellite mass is about kg; its useful load is about 800 kg. The MTVZA operated validly till the summer of 2002, and during the next 1-year period – only in the along-the-trace regime because of malfunction of the antenna scanning system.

The MTVZA (multichannel air temperature and humidity sounder) (see Fig. 5.1) was designed for long-term observations (monitoring) of meteorological and oceanographic of the Earth. It is an attempt here to combine with this device the possibilities of all subsystems of the DMSP complex – the radiometers SSM/I, SSM/T, and SSM/T2. The orbital parameters of the Meteor-3M satellite and its radiometric complex MTVZA are presented in Tables 5.1, 5.5, and 5.6 (Cherny and Raizer 1998; Cherny et al. 1998). One of the goals of this project is to provide a spacious ocean coverage from space – about 2,200 km, when this characteristic for the systems MIMR, SSM/I, SSM/T, SSM/T2, and
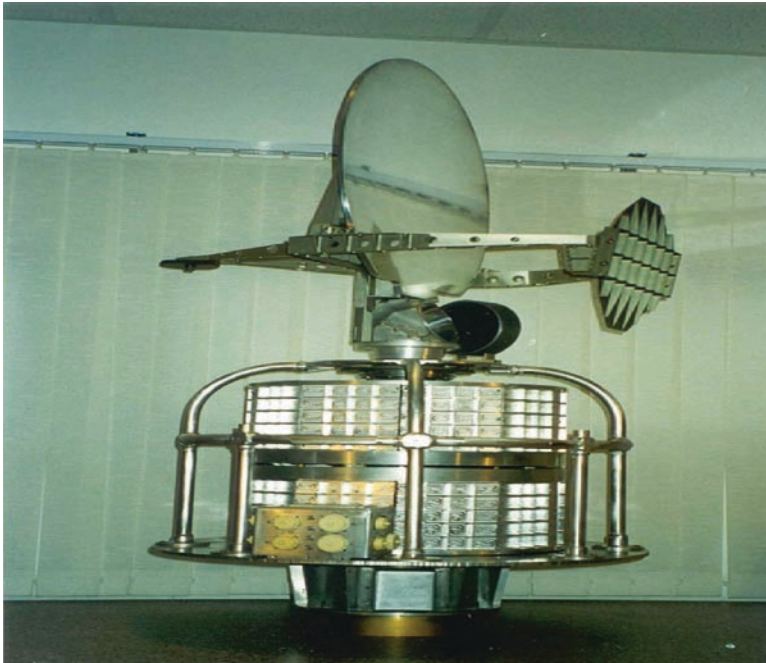
Fig. 5.1 The multichannel air temperature and humidity sounder MTVZA

Table 5.5 Parameters of the MTVZA complex

Frequency (GHz)	18.7	22.2	33.0	36.5	42.0	48.0	52-57	91.6	183
Sensitivity in pixel (K)	0.25	0.25	0.35	0.38	0.45	0.45	0.3	0.5	0.4
Absolute error of the antenna temperatures measure- ments (K)	0.5	0.5	0.6	0.6	0.7	0.7	1.0	1.0	1.1
Antenna efficiency (%)	93.7	93.4	93.5	93.5	92.8	93.9	94.2	95	95
Spatial resolution (km)	76× 136	68× 124	45× 82	41× 75	36× 65	32× 58	30× 55	18× 33	12× 22
Incidence angle (°)	69								
Swath (km)	2,200								
Mass (kg)	107								
Power supply (W)	110								

Table 5.6 Parameters of the MTVZA radiometric channels

	Central frequency (GHz)	Number of pass bands	Pass band width (MGz)	Polarization	Height of peak of sensitivity (km)
1–2	18.7	1	800	V, H	–
3	22.235	1	1,600	V	–
4–5	33	1	2,000	V, H	–
6–7	36.5	1	2,000	V, H	–
8–9	42	1	2,000	V, H	–
10–11	48	1	2,000	V, H	–
12	52.8	1	400	V	2
13	53.30	1	400	V	4
14	53.80	1	400	V	6
15	54.64	1	400	V	10
16	55.63	1	400	V	14
17–18	91.65	2	3,000	V, H	Earth surface
19	183.31±7.0	2	1,500	V	1.5
20	183.31±3.0	2	1,000	V	2.9
21	183.31±1.0	2	500	V	5.3
22	57.290344±0.3222	4	50	H	20
23	57.290344±0.3222	4	20	H	25
24	57.290344±0.3222	4	10	H	29
55	57.290344±0.3222	4	5	H	35
26	57.290344±0.3222	4	3	H	42

AMSR-E is varied from 1,200 to 1,600 km. This improvement is reached by increasing the viewing angle ranges upto 65° and using the more high satellite orbit (1,024 km).

5.1.10 EOS Aqua Satellite Complex

The EOS Aqua satellite has the polar, sun-synchronous, circular orbit (see Table 5.1). Six remote sensing devices – AIRS, MODIS, CERES, including three MCW radiometers (ASMR-E, AMSU-A, and HSB) – are on a board of the satellite. A useful load is of 1,100 kg, the average power supply of the devices is about 1,200 W, and the output information flux is about 7.7 MB s^{-1}.

5.1.10.1 AMSR-E – Advanced Microwave Scanning Radiometer

AMSR-E radiometer is a modification of the ADEOS-II AMSR radiometer designed in NASDA in a frame of the EOS program prolonging a development of the conception of the DMSP SSM/I radiometers.

The radiometer provides a monitoring of geophysical parameters of atmosphere, ocean, land, and cryosphere. A global covering of the Earth completes during every 3 days and nights (72 h), during 48 h the covering is of 98.8%, and during 24 h, of 82%. When studying the atmosphere, a determination of liquid water and ice content of the clouds, the integral water vapor content, rainfall intensity, and a monitoring of typhoons is carried out. The oceanographic parameters of interest are the water surface temperature and near-surface wind speed. Also, an important task is a determination of the CO_2 changes in the ocean–atmosphere interface. The cryosphere studies include mapping the ice, estimating its type and concentration. When studying the land surface, the snow coverage and its water equivalent, freez/thaw boundaries, the soil moisture, and vegetation characteristics are determined.

Parameters of the AMSR-E radiometric complex are given in Table 5.7 (Kawanishi et al. 2003). The specific feature of the AMSR-E radiometer in comparison with the SSM/I device is a midday time of the Earth equator crossing. This peculiarity enlarges its potential for solving some tasks of the studies of the ocean and land surface, and in particular, it is important for estimation of vegetation characteristics at the frequencies 10.65 and 6.8 GHz.

5.1.10.2 AMSU – Advanced Microwave Sounding Unit

This MCW radiometer was operated in USA for determination of the temperature profiles in stratosphere, filtration of the cloudiness effect in troposphere, and estimating the cloud liquid water content (Kondratèv et al. 1992; MTPE EOS Reference Handbook 1995). The radiometer AMSU is the 15-channel transversally

Table 5.7 Parameters of the AMSR-E radiometric complex

Frequency (GHz)	6.9	10.65	18.7	23.8	36.5	89
Polarization (V/H)	V, H	V, H	V, H	V, H	V, H	V, H
Sensitivity (K)	0.3	0.6	0.6	0.6	0.6	1.1
Width of a directional pattern (°)	2.2	1.4	0.8	0.9	0.4	0.18
Antenna efficiency (%)	95.3	95	96.3	96.4	95.3	96.0
Spatial resolution (km)	76×43	51×30	27×16	31×18	14×8	6×4
Angle of sounding (°)	55					
Swath (km)	1,445					
Antenna diameter (m)	1.6					
Mass (kg)	324					
Power supply (W)	350					
Output information flux (Kb s^{-1})	87.4					

scanning system with the survey width of 1,650 km and spatial resolution (in nadir direction) of 40 km. The survey is carrying out in the range of angle ±49.5° with resolution 3.3°. Channels 3–14 are working in the resonant regions of the atmosphere oxygen (50–60 GHz), channel 1 corresponds to the resonant frequency of the atmosphere water vapor (22.235 GHz) and used for estimating its total content, and channel 2 (31 GHz) is used for rain rate indicating.

Output information flux is 3.2 Kb s^{-1}, power supply-125 W, mass – 125 kg, and dimensions – $65.5 \times 29.9 \times 59.2$ cm.

5.1.10.3   HSB – Humidity Sounder for Brazil

This device is designed for determination of the atmosphere humidity and selection of precipitations under clouds with 13.5 km spatial resolution (in nadir). The radiometer HSB is the 4-channel system: 3 channels are operating in the resonant region 183.3 HGz of the atmosphere water vapor and the fourth channel has the frequency 150 GHz. The radiometer is scanning transversally to satellite trace in a swath of 1,650 km in range of angles ±49.5° with resolution 1.1° (Kondrat`ev et al. 1992; MTPE EOS Reference Handbook 1995).

Output information flux is 4.2 Kb s^{-1}, power supply – 85 W, mass – 66 kg, and dimensions – $77.4 \times 99 \times 56$ cm.

5.1.10.4   AIRS – Atmospheric Infrared Sounder

The infrared radiometer of a very high resolution AIRS is operating at the range of electromagnetic waves 0.4–15.4 mcm, carrying out simultaneous measurements in 2,300 spectral channels; the spectral resolution ($\lambda/\Delta\lambda$) is 1,300.

The channels of visible and near IR ranges are used for selection of the cloudiness lower layer and various types of land surface including the snow and ice covers. Besides, the channels of a visible range are used for determination of the cloud, land, and ocean parameters with an account of the atmospheric correction. The AIRS radiometer is capable of retrieving the atmosphere temperature and humidity vertical profiles, and the temperature and emissivity of the surface observed with the spatial resolution of 13.5 km (in nadir). The radiometer is scanning transversally to satellite trace in the swath of 1,650 km in range of angles ±49.5° with resolution 1.1°.

Output information flux is 1.44 Mb s^{-1}, power supply – 256 W, mass – 156 kg, and dimensions – 139.7×77.5×76.2 cm.

5.1.10.5   MODIS – Moderate-Resolution Imaging Spectroradiometer

The multispectral spectroradiometer of a moderate resolution MODIS serves for analysis of biological and physical processes with a periodicity 1–2 days. It was designed for long-term observations of global dynamics of such Earth characteristics as landscape, surface temperature, snow cover, vegetation (on the land), water surface temperature and chlorophyll concentration (in the ocean) and aerosol, clouds, air water vapor, and temperature profiles (in the low atmosphere). The optical scheme of the MODIS device provides image formation in 36 discrete bands ranged from 0.4 to 14.5 μm. The optical scheme of the MODIS device provides image formation in 36 discrete bands ranged from 0.4 to 14.5 mcm. These spectral bands have a spatial resolution 250 m (2 bands), 500 m (5 bands), and 1,000 m (29 bands) in nadir. The ratio signal/noise exceeds 500 under 1-km spatial resolution for the zenith angle of the Sun of 70°. An accuracy of radiation flux is not less than ±5% in the spectral region 0.4–3 mcm and 1% in region 3.7–14.5 μm.

The radiometer is scanning transversally to satellite trace in the swath of 2,300 km in the range of angles ±55.5°.

Output information flux is 10.5 MB s^{-1} in the daytime and 3.3 MB s^{-1} in nighttime, power supply – 163 W, mass – 229 kg, and dimensions – 104.4×118.4×163.8 cm.

5.1.10.6   CERES – Clouds and the Earth's Radiant Energy System

The CERES sensor was designed for the Earth radiation balance measurements in the absence and presence of the cloudiness. The measurement data of the cloudiness characteristics and the radiation fluxes are used as basic parameters in the models of the ocean and atmosphere energy transfer. The device consists of two wideband radiometers with three channels: the first one operating in range 0.3–100 mcm serves for the measurement of the total radiation; the second (0.3–0.5 μm) for the short-wave radiation measurements; also the spectral window (8–12 μm) for the IR radiation measurements is available.

Output information flux is 20 KB s^{-1}, power supply – 94 W, mass – 100 kg, and dimensions – 2×(60×60×70 cm).

5.1.11   Complex of the ADEOS-II Satellite

ADEOS-II is advanced modification of the ADEOS-I satellite with measurement complex designed and manufactured by Japan space agency NASDA. This complex includes the spectrometer global imager (GLI) for a global monitoring of biological and physical processes in the atmospheric ozone, advanced spectrometer ILAS-II - Improved Limb Atmosphere Spectrometer, advanced radiometer AMSR-E – Advanced Microwave Scanning Radiometer, and SeaWinds scatterometer providing the global and precise estimates of the near-surface wind speed and direction (Kondrat`ev et al. 1992; Shilin and Tronin 1995). The studied objects of the ADEOS-II satellite are the earth surface, atmosphere, and global ocean. The satellite has the sun-synchronous orbit with inclination 98.6°, the height 800 km, and the equator crossing local time 10:00.

SeaWinds is the scatterometer designed for the all-weather global monitoring of the vector of wind speed over the ocean and an effective square of land reflection, and ice and ocean reflectivity with a high spatial resolution. These data are used for studying the troposphere dynamics, eddy flowers in upper layers of the ocean, ocean–atmosphere interface characteristics, and for weather forecasting at the global and regional scales. The scatterometer is operating at the frequency 13.4 GHz in the swath about 1,800 km; the Earth coverage is 90% per 24 h. The range of angles is ±51° from nadir.

Output information flux is 40 KB s^{-1}, power supply – 220 W, mass – 220 kg, and dimensions – 81×91×43 cm (without antenna).

5.1.12   Complex of the Sich-1M Satellite

The satellite optical/microwave scanner MTVZA-OK is designed for a global monitoring of the atmosphere, ocean, and land surface. This device is the modification of the MTVZA (see Fig. 5.2) device developed by the ROSCOSMOS Center of Program Researches and installed on a board of the satellite METEOR-3M No. 1. The Sich-1M with the MTVZA-OK scanner was launched in 2004 (Cherny et al. 2001).

5.1.13   The Measurement Complex of Russian Satellite
Meteor-M No. 1

The goals of this satellite project are:

• Determination of the atmosphere temperature and humidity vertical profiles
• Determination of integral air water vapor and cloud liquid water content, rain rate, and near-surface wind speed over oceans

Fig. 5.2 The satellite optical/microwave scanner MTVZA-OK

- Determination of the ocean surface temperature
- Monitoring the ice and snow covers
- Diagnosis of processes in the ocean upper layer
- Determination of the ocean water color and biological productivity;
- Studies of vegetation covers

The characteristics of the MTVZA-OK (see Table 5.8) are in agreement with the requirements of the World Meteorological Organization. Its unique property is synchronous and combined scanning in optical and MCW blocks.

The microwave scanner/sounder MTVZA GY. Nakonechny et al. (2004) has elaborated for the spacecraft "Meteor-3M;" its launch is planned in 2009 year and designed for retrieving the temperature and humidity atmosphere vertical profiles, as well as for remote sensing of the ocean and land covers. This radiometer is the

Table 5.8 Parameters of the optical/MCW scanner MTVZA-OK

Device	MCW-block	Optical block
Frequency (wavelength) ranges (GHz, mcm)	6.9, 10.6 GHz	0.37–0.45 mcm
	18.7, 23.8	0.45–0.51
	31, 36.5	0.58–0.68
	42, 48	0.68–0.78
	52.3–7.0	3.55–3.93
	89	10.4–11.5
	183.31	11.4–12.6
Period of scanning (s)	1.8	
Spatial resolution (km)	12–50	1.1
Antenna size (m)	0.6	
Output information flux (K s^{-1})	665.4	
Type of Scanning	Conical	
Swath (km)	2,200–800	
MASS (kg)	100	
Power supply (W)	240	

Table 5.9 Technical characteristics of the MTVZA_GY radiometer

Parameters	MTVZA_GY
Frequency (GHz)	10.6; 18.7; 23.8
	31.5; 36.7; 42, 48
	52–57, 91, 183, 31
Spatial resolution (*km*)	
in horizontal	16–198
in vertical	1.5–7
Survey width (km)	1,500
Scanning method	Conical
Regime	Incessant
Period of scanning (s)	2.5
Output information flux (Kb s^{-1})	35

advanced version of the multichannel scanning MCW radiometer MTVZA from spacecraft "Meteor-3M" and Sich-1M. Its characteristics correspond to the foreign analogs, the MCW radiometer AMSU-A, B, boarded at the NOAA satellites and the DMSP-16 scanner/sounder SSMIS device.

Table 5.9 illustrates the main technical characteristics of the radiometer MTVZA-GY; its photograph is shown at Fig. 5.3.

The radiometric channels of the MTVZA-GY scanner will be operated at the frequencies in the spectral windows 10.6, 18.7, 23.8, 31.5, 36.7, 42, 48, and 91 GHz; working frequencies of the sounder are located in the lines of atmospheric molecular oxygen (52-57 GHz) and a water vapor (183 GHz) attenuation.

Fig. 5.3 Microwave scanner/sounder MTVZA GY

Microwave radiometers at the frequency range 10–48 GHz are constructed with the scheme of receivers of direct amplification (of the compensation type). The radiometers at the frequency ranges 52–57, 91, and 183 GHz were constructed as the superheterodyne receivers. Table 5.10 shows the main parameters of the radiometer in Table 5.10.

Table 5.10 Parameters of the MTVZA-GY channels

Channel number	Central frequency (GHz)	Number of spectral bands	Frequency spectral bands (MGz)	Sensitivity of the radiometers (K s^{-1})	Type of polarization (V or H)	Type of the receiver (direct (D) or superheterodyne (S)
1	10.6	1	100	0.06	V	D
2	10.6	1	100	0.06	H	D
3	18.7	1	200	0.05	V	D
4	18.7	1	200	0.05	H	D
5	23.8	1	400	0.04	V	D
6	23.8	1	400	0.04	H	D
7	31.5	1	1,000	0.05	V	D
8	31.5	1	1,000	0.05	H	D
9	36.7	1	1,000	0.06	V	D
10	36.7	1	1,000	0.06	H	D
11	42	1	1,000	0.07	V	D
12	42	1	1,000	0.07	H	D
13	48	1	1,000	0.07	V	D
14	48	1	1,000	0.07	H	D
15	52.80	1	400	0.08	V	S
16	53.30	1	400	0.08	V	
17	53.80	1	400	0.08	V	
18	54.64	1	400	0.08	V	
19	55.63	1	400	0.08	V	
20	57.290344 ±0.3222±0.1	4	50	0.12	H	S
21	57.290344 ±0.3222±0.05	4	20	0.2	H	
22	57.290344 ±0.3222±0.025	4	10	0.3	H	
23	57.290344 ±0.3222±0.01	4	5	0.45	H	
24	57.290344 ±0.3222±0.005	4	3	0.5	H	
25	91.655	2	2,500	0.04	V	S
26	91.655	2	2,500	0.04	H	S
27	183.31±7.0	2	1,500	0.08	V	S
28	183.31±3.0	2	1,000	0.1	V	
29	183.31±1.0	2	500	0.15	V	

5.1.14 Complex of the NPOESS Satellite

Satellites of the NPOESS (National Polar-orbiting Operational Environmental Satellite System) series (http://www.ipo.noaa.gov/) have the polar, sun-synchronous,

circular orbit with the height 833 km and inclination 98.7°. The equator crossing local time is 05:30 and 13:30 for the USA satellites and 21:30 for the European satellites.

The following satellites of the NPOESS series represent the next stage of the DMSP satellites.

VIIRS – Visible/infrared imager/radiometer suite: This device is designed for accumulating the data of measurements of the earth atmosphere, ocean, and land surface in visible and IR-ranges These data bring a general information on the atmosphere, its clouds, Earth radiation budget, surface land and ocean temperature, and the color of the ocean surface waters.

CrIS – Crosstrack infrared sounder: It is the IR sounder designed for determination of the atmosphere temperature, humidity, and air pressure vertical profiles.

GPSOS – Global positioning system occultation sensor: The GPSOS device will be used in the analysis of the refraction effect at microwaves with the GPS and Russian GLONASS systems.

OMPS – Ozone mapping and profiler suite: The OMPS device designed for estimating the horizontal and vertical distribution of the ozone in the Earth atmosphere.

SESS – Space environment sensor suite: This device is useful for studying the magnetic fields, electronic concentration in the ionosphere, and the effect of the aurora.

ATMS – Advanced technology microwave sounder: The ATMS device is the MCW sounder served for a global observations of the atmosphere temperature and humidity with a high temporal resolution (about 24 h).

MIS – Microwave imager/sounder: Determination of the following parameters is the function of this device:

- Atmosphere temperature, humidity, and pressure vertical profiles
- Images of the surface sensed at all satellite
- Wind speed and its direction
- All-weather estimates of the soil moisture
- Ocean surface temperature
- Integral water vapor content of the atmosphere
- Precipitation: type and intensity
- Height of the cloud low
- Cloud liquid water content
- Snow coverage and its thickness
- Separation of the boundaries of the clear water and ice mixing zones
- Temperature of the ice covers
- Age of the ice covers and their boundaries changes
- Near-surface wind stress
- Land surface temperature
- Vegetation characteristics

The radiometer is scanning conically the underlying surface and atmosphere with the reflectors of diameter of 1.8 m. The satellite survey width is about 1,700 km. Spectral channels are able to measure a natural Earth MCW radiation at the frequencies 10, 23, 18, 37, and 89 GHz on the vertical (V) and horizontal (H) polarizations.

The atmosphere sounder is functioning in the atmospheric resonance areas at the frequencies 50.3–57, 150/166, and 183.31 GHz.

The low-frequency channel receives emission at the frequency 6.8 GHz on vertical and horizontal polarizations; it is supplied by the system of reduction of radio-interference influence. The sounder of upper atmosphere operates in the frequency range 60–63 GHz.

Output information flux is 500 KB s^{-1}, power supply – 357 W, and mass – 475 kg.

5.1.15   Complex of the PROTEUS Satellite

At present, a sensible progress in the development of satellite MCW radiometric means operating at decimeter range of wavelengths (L-band) is observed; in European Space Agency (ESA), special efforts are undertaken in designing the L-radiometers with a synthesized aperture. In Finland and Germany, a successful testing of the aircraft variants of such radiometers took place. Specialists of ESA have finished a design of satellite version of the L-radiometer with a synthesized aperture MIRAS for global monitoring of the soils moisture, the temperature, and salinity of waters (Borges et al. 2000). Spatial and temporal variations of the soil moisture fields are an important factor in the weather and climate models, and are also used as the key characteristic in the Earth hydrological cycle. The heat and moisture fluxes in the land-atmosphere interface strongly depend on the soil moisture, which rules by the processes of evapotranspiration and insolation. In oceans, the upper layer salinity plays an important role in the North Atlantic subpolar zone where the intrusive fluxes with a low salinity influence the depth of thermohaline circulation and meridional heat transfer. Salinity variations also influence subsurface dynamics of tropical oceans where rain changes a flotation of the water surface and an intensity of heat fluxes in near-surface layer.

The radiometer MIRAS has the Y-type configuration and includes 27 radiometric receivers supplied by microstrip antennas. Each antenna consists of four oscillators providing signal received on vertical and horizontal polarizations with isolation not less than 25 dB. The output signals of receivers are the Stock parameters *I* and *Q* in digital form. The radiometer sensitivity varies from 0.8 to 3 K on both polarizations; the spatial resolution is of 30–50 km. The satellite PROTEUS has the polar, sunsynchronous orbit with height 670 km and the equator crossing local time 6:00. The swath is 934 km. The image synthesis is carried out in the range angles that varies from 0° to 55°.

5.1.16   Russian Sensing Complex "MKA-FKI" No. 1

This complex will be mounted on the board of small-size satellite (micro-satellite) developed in the Lavochkin Designing Bureau. The mission is planned to start in 2010.
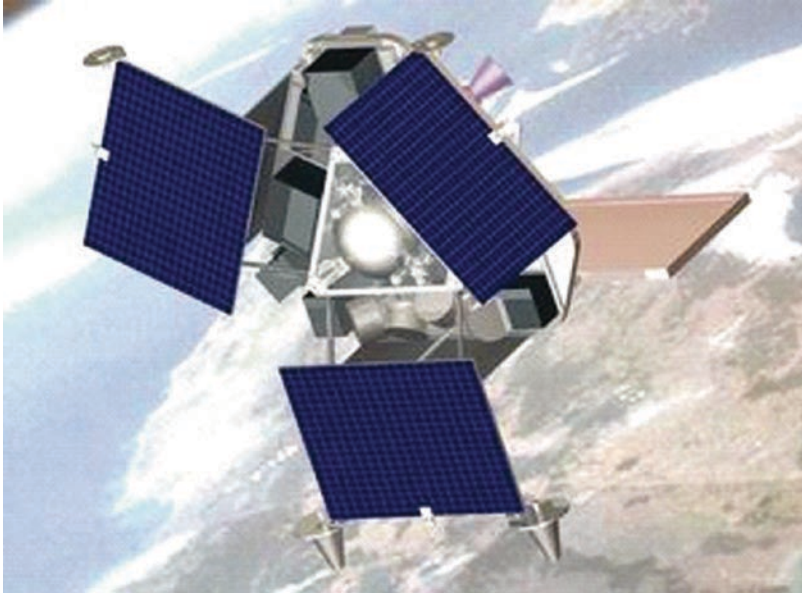
Fig. 5.4 Experiment "Zond": space platform "Karat" with L-radiometer (to the *right*)

Microsatellites equipped by the scientific devices will be launched as the additional useful attachment to usual spacecraft. As the future paramount realistic projects, in the focus of the Russian Academy of Sciences are five experiments with the microsatellites. In the first place, this is the experiment "Zond-PP" with the Institute of Radioengineering and Electronics RAS as its producer (see Fig. 5.4). This project was designed for studying the earth covers with the radiometer operating at microwaves in L-band (L-radiometer); it is directed to mapping the soil moisture and waters salinity (Armand et al. 2008). The results obtained will be used in the analysis and forecasting of the global changes of environment.

The main goals of studies with the spacecraft "MKA-FKI No.1" are as follows:

- Elaboration of radiophysical methods of the Earth remote sensing in perspective ranges of radiowaves for study of physical phenomena and processes in the system atmosphere-earth surface.
- Analysis of influence of outside factors (galactic background radiation, ionosphere radiation/absorption, etc.) as well as the radiointerference on the earth characteristics measured.
- Development of methods of improving the spatial resolution supplied by the L-radiometer.

The main scientific tasks are as follows:

- Mapping the moisture of the open and forest-covered soils (regional and global scales)

Table 5.11 Main characteristics of the spacecraft

Mass (kg)	120
Mass of payload (kg)	40
Orbit height (km)	650/664
Orbit inclination (°)	82.5
Output information flux (Kb s^{-1})	58
Power supply (W)	100–150
Life time (years)	5

Table 5.12 Main characteristics of MCW radiometer

Number of antenna beams	2
Swath (km)	580–600
Polarization	linear
Central frequency (GHz)	1.415
Frequency width (MHz)	20
Sensitivity (K)	0.3
Power supply (W)	60
Mass (kg)	13
Dimensions (mm): Radiometer	$400 \times 300 \times 50$
antenna	$800 \times 510 \times 40$

- Study of the temperature and moisture characteristics of the forest/bog systems
- Study of biometric characteristics from space
- Estimation of the water salinity
- Study of glaciologic and congelated ground zones
- Study of the energy exchanges in the system ocean-land-atmosphere (jointly with another sensors)
- Study of the Earth geothermal-active zones, estimation of their boundaries and the temperature regime
- Development of the methods of co-processing the data of sensors derived with various spatial resolution

Main characteristics of the FKA-MKI No. 1 spacecraft expected are presented in Table 5.11; the characteristics of its radiometers are illustrated in Table 5.12.

5.2 Comparison of Potentials of the SSM/I and MTVZA Radiometers for Analysis of the Ocean-Atmosphere Interaction

5.2.1 Background of Study

Technical characteristics of the MTVZA radiometer made us consider this device as a perspective instrument for determination of the cloud liquid water content, rain

rate, integral water vapor content of the atmosphere over oceans, near-surface wind speed, ice covers spatial distribution, concentration and age, snow water equivalent, and temperature and moisture of the land surface.

The most important point of the Program of scientific and applied researches with the satellite Meteor-3M No. 1 was an analysis of large-scale heat and dynamic ocean–atmosphere interaction including estimation of an intensity of vertical turbulent fluxes of heat and impulse (momentum) at the ocean surface as the climate-forming parameters of the system ocean–atmosphere. At present, a positive experience in studying the synoptic, seasonal, and climatic dynamics of heat and momentum fluxes in energy active zones of the North Atlantic has been accumulated using the SSM/I measurement data (Grankov et al. 2001; Grankov and Milshin 2001), which has the technical characteristics similar to the characteristics of the MTVZA radiometer in the frequency range 19–91.6 GHz (0.3–1.6 cm). In this respect, we proposed at the stage prior the launch of the Meteor-3M No. 1 satellite the following idea:

(a) Testing of the MTVZA radiometer potential by way of modeling its simulated measurement results at the same areas of the ocean and in the same intervals of the oceanographic and meteorological parameter variations where possibilities of the SSM/I radiometer were tested – namely in the areas of the North Atlantic observed in the experiments NEWFOUEX-88 and ATLANTEX-90.
(b) Comparison of these results with in situ measurement data derived from the SSM/I radiometer keeping in mind two levels of such comparative analysis: the SOA brightness temperatures, measured with the MTVZA and SSM/I radiometers, and the products of their interpretation, i.e., the heat fluxes.

The conditional experiment allowed to evaluate in advance capabilities of the MTVZA radiometer in studying the ocean–atmosphere interaction processes and optimal planning the real experiment. A similar approach was approbated in Vazhnik and Chistyakova (1989) where data of the brightness temperature measured by the SSM/I channel 37V were used for validation and calibration of analogical MCW radiometric channel of Russian orbital complex OCEAN-01 (Akvilonova et al. 2002).

Modeling of results expected from the MTVZA radiometer was based on the oceanographic, meteorological, and aerologic direct measurement data derived from research vessels *Victor Bugaev*, *Musson,* and *Volna* in the Newfoundland active zone of the North Atlantic at the stationary phase of the experiment Atlantex-90:

– Hourly values of the oceanic water surface temperature and near-surface wind speed
– Hourly values of the air temperature, humidity, and pressure

The typical model of relations between the ocean–atmosphere brightness temperature at microwaves and the SOA parameters (see Sect. 2.2 of Chap. 2) was used. The effect of cloudiness was ignored as the cloud liquid water content in the experiment ATLANTEX-90 was estimated visually with the use of the "optical" ten-point scale, which is of little interest at microwaves.

5.2.2 Comparison of MTVZA Simulated and SSM/I-Derived Brightness Temperatures

We compared the MTVZA simulated and SSM/I measured brightness temperatures at the wavelength 1.35 cm and the wavelength intervals 1.55−1.58 cm and 0.81−0.82 cm coinciding for both devices at the points of locating the R/Vs *Victor Bugaev*, *Musson,* and *Volna*. These spectral intervals are used traditionally for determining the most dynamical parameters of the SOA, such as the integral water vapor content in the atmosphere, cloud liquid water content, near-surface wind speed, as well as the boundary fluxes of sensible, latent, summer heat, and moment. Let us note that both the radiometers have the pass bands of 1,000 MHz; so their central frequencies (22.235 GHz for the MTVZA and 22.2 GHz for the SSM/I devices) can be assumed to be as same.

Unlike the calculated brightness temperatures derived for the cloudless atmosphere, the data of the SSM/I measurements include a radiation increment caused by the MCW absorption in clouds. To estimate this effect, we retrieved the cloud liquid water content (W) from the radiometer SSM/I with the method developed in (Bunker 1976) at the stationary phase of the experiment ATLANTEX-90 (see Fig. 5.5). It is seen from the figure that a value of the parameter W did not exceed 0.4 kg m^{-2}; this value corresponds to the weather situation "moderate cloudiness."

Figure 5.6 compares the simulated MTVZA and measured SSM/I brightness temperatures at the area where R/V *Victor Bugaev* was settled; such comparison was made (a) at the wavelengths 1.35 cm (channels 22V of the MTVZA and SSM/I radiometers), (b) 1.58 cm (MTVZA channel 19V) and 1.55 cm (SSM/I channel 19.35V), and (c) 1.58 cm (MTVZA channel 19H) and 1.55 cm (SSM/I channel 19.35H).

The correlation coefficient r and mismatch (*rms* difference) σ between the simulated and measured brightness temperatures are shown in the figure.

Distinctions of the Earth surface sensing angles (69° for the MTVZA and 55° for the SSM/I radiometers) and the time asynchronism of the satellite orbits result in essential increase of the difference between the absolute values of the MTVZA and SSM/I evaluated brightness temperatures (of 30−40 K); nevertheless, its *rms* difference is varied between 2.5 and 7 K, i.e., 8−15% from the brightness contrasts measured with the SSM/I; the correlation coefficient is varied from 0.71 to 0.88. A best compliance between these data is observed at the wavelength 1.35 cm (see Fig. 5.6a) where the MCW resonance absorption in the atmosphere water vapor is the dominating factor and an influence of the cloudiness is in the background here. The picks of the cloud liquid water content marked at the Fig. 5.5 influence appreciably the mismatch between the SOA simulated and experimental brightness temperatures; this effect is seen more clearly in the area of the R/V *Victor Bugaev* location on April 6–7 and 14–16, 1990.

More vast list of the σ and r value estimates for various channels of the SSM/I and MTVZA radiometers as well as for all research vessels used in the stationary phase of the experiment ATLANTEX-90 is contained in Table 5.13.
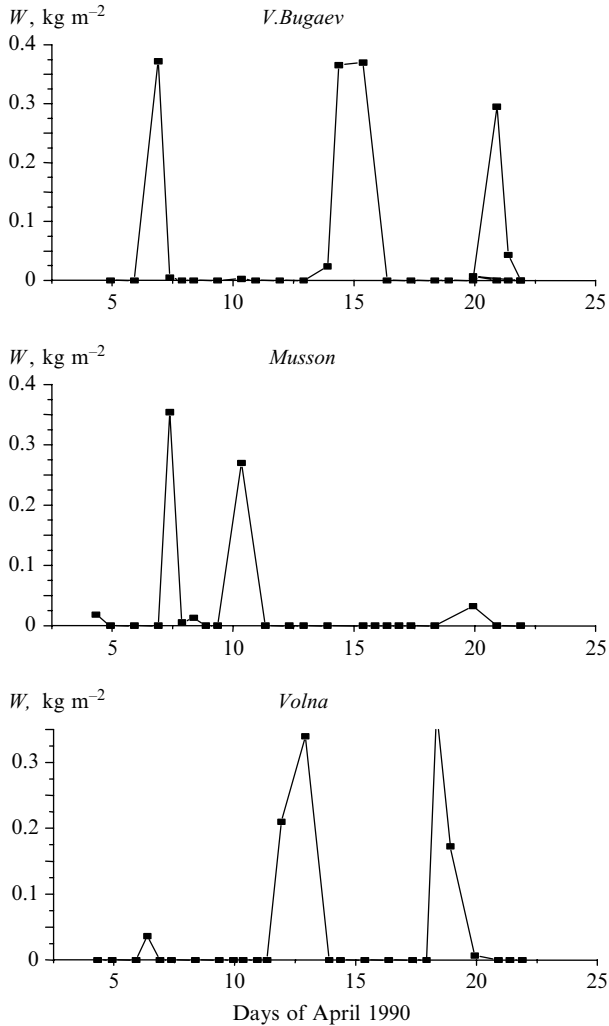
Fig. 5.5 Satellite estimates of the cloud liquid water content W resided to the regions of the R/Vs *V.Bugaev*, *Musson*, and *Volna* at the stationary phase of the experiment ATLANTEX-90

Aside from the cloudiness, the following factors influence discrepancy between simulated (MTVZA) and experimental (SSM/I) brightness temperature estimates:

(a) Time shift of satellite measurement samples relative to meteorological measurements – of 30 min (see Subsect. 3.2.4. of Chap. 3) and, especially, to aerologic measurements (up to 3 h); the complementary error can reach 6−7 K at the wavelength 1.35 cm.

(b) Availability of appreciable horizontal gradients of the atmosphere parameters (see Subsect. 3.2.4 of Chap. 3), which determine an uncertainty of spatially
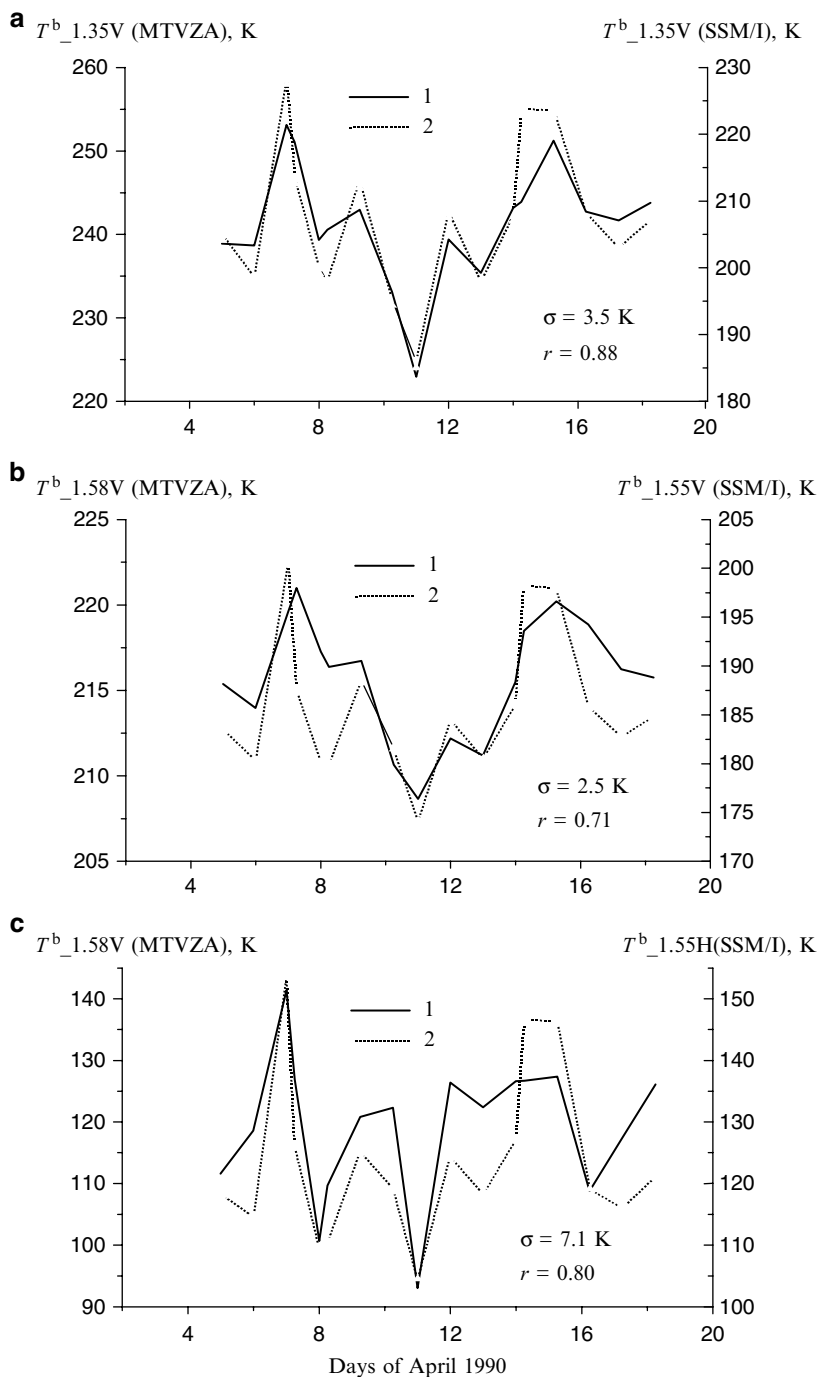
Fig. 5.6 Comparison of the evaluated SOA brightness temperature, during April 4–21, 1990 (experiment ATLANTEX-90, R/V *Victor Bugaev*): 1 – simulated data; 2 – measured (SSM/I) data: (**a**) σ = 3.5 K, r = 0.88, (**b**) σ = 2.5 K, r = 0.71 and (**c**) σ = 7.1 K, r = 0.80

Table 5.13 Mismatch (*rms* difference) σ and correlation coefficient r between simulated and measured SOA brightness temperatures at the stationary phase of the ATLANTEX-90 experiment

| Vessels | Radiometer channels | | σ_1 (K) | r_1 | σ_2 (K) | r_2 |
	MTVZA	SSM/I				
V.Bugaev	1.35V	1.35V (1)	3.5	0.88	–	–
	1.35V	1.35V+0.81V, H (2)	–	–	1.0	0.99
	1.58V	1.55V (1)	2.5	0.71	–	–
	1.58V	1.55V+0.81V, H (2)	–	–	1.3	0.94
	1.58H	1.55H (1)	7.1	0.8	–	–
	1.58H	1.55H+0.81V, H (1)	–	–	3.6	0.85
Musson	1.35V	1.35V (1)	2.6	0.83	–	–
	1.35V	1.35V+0.81V, H (2)	–	–	2.1	0.91
	1.58V	1.55V (1)	5.6	0.46	–	–
	1.58V	1.55V+0.81VH (2)	–	–	1.1	0.82
	1.58H	1.55H (1)	4.1	0.52	–	–
	1.58H	1.55H+0.81V, H (2)	–	–	2.8	0.82
Volna	1.35V	1.35V (1)	2.8	0.9	–	–
	1.35V	1.35V+0.81V, H (2)	–	–	2.4	0.94
	1.58V	1.55V (1)	1.6	0.42	–	–
	1.58V	1.55V+0.81V, H (2)	–	–	1.2	0.75
	1.58H	1.55H (1)	5.2	0.82	–	–
	1.58H	1.55H+0.81V, H (2)	–	–	4.4	0.89

averaged satellite estimates of the SOA brightness temperature (upto 4–5 K) in comparison with the simulated estimates based on the "spot" measurements from vessels.

Figure 5.7 shows results of imitation of the MTVZA measurements and the SSM/I real measurements at the wavelengths 1.35 cm and 1.55–1.58 cm for various values of the atmosphere integral water vapor content Q calculated from aerologic measurements and near-wind speed V in the area measured directly from the R/V *Volna* disposal during April 4–21, 1990. In both cases, a perceptible sensitivity of the SOA brightness temperature to the parameter Q variations (mainly at the wavelength 1.35 cm) and to variations of the parameter V registered by the SSM/I 1.55H and MTVZA 1.58H channels is observed; a scattering of these results is caused by the influence of the cloudiness.

5.2.3 Interrelation of the MTVZA and SSM/I Brightness Temperatures with Heat Fluxes

We studied the response of the MTVZA simulated and SSM/I measured brightness temperatures to the vertical turbulent heat fluxes registered in the experiment ATLANTEX-90 and analyzed their correlations. Figure 5.8 compares the SOA
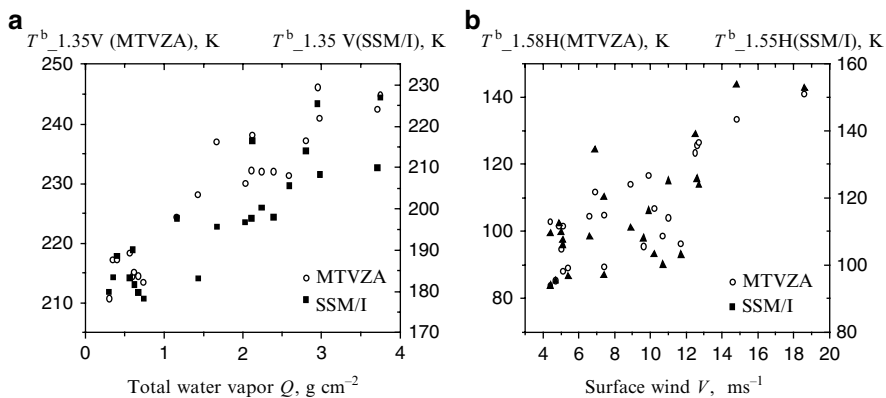
Fig. 5.7 Comparison of the MTVZA and SSM/I data: (**a**) MTVZA and SSM/I channels 1.35V under variations of integral water vapor and (**b**) MTVZA channel 1.58H and SSM/I channel 1.55H under variations of surface wind (R/V *Volna*)
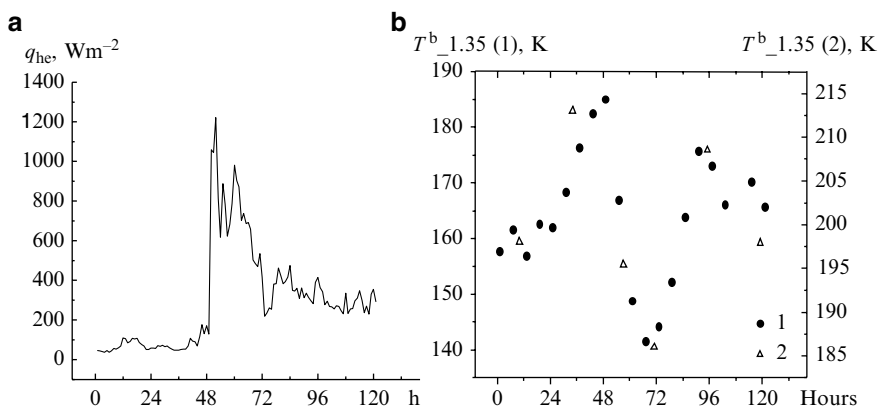
Fig. 5.8 Variations of total heat fluxes q_{he} (**a**), SOA brightness temperature (**b**) during April 8–13, 1990 in the area of the R/V *Victor Bugaev* settlement (**b**): 1 MTVZA simulated estimates; 2 SSM/I estimates

simulated brightness temperature at the wavelength 1.35 cm based on the data of meteorological and aerologic measurements from the R/V *Victor Bugaev* with 1-h time resolution and the F-08 SSM/I brightness temperature data with ~24-h resolution and the MTVZA brightness temperature data with 6-h resolution against a diurnal variability of the surface total heat fluxes in this area of the North Atlantic. These results demonstrate good accordance between simulated and experimental brightness temperature values in the water vapor resonant line of MCW absorption; at the same time, a clear reaction of these values to synoptic variations of the surface total heat fluxes is observed.

We analyzed also relations of the vertical turbulent fluxes total (sensible + latent) heat q_{he} and impulse q_v in the areas where the R/Vs *Victor Bugaev*, *Musson,* and *Volna* were resided and their estimates in the form of linear combinations ofcalculated MTVZA brightness temperatures in the channels 1.35V, 0.81V, 0.81H and measured SSM/I brightness temperatures in the channels 1.35V, 0.82V, 0.82H. These combinations are constructed in such a way to ensure the minimum *rms* difference (mismatch) between satellite estimates and original values of q_{he} and q_v. Figure 5.9 compares results of direct (vessel-derived) and indirect (satellite-derived) estimates of the parameters q_{he} (a) and q_v (b) for the R/V *Volna*.

Figure 5.9 shows that the SOA brightness temperature variations reproduce fair variations of heat and impulse fluxes at the stationary phase of the ATLANTEX-90 experiment. The correlation coefficients of heat fluxes and their satellite estimates are as high as $r = 0.84$ (SSM/I) and $r = 0.83$ (MTVZA), similar coefficients for q^v range from 0.85 (SSM/I) to 0.88 (MTVZA). The mismatch between surface fluxes and their estimates is of $36-37$ W m^{-2} (heat flux) for both radiometers, i.e., reaches $14.2-14.6\%$ of magnitude of the q_{he} parameter variations and $0.49-0.52$ N m^{-2} (impulse flux) – $11-12\%$ of the q^v variation magnitude.

Thus, in the case of a weak cloudiness, we can observe good qualitative and quantitative agreement between simulated and experimental values of the SOA brightness temperature at the wavelengths 1.35 and $1.55-1.58$ cm. The distinction between brightness temperatures (of 10–40 K) is caused first of all by the difference of incidence angles of the MTVZA and SSM/I radiometers. In consequence of the cloudiness influence on the SSM/I measurement data at the wavelengths 1.35 and 1.55 cm, their correct comparison with the MTVZA simulated data (which do not account the effect of the cloudiness) must be carried out with auxiliary measurements of the SOA brightness temperature at the wavelength 0.81 cm.
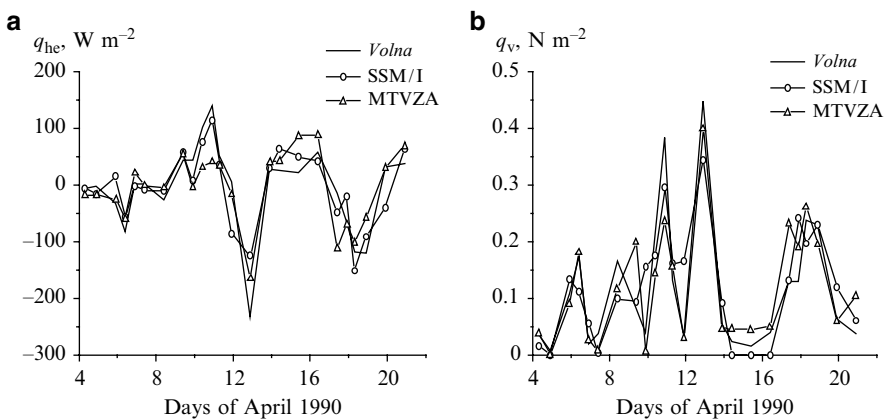
Fig. 5.9 Comparison of direct heat (**a**) and impulse (**b**) fluxes recorded from vessel *Volna* with their estimates obtained from simulated MTVZA and measured (SSM/I) brightness temperatures

Another reason that evoked the divergence of simulated and experimental data is the distinction between satellite and vessel measurements periodicity as well as their spatial resolution.

5.2.4 Comparison of the MTVZA and SSM/I Measurement Data

Here, we will show some results of comparison of the measurement data from the radiometer MTVZA with the data of quasi synchronous measurements from radiometer SSM/I of the DMSP satellite F-13 at the wavelength 1.35 cm in April and May of 2002. These data were compared for various areas of the North Atlantic located along the beds of the Gulf Stream and the North Atlantic Current (or adjacent areas) characterized by strong contrasts of the SOA parameters and its brightness temperature. The brightness temperature contrasts here are several tens of times greater than the circuit noise and calibration errors of the MTVZA and SSM/I radiometers: these factors provide favorable premises for the comparative analysis of data derived from these devices. In addition, the long-term (in terms of climate) repeatability of the basic features of large-scale temperature fields of the ocean surface as well as of the atmospheric temperature and humidity (which have a strong effect on the SOA brightness temperature measured at the wavelength 1.35 cm) makes it expedient to use these ocean areas for solving the problems of interest to us. This factor is very important in our case since no shipborne, buoy, or probe sensor aids were present in the satellite-covered area during the measurements performed with the MTVZA and SSM/I radiometers in spring 2002.

Figures 5.10 and 5.11 show sampled data measured by the MTVZA radiometer (in the form of spatial distributions of telemetry signals) and by the SSM/I radiometer (in the form of spatial distributions of the SOA brightness temperature) in the North Atlantic region in April and May, 2002. Below, only the data obtained in the descending orbits are considered since in the ascending orbit, the pattern of the MTVZA radiometer antenna system is markedly affected by the solar panels of the Meteor-3M No. 1 satellite. The images shown are based only on in situ satellite measurements and no mathematical procedures for their smoothing or other corrections were used.

In Figs. 5.10 and 5.11, the gray regions are the fragments of the southern extremity of Greenland, of the Labrador Peninsula and the island of Iceland (Fig. 5.10), and the fragment of the island of Newfoundland (Fig. 5.11); the white regions in the figures are the images of the areas observed by the MTVZA radiometer and affected by distortions due to an influence of the solar panels when being in sight of receiving antennas; the black regions are the gaps in the measurements performed with the MTVZA and SSM/I radiometers.

An analysis of the experimental data from the MTVZA and SSM/I radiometers for the period from April 17 to May 5, 2002 shows that this episode can be treated as a special case since ocean currents are rarely accompanied by atmospheric
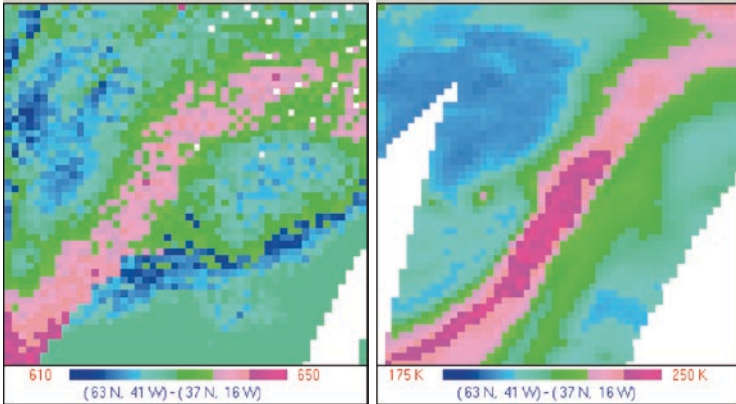
Fig. 5.10 MTVZA telemeter data (**a**) and SSM/I brightness temperature data (**b**) measured on April 23, 2002 over North Atlantic. The range of signals measured is 610–650 mV (MTVZA) and 175–250 K (SSM/I). Working frequencies used are 22.2 GHz (MTVZA) and 22.235 GHz (SSM/I)
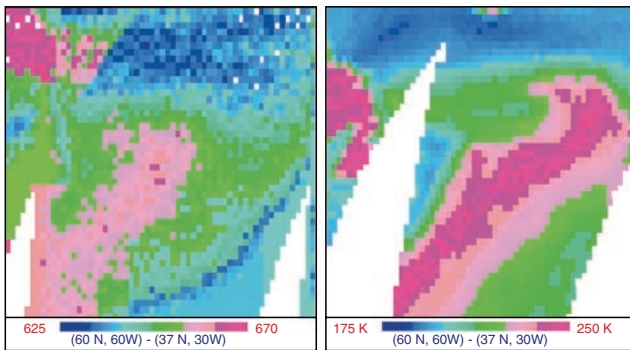
Fig. 5.11 MTVZA telemeter data (**a**) and SSM/I radiometric data (**b**) measured on May 4, 2002 over North Atlantic. The range of signals measured is 625–670 mV (MTVZA) and 175–250 K (SSM/I). Working frequencies used are 22.2 GHz (MTVZA) and 22.235 GHz (SSM/I)

images (e.g., in the form of water vapor). The phenomenon observed on April 23 was probably caused by the passage of an extended atmospheric front across the North Atlantic Current, which caused a sharp increase in the integral water vapor content along the Current and the SOA brightness temperature at the wavelength 1.35 cm sensible to variations of this parameter. The difference between the data under comparison is primarily determined by the time difference between the measurements performed with the MTVZA and SSM/I radiometers, rather than the differences in the spatial resolution of these instruments. This time the difference is

about 9 h judging from the difference in the equator cross time of the Meteor-3M No. 1 (9:15 a.m.) and the F-13 (5:42 p.m.) satellites. Our experience gained in the course of processing of the data measured by the SSM/I radiometer of the F-08 satellite indicates that the spatial distribution of the atmospheric water vapor spatial fields in this area of the North Atlantic region can radically change within 12 h owing to the cyclonic activity in the atmosphere (Grankov et al. 2001). Nevertheless, in both illustrations, similar features can be observed in spatial distribution of the atmosphere integral water vapor in the area of the North Atlantic Current, which correspond to the location of this distribution in the North Atlantic region known from the averaged climatic data.

Figures 5.10 and 5.11 indicate an important role of an intensity of MCW radiation measured at the wavelength 1.35 cm, which is closely related to the integral water vapor content of the atmosphere as the characteristic of the Gulf Stream dynamics. Although the agreement between the images is incomplete, the similarity between the contrast of the brightness temperature measured by the SSM/I radiometer and the contrast determined from the telemetry data of the MTVZA radiometer can be observed for this area of the North Atlantic region.

5.3 Conclusion

Data measured by the MTVZA microwave radiometer carried by the Meteor-3M No. 1 satellite and the quasi-synchronous experimental data obtained from the SSM/I radiometer carried by the F-13 satellite (DMSP series) in the water vapor absorption region at the wavelength 1.35 cm give similar patterns of spatial distributions of an intensity of brightness temperature of the ocean–atmosphere system in the areas of the North Atlantic region that are characterized by a strong variation (contrast) of heat and dynamic characteristics of the system. A comparison of the results of satellite microwave radiometric measurements performed at this frequency confirms an important role of the atmospheric water vapor as a factor that is actively involved in the processes of heat and moisture exchange between the ocean and the atmosphere and, at the same time, is an important indicator for these processes in the course of satellite monitoring of the ocean.

Time difference of approximately 9 h between the measurements performed with the MTVZA and the SSM/I radiometers, which is a consequence of the time asynchronism between the orbits of the Meteor-3M No. 1 and DMSP F-13 satellites, makes it difficult to perform a final estimate of the equivalence of the measurement results because these results are based on the analysis of "instantaneous" satellite snapshots of fast processes in the system "ocean–atmosphere" whose lifetime is several days. At the same time, a comparison of these data indicates that the dynamics of these processes can be estimated by integrating data of satellite microwave radiometric measurements received from similar spacecraft such as satellites of the Meteor, DMSP, and EOS Aqua series.

References

Armand NA, Tichsenko JuG, Ablyazov VS, Khaldin AA (2008) Satellite L-microwave radiometers. In: Actual problems of the Earth Remote Sensing from Space (Collected Papers), Poligraph Service, pp 139–145

Borges A, Solana A, Plaza et al (2000) The MIRAS Demonstrator Pilot Project. In: Proceedings of IEEE IGARSS'2000, 24–28 July, Honoluly (oral report)

Bunker AF (1976) Computations of surface energy flux and annual sea-air interaction cycles of the North Atlantic Ocean Mon. Weather Rev 96:1122–1140

Cherny IV, Raizer V Yu (1998) Passive microwave remote sensing of oceans. Wiley, UK, p 300

Cherny IV, Chernyavsky GM, Gorobetz NN et al (1998) Satellite Meteor-3M microwave radiometer MTVZA. In: Proceedings of International Symposium on Remote Sensing (IGARSS'98): Collected Papers, Seattle, USA, pp 556–558

Cherny IV, Chernyavsky GM (2001) Combined Optical-Microwave Imager/Sounder MTVZA-OK. In: Proceedings of International Symposium on Remote Sensing (IGARSS'2001): Coll. Papers. Sydney, pp. 2016–2018

Defense Meteorological Satellite Program (DMSP) (1997) Satellite source/Platform document . NOAA Satellite Active Archive

Dubach L, and C. Ng (1988) NSSDC's Compendium of Meteorological Space Programs, Satellites, and Experiments, March 1988

Falcone VJ, Griffin MK, Isaacs RG et al (1992) DMSP F11 SSM/T-2 calibration and validation data analysis. Phillips Laboratory, Hanscom Air Force Base, MA

Grankov AG, Milshin AA (2001) Evaluation of usefulness of the SSM/I data for study of climatic parameters of the ocean and atmosphere in the North Atlantic. Issledovanija Zemli iz kosmosa 5:70–78 In Russian

Grankov AG, Milshin AA, Shelobanova NK (2001) Specific features of the subpolar hydrological front from microwave radiometric satellite data. Russian Meteorol Hydrol 8:34–40

Hollinger PH, Peirce JL, Poe GA (1990) SSM Instrument evaluation. IEEE Trans Geosci Remote Sens 28:781–790

Kawanishi T, Sezai T, Ito et al (2003) The Advanced Microwave Scanning Radiometer Radiometer for the Earth Observing System (AMSR-E), NASDA's Contribution to the EOS for Global Energy and Water Cycle Studies. IEEE Trans Geosci Remote Sens 48:173–183

Kondrat`ev KJa, Buznikov AA, Pokrovskii OM (1992) Global ecology: remote sensing. atmosphere, ocean, space – "Razrezy" Program, VINITI, Moscow 14:145–165 (in Russian)

Nakonechny VP, Pantzov VJu, Prokhorov JuN (2004) Optical/microwave scanner/sounder MTVZA-OK. In: Actual problems of the Earth Remote Sensing from Space (Collected Papers), issued annually. Poligraph Service, pp 139–145 (in Russian)

Njoku EG (1982) Passive microwave remote sensing of the Earth from Space. IEEE Proc 70:728–750

Njoku EG, Rague B, Fleming K (1995) Nimbus-7 scanning multichannel microwave radiometer (SMMR): brightness temperature data (SMMR level 1B pathfinder). JPL Publication, Jet Propulsion Laboratory, Pasadena, CA

MTPE EOS Reference Handbook (1995) Asrar G. and Greenstone R. (eds). EOS Project Science Office, NASA/GSFC, 277 pp

Remote Sensing Applications (1998) Putting NASA's Earth science to work. – Raytheon Systems Company, Mariland 1–36

Shilin BV, Tronin AA (1995) First sympozum (advanced earth observing satellite – ADEOS). Issled Zemli iz kosmosa 5:117–119 In Russian

Special Sensor Microwave Imager (SSM/I) User's Interpretation Guide UG32268–900, Rev C 29 November 2000

Special Sensor Microwave Imager and Sounder (SSMIS) Antenna brightness temperature data record (TDR) (2007). Calibration and validation user manual. Center for Satellite Applications and Research NOAA/NESDIS

Tadepalli K (1994) SSM/T-2 Level 1b interface control document NOAA/NESDIS: Suitland, MD,
     11 July
Vazhnik TP, Chistyakova EA (1989) A method for forecasting the air-sea anomalies in the
     Northern Atlantic and the European territory of the USSR in western Siberia and North
     Kazhakstan using the water temperature in active zones of the North Atlantic Search Earth
     from Space. Tr GidrometCenter 303:127–134 In Russian

Appendix

Key Terms and Abbreviations

Atmosphere boundary layer (ABL) The atmospheric turbulent layer with the upper boundary of 1,500 m (850 HPa).

   Free atmosphere The atmospheric layer disposed above the ABL.

   Mesometeorological variations The components of atmospheric processes varied from some minutes to some hours.

   Near-surface atmosphere The lower (10-m) air layer.

   Ocean boundary layer (OBL) The upper oceanic layer (tens of meters), which is immediately acting in the energy interchanges with an atmosphere.

   Seasonal variations The components with the annual rhythm and its harmonics.

   Synoptic variations The components of atmospheric processes varied from some hours to some days.

   BT Brightness temperature.

   cm Centimeter wavelength range.

   dm Decimeter wavelength range.

   EAZO Energy active zones of the ocean.

   HP Horizontal polarization.

   IR Infrared range of wavelengths.

   MCW Microwave range of wavelengths.

   mm Millimeter wavelength range.

   SOA The system ocean–atmosphere.

   SST Sea surface temperature.

   VP Vertical polarization.

Index